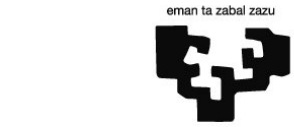


# DIFFUSIVE RANDOM LASERS IN MICRO/NANOSTRUCTURED MATERIALS BASED ON ORGANIC DYES AND RARE-EARTH IONS

DISSERTATION
submitted for the degree of Doctor of Philosophy by

**M. MACARENA BARREDO ZURIARRAIN**

*Supervisors:*
Dr. Joaquín Fernández
Dr. Ignacio Iparraguirre

Grupo de Láseres y Materiales Fotónicos
Departamento de Física Aplicada I
Escuela de Ingeniería de Bilbao

**UNIVERSIDAD DEL PAÍS VASCO**
**EUSKAL HERRIKO UNIBERTSITATEA**

2017

A mi familia

# Agradecimientos

Muchas son las personas que me han apoyado y ayudado a lo largo de estos cuatro años y las que han contribuido a la elaboración de este trabajo. A todas ellas quiero expresarles mi agradecimiento:

A mis directores de tesis, Joaquín Fernández e Iñaki Iparraguirre, por su apoyo, dedicación y el conocimiento que me han transmitido. Ha sido una gran e interesante experiencia poder trabajar con ellos.

A los demás miembros del Grupo de Láseres y Materiales Fotónicos. A mi compañera Sara García, por su tiempo y la paciencia que ha ejercitado conmigo tanto en el laboratorio como con el procesado de los datos y la literatura, por su cercanía y buenos consejos, que también me han prestado Jon Azkargorta, mi tutora Rolindes Balda y Adrián Miguel.

A todos mis compañeros de despacho, comidas, cafés y buenos ratos a lo largo de estos años: Raquel, Imanol, Alazne, Nelson, Vitalii, Ángel, Vasyl, Rubén, Adrián, Iñaki, Itziar, Kelly, Itsaso y Arrate. Gracias por el buen ambiente, vuestros consejos y apoyo.

Al personal del departamento por su buena acogida y calidez.

Al MINECO, por la financiación bajo el programa de Formación Personal Investigador 2012.

De mi estancia en el Karlsruhe Institut of Technology me gustaría agradecer al profesor Wegener su acogida y a los doctorandos Yatin Mange, Christian Kern y Patrick Mller el compartir conmigo sus conocimientos sobre escritura láser y resinas.

También son muchas las personas que, fuera de la Escuela, han compartido conmigo estos años y se han interesado por mi trabajo y avances. Gracias a mis compañeros y directores del coro de la universidad por todos los buenos ratos compartidos. A mis compañeras de piso, Irati y Cristina. A todas mis amigas, las de la carrera y las de Asturias, pero especialmente a Patricia, Nora, Carla, Laia, Sara, Cristina y Raquel, y a Santi, por acompañarme todo este tiempo. Gracias Guille por tus canciones.

Y a mi familia, quienes más me han sufrido y más me han cuidado; a mis hermanos y a mis padres, al "magister" José Larrea†, porque todo lo bueno se lo debo a ellos y a su ejemplo.

A todos, muchas gracias.

# Contents

# List of Tables

# List of Figures

# Summary

Random lasers are systems able to generate laser light above a certain pumping threshold thanks to the multiple scattering processes that can create enough amplification to compensate the losses. Although, unlike traditional lasers, they have no cavity they still present laser modes determined by the multiple scattering of the random dielectric structure. They have been studied since the 1990s in very diverse materials, and can present two different configurations: they are composed by either a gain medium with added scatterers or a medium with scatterers which have gain.

Among random lasers one category known as diffusive random lasers attracts special attention. Nevertheless, the understanding of some of their features remains a challenge. In this thesis we study the emission properties and modal dynamics of two different materials, a di-ureasil doped with Rhodamine B and neodymium doped crystal powders, and the dependences of the emission features on the experimental configuration and material properties such as concentration and grain size.

The spatiotemporal dynamics and spatial coherence of the Rhodamine B doped di-ureasil under one and two photon pumping is analysed thanks to a spatial filtering method to allow for mode selection. A streak camera provides time and wavelength-resolved images of single shot measurements of both the pump pulse and the sample emission.

We also present a detailed study of the emission of several $Nd^{3+}$ stoichiometric and low-doped powders and explore their laser slope, threshold energy, absorption and the spatially integrated pulse dynamics.

Lastly, we explore two applications of the studied phenomena. On the one hand, we study the suitability of $Nd^{3+}$ doped powder samples as NIR source for speckle-free imaging and, on the other hand, the cooling of discrete regions by anti-Stokes processes of $Nd^{3+}$ doped oxysulfide powders.

This thesis is the result of a four-year doctorate in the Escuela de Ingeniería de Bilbao of the Basque Country University (UPV/EHU) under the supervision of Prof. J. Fernández and Prof. I. Iparraguirre and has been supported by a FPI grant of the MINECO (Spanish Government).

The work described in this thesis has been published in the following papers and

proceedings:

- J. Azkargorta, I. Iparraguirre, M. Bettinelli, E. Cavalli, **M. Barredo-Zuriarrain**, S. García-Revilla, R. Balda, and J. Fernández, "Effects of pumping wavelength and pump density on the random laser performance of stoichiometric Nd crystal powders," *Opt. Express*, vol. 22, no. 22, p. 27365, 2014.
- S. García-Revilla, J. Fernández, **M. Barredo-Zuriarrain**, L. D. Carlos, E. Pecoraro, I. Iparraguirre, J. Azkargorta, and R. Balda, Spectral dynamics of a diffusive random laser under two photon pumping," *Adv. Device Mater.*, vol. 1, pp. 3845, 2015.
- J. Fernández, R. Balda, **M. Barredo-Zuriarrain**, O. Merdrignac-Conanec, N. Hakmeh, S. García-Revilla, and M. A. Arriandiaga, "Spectroscopic and thermal study of Er-doped oxysulfide crystal powders," in *Proceedings of SPIE*, 2015, vol. 9380, pp. 110.
- S. García-Revilla, J. Fernández, **M. Barredo-Zuriarrain**, L. D. Carlos, E. Pecoraro, I. Iparraguirre, J. Azkargorta, and R. Balda, "Diffusive random laser modes under a spatiotemporal scope," *Opt. Express*, vol. 23, no. 2, p. 1456, 2015.
- S. García-Revilla, J. Fernández, **M. Barredo-Zuriarrain**, and E. Pecoraro, "Coherence characteristics of random lasing in a dye doped hybrid powder," *J. Lumin.*, vol. 169, pp. 472477, 2016.
- I. Iparraguirre, J. Azkargorta, K. Kamada, A. Yoshikawa, U. R. Rodríguez-Mendoza, V. Lavín, **M. Barredo-Zuriarrain**, R. Balda, and J. Fernández, "Random laser action in stoichiometric $Nd_3Ga_5O_{12}$ garnet crystal powder," *Laser Phys. Lett.*, vol. 13, p. 035402, 2016.
- J. Azkargorta, I. Iparraguirre, **M. Barredo-Zuriarrain**, S. García-Revilla, R. Balda, and J. Fernández, "Random Laser Action in Nd:YAG Crystal Powder," *Materials (Basel).*, vol. 9, no. 5, p. 369, 2016.
- J. Azkargorta, L. Marciniak, I. Iparraguirre, R. Balda, W. Strek, **M. Barredo-Zuriarrain**, S. García-Revilla, and J. Fernández, "Influence of grain size and $Nd^{3+}$ concentration on the stimulated emission of $LiLa_{1-x}Nd_xP_4O_{12}$ crystal powders," *Opt. Mater. (Amst).*, pp. 38, 2016.
- R. Balda, N. Hakmeh, **M. Barredo-Zuriarrain**, O. Merdrignac-Conanec, S. García-Revilla, M. A. Arriandiaga, and J. Fernández, "Influence of Upconversion Processes in the Optically-Induced Inhomogeneous Thermal Behavior of Erbium-Doped Lanthanum Oxysulfide Powders," *Materials (Basel).*, vol. 9, no. 353, p. 13, 2016.
- J. Fernández, R. Balda, **M. Barredo-Zuriarrain**, O. Merdrignac-Conanec, N. Hakmeh, and S. García-Revilla, "Progress in the spectroscopic and thermal studies of Er-doped oxysulfide crystal powders," in *Proceedings of SPIE*, 2016, vol. 9765, pp. 111.

- **M. Barredo-Zuriarrain**, I. Iparraguirre, J. Fernández, R. M. Balachandran, and R. Balda, "Speckle-free near-infrared imaging using a $Nd^{3+}$ random laser source," *Laser Phys. Lett.* Accepted.

# Chapter 1

# Random lasers: Background and current status

## 1.1 Introduction

Random Lasers (RLs) generate laser light above a power threshold by the light scattering induced by disorder and mediated by random fluctuations of the dielectric constant in space. In these systems, multiple scattering can keep light long enough inside the material so enough amplification can compensate the losses leading to the clamping of the population inversion, and therefore of the gain, around threshold.

In traditional lasers the cavity determines the modes of the laser, the frequency and directionality. Scattered light from a particular lasing mode can form a new mode and amplified by stimulated emission if the feedback overcomes the losses of the system. This is what allows lasing in random media [1] and what makes multiple scattering determine random laser modes.

Ambatsumyan et al. proposed in the 1960s a new type of laser with nonresonant feedback based on reflection off a highly scattering surface. They proposed several configurations of multimode cavities in which nonresonant feedback conditions could be fulfilled [2, 3]. During that time, Letokhov predicted laser emission from scattering particles with negative absorption and with a mean free path much smaller than the dimensions of the system [4], detailing the behaviour, the slow kinetics of the spectral narrowing, the existence of relaxation oscillations... He also suggested that such a scattering medium would show a large number of strongly coupled modes and large radiation losses [5], which creates such an overlapping of the modes spectra that the spectrum becomes a continuum, i.e., if the number of modes is sufficiently large, the feedback becomes nonresonant [6]. Varsanyi in 1971 observed a miniature source of stimulated emission, a powder laser [7]. Markushev in 1986, while studying several powders doped with neodymium, found that above a certain energy threshold the duration of the emission shortened several orders of

magnitude, the intensity increased at the frequency of maximum gain, the spectra narrowed significantly up to a single line and the input-output energy dependence was similar to that of conventional lasers [8–10]. Although the emission presented a lasing behaviour it was explained in terms of stimulated emission from excited powders [6]. The main two ingredients needed in an RL are multiple scattering and gain. There are two main classes of RL: a gain medium with added scatterers and scatterers which have gain. Random laser emission has been reported in very diverse materials such as semiconductor powders like ZnO [11–13], powdered crystals [14–16], dye solutions with nanoparticles [17, 18], plasmonic nanostructures [19, 20], photonic fibres [21–23], biological tissues [24–30], polymeric films [31–33], died paper [34], microdroplets [35, 36], solutions with scatterers [17, 37] or liquid crystals [38–43].

## 1.2 Diffusive Random Lasers

Many fundamental questions remain unsolved and some basic features of RLs are still unfixed. As van der Molen et al. explains, one of the reasons there is not a unique definition of what an RL is or how it behaves relies on the widespread kinds of emitting materials and scattering regimes, which give very different behaviours on emission spectra, energy efficiencies, pulse time-ranges, spatial profiles, etc. In addition, the parameters used to describe the results vary from author to author and sometimes are not completely described, hindering the understanding among the scientific community [44]. It is difficult to study all systems with a unique theoretical treatment [45] because the nature and morphology of each amplifying disordered medium determine the feedback mechanism [6, 46]. Results of different RL experiments can be influenced by experimental conditions: sample excitation, the emission collection method, boundaries imposed by the sample holder... [11,12]. However, many efforts have been done to develop a general theoretical treatment, for their temporal dynamics [47–50], their spectral behavior [44, 51, 52], the threshold and output energies, etc.

Diffusive random lasers (DRLs), RLs in which light undergoes diffusive motion within the gain medium and hence present a strong modal interaction, are of particular interest since a clear modal picture of such extremely leaky systems is still missing in the literature. As with most lasers, in a DRL, lasing occurs above a pumping power threshold. However, pump and emitted photons are involved in multiple scattering processes which increase the dwell time of photons inside the material and allow for enough amplification to compensate for absorption and leakage of light through its boundaries creating gain saturation. A classical DRL is usually realized by closely assembled optically active particles (such as laser crystal or amorphous powders) that scatter light and have gain, or by passive scatterers embedded in an amplifying medium. Note that random lasing in diffusive systems with a continuum spectrum was the first observed and theorized. Under certain conditions the emission spectrum of DRLs shows a narrowed emission band made of

overlapped spikes. These spikes can appear as a result of localized modes and also extended modes [53]; in some materials these can co-exist and produce a coherent emission. Experimental conditions are critical in the analysis of the spectral structure of this systems because the strong coupling they suffer determines the statistical regime of the fluctuations and the spectral features [54]. It is then essential to study these systems under adequate experimental conditions. For instance, it is necessary to use a quasi-instantaneous pumping source, a picosecond laser – longer pulses create an overlapping of the modes and a smooth spectra without spikes –, but other experimental parameters such as the pumping energy, the size of the pumped area, the absorption of the material, the extension of the analysed area... are also critical and have to be considered.

Depending on the experimental configurations nonresonant or resonant feedback can appear on the material. The emission dynamics of early experiments in colloidal dye solutions showed spectral narrowing above threshold and increase of intensity at the frequency of maximum gain [17] could be described by a diffusion equation with gain where the phase of the light field does not play any role [55, 56]. This laser emission showed a smooth and broad spectrum with no frequencies of a resonator was said to have nonresonant feedback. Later experiments in semiconductor powder samples by Cao et al. [57] revealed multiple spikes in the emission spectrum; these lasing systems are called systems with resonant feedback. The emitted light had Poissonian photon statistics which reveals the temporal coherence of the emission [58]. Several authors [59–61] first suggested that certain cavities could be providing resonant feedback thus creating a localization regime with narrow spikes. However, other experiments dismissed this explanation for the spikes arguing that the spikes appeared in different scattering regimes: strong, diffusive and weak [42, 62, 63]. The scattering strengths are defined by three important parameters: the transport mean-free path $l_t$ over which the direction of light is randomized, the size of the sample $L$ and the wavelength [64]. Apalkov et al. [65] suggested that ring-shaped resonators might have some nonnegligible probability to exist in the diffusive regime ($\lambda \ll l_t \ll L$). This model is supported by random lasing experiments in $\pi$-conjugated polymers [66, 67]. However, these configurations can only exist if spatial fluctuations of the refractive index are correlated over large enough distances, so they will not appear in all weakly scattering cases [68]. Mujumdar, on the other hand, suggested that among the spontaneously emitted photons of a random system with gain, there exists a subset of rare photons that travel much longer distances than the average ones. These "lucky photons" accumulate enough gain to activate a new lasing mode with a different wavelength after each excitation shot, and give rise to random spikes in the spectrum [63, 69]. The experimental study performed by Chabanov et al. has brought forward the existence of long-lived extended modes in regular diffusive materials which might be responsible for the observed narrow spikes in RLs [70]. However, Fallert et al. showed that strongly localized modes can co-exist with modes of much larger spatial extension which become more easily coupled from mode competition. Depending on the material studied, both localized and extended modes can thus lase and provide a coherent RL mechanism [53]. On the other hand, DRLs are highly multimode as many spatially overlapping modes exist, so mode

mixing, which obscures the characteristics of individual modes and is likely to be modified by the boundary conditions, is particularly important. If the mode overlap is significant, complex nonlinear processes such as temporal oscillations [71, 72] or spatial hole burning [73] may appear. Gain mode competition may also play a crucial role when determining the condition of the different statistical regime of fluctuations and spectral profiles of RLs [54]. The intensity distribution of RLs obeys a Lèvy type defined power-law tails [74]. However, different statistical regimes and crossovers are possible depending on gain, scattering strengths, excitation energies, and sample sizes [75–77]. Furthermore, the mode coupling between long-lived extended modes together with the stochastic behaviour inherent in the spontaneous emission from which the RL starts at each shot, can explain the strongly stochastic behaviour in the positions of the narrow emission lines of an RL with static disorder reported by Mujumdar et al. [69].

The presence of coherent multimode lasing even in the diffusive regime, has been a challenge for conventional laser theory. The focus of theoretical research in this field is to extend the semiclassical multimode lasing theory to open and irregular systems, the modes of which have a broad distribution of radiative lifetimes and an irregular spatial pattern [78]. As the usual methods for introduction of modes and quantization based on eigenvectors of hermitian operators are not applicable in such a case, alternative methods for defining electromagnetic modes are proposed by using the quasimodes, quasi-bound (QB) states, or resonances of the passive system without gain [78, 79]. In the strong scattering regime, the eigenvectors resulting in these theoretical explorations are nearly identical (within the scattering medium) to the threshold lasing modes. However, the difference between them increases for more lossy systems such as DRLs [79]. A recent time-independent theory based on the so-called constant-flux (CF) states which can find the random lasing modes and frequencies self-consistently (with no relation with the QB states), allows one to study the multimode regime in DRLs, and provides detailed information about the effects of mode competition through spatial hole burning [80–82]. Within this approach, uniformly spaced frequency spectra are expected in DRLs due to their modal interaction through the gain medium. In accordance with it, some experimental observations show more or less regularly spaced lasing frequencies exhibiting mode repulsion [68, 83, 84]. No significant changes in the lasing frequencies were either predicted for different pump strengths or spatial profiles of the pump whereas the intensities vary strongly. Nonetheless, the CF theory only improved the understanding of the properties of lasing modes in the stationary regime. RLs are intrinsically time-dependent systems due to the different time scale of transport and population dynamics, so in order to address the description of the dynamics, structure, frequency or intensity statistics of lasing modes in a DRL, a time-dependent model in three-dimensional (3D) RL structures, suitable under local and pulsed-pumping conditions, might be necessary.

In the diffusion approximation, far from the localization condition $kl_s \gg 1$, the propagation of the intensity is described as a random walk with a characteristic mean free path $l$. In order to characterize the propagation of light in the scattering material it is important to analyse the main parameters, the mean-free-path lengths

involved in the scattering process: the scattering mean-free-path $l_s$, defined as the average distance between two successive scattering events and the transport-mean-free-path $l_t$ is the average distance the light travels before its direction of propagation is randomized [64]. In a steady state regime and for a density of scatterers $\rho$:

$$l_s = \frac{1}{\rho\sigma_s} \tag{1.1}$$

$$l_t = \frac{1}{\rho\sigma_t} \tag{1.2}$$

where $\sigma_s$ is the scattering cross-section and $\sigma_t$ the transport cross-section. The lengths that describe the photon propagation are the inelastic length and the diffusive absorption length: $l_i$, which is defined as the travelled length over which the intensity is reduced to e1 of the initial value due to absorption by scatterers and labs, the average distance between the beginning and the end points of paths of length $l_i$.

$$l_i = \frac{1}{\rho\sigma_a} \tag{1.3}$$

$$l_{abs} = \sqrt{\frac{l_t l_i}{3}} \tag{1.4}$$

where $\sigma_{abs}$ is the absorption cross-section at pump wavelength, $\rho$ the concentration in ions per unit volume and $\sigma_t$ the transport cross-section.

And the gain length is,

$$l_g = \frac{1}{N_s\sigma_{em}} \tag{1.5}$$

, where $\sigma_{em}$ is the stimulated emission cross- section, $N_s$ the population inversion in particles per unit volume:

$$N_s = \frac{\eta E}{h\nu A l_{abs}} \tag{1.6}$$

being $E$ the pumping energy, $h\nu$ the pump photon energy, $\eta$ the absorbance of the sample and $A$ the pumping area.

At the threshold condition, $l_g = l_{res}$, where $l_{res}$ is the mean residence length of the stimulated emission photons. Then, according to the one dimensional theory [85, 86],

$$\frac{E_{th}}{h\nu A} = \frac{l_{abs}}{\eta\sigma_{em} l_{res}} \tag{1.7}$$

In stoichiometric materials (Part II) it is very difficult to measure the inelastic length; instead, the ratio between the transport length and the absorption length can be estimated from absorbance spectrum using the Kubelka-Munk theory [87]:

$$\frac{l_t}{l_i} = \frac{\eta^2}{2(\eta - 1)} \tag{1.8}$$

## 1.3 Current status and motivation

The observation of isolated narrow lines or a global narrowing of the RL spectrum often depends on the chosen experimental configuration. The ideal conditions for observation of spiky spectra are the use of a short-time pump pulse duration ( 30 ps) and single-shot observation. Both the collection of several emission shots, or the use of a long enough single excitation pulse, may lead to an averaging mechanism among modes which reduces the previously mentioned fluctuations and gives rise to a smooth emission structure. This is probably the reason why some early RL experimental studies missed the observation of narrow spectral features in DRLs [88]. A reduction of the spikiness of the emission spectra, accompanied by an increase of the intermode spectral correlation, can be also achieved by adjusting the shape of the pump beam with a spatial mode modulator to incrementally excite larger numbers of spatially separated lasing modes [89]. The observed transition from a spiky to a smooth emission profile was explained by a phase locking between modes. On the contrary, the reduction of the spatial extent of the pump applied to the gain material by using a tightly focused beam, facilitates the experimental observation of well separated sharp peaks [1]. When a large enough pump spot is employed, narrow lasing lines overlap and the emission spectrum becomes smooth. In contrast, smaller pump areas excite fewer modes, so a fine structure can thus be observed [90].

Thus, the aim is to give experimental evidences of the modal structure and modal oscillation dynamics of our diffusive scattering system after single shots of 30 ps pulse duration. As already pointed out, the difficulty in unscrambling the complex lasing behavior of a DRL is caused by the large number of modes that can simultaneously lase and randomly couple. As a result, the lasing modes dynamics of a DRL is rarely investigated experimentally [91, 92]. In almost all reported RL experiments with pulse laser excitation, time-integrated data are recorded. Under these circumstances, it is hard to extract any detailed information about individual lasing modes and thus impossible to know whether different modes coexist at the same time or appear subsequently. However, these difficulties can be avoided with the novel experimental arrangement adopted in this work. Our set-up was specially designed to enable spatial mode selection, which favours the observation of individual lasing spikes, as well as accurate time-resolved measurements which permit to follow experimentally their dynamics response. The use of a streak camera allows a 2 ps time resolution which is a crucial requirement in this regard. The way to resolve lasing modes consists both in using a small enough pump spot size and in selecting a small enough emitting surface area by spatial filtering in the detection.

The performed systematic study of the temporal evolution of the spectrally resolved emission evidences that different lasing modes stem from different time intervals showing a different temporal behaviour in a DRL, and illustrates the existence of relaxation oscillations from the time traces of individual lasing modes. In this approach, the modal density dependence on the pump energy and pump spot size is also accessed experimentally . Careful examination of the temporal and spectral response of the corresponding sharp lasing peaks allows us to assess the stability of the mode structure between different shots and, therefore, to evaluate the stochastic behaviour of these active random media. The analysis of the results shows that our powder system lases in different modes in successive excitation events under constant experimental conditions. Parallel to this research, we have examined the spatial properties of the RL emission of this sample. We herein explore whether the imaging of the RL light on the dye doped powder surface is spatially restricted to the pumped domain (as suggested in the literature [1]), or else it is extended over a larger area of the scattering medium.

In addition, we have studied the coherence of these systems. In RLs, light is trapped through multiple scattering and the spatial modes are inhomogeneous and highly irregular. With external pumping, a large number of modes can lase simultaneously with uncorrelated phases, which accounts for the low spatial emission coherence of these unconventional lasers [93]. In such disorder media, laser light is the weighted sum of the light emitted from various spatial regions, so that light intensity from sample zones separated by more than a given coherence length becomes uncorrelated. A valid assumption for RLs lies in regarding a transversal coherence length of the same order of the transport mean free path [92]. The first approach to this research field was carried out on a Rhodamine 6G-titania system in a polymer matrix where a partially coherent emission was found [94]. However, Cao et al. demonstrated in a ZnO pellet that above threshold, light emitted from a disordered material structure with resonant feedback exhibits coherence properties characteristic of true laser light [58]. Both conflicting results evidence a heavy dependence of the temporal coherence properties of RLs on the specific system in question, and particularly, on their mode competition [95]. More recently, Redding et al. found significant variations of the spatial coherence properties of the RL emission of dye solutions containing nanoparticles, depending on scattering strength and the pump area. These observations were also qualitatively explained in terms of the number and characteristics of the active RL modes [96]. Note that the investigation about coherence in RLs is not only of theoretical interest [95, 97, 98], but also of practical importance. Since their spatial and temporal coherence characteristics are quite different from those of conventional lasers, RLs could be well suited for a host of applications in which they could outperform conventional lasers [93].In particular, the versatility of RLs combined with their unique ability to provide controllable coherence and laser-level intensity, open the possibility of developing a new kind of illumination sources for specific imaging applications. In fact, the feasibility of RLs for full- field imaging or time-resolved microscopy has already been reported [92, 93, 95, 97–99].

The system response under two photon pumping is also studied. In practical

terms, multiphoton pumping can be highly useful for data storage, or frequency up-conversion imaging [100] whereas RLs find an increasing use in photonics, biotechnology, medicine or bio/chemical sensing [6, 88]. In particular, RLs have already proved their value for medical diagnostic purposes [24]. The conjoint use of multiphoton excitation by means of NIR sources (desirable for tissue penetration), with techniques based on the knowledge of multiple light scattering in random systems, such as a biological tissue containing a statistical inhomogeneity (tumor), opens exciting avenues in biophotonics for monitoring thick biological objects with spatial resolution. For this purpose, dyes with a large multiphoton absorption coefficient to be used in the NIR, which also assure compatibility with the biological materials, are required [100]. Despite these new possibilities for applications, multi-photon induced random lasing has become the subject of just a few works which report observation of this phenomenon. Random lasing utilizing a two photon (TP) pumping scheme was firstly observed in dye doped gelatin cubes excited with femtosecond laser pulses at 800 nm [101]. Afterwards, experimental evidences of anti-Stokes RL emission were found in dye solutions doped with $TiO_2$ nanoparticles, in micrometre size powder of GaAs, in different morphologies of ZnO, and in a disordered InGaN/ GaN quantum-disk (Q-disks) ensemble [102–109]. The theoretical study performed by Burin et al. within the diffusion model framework, suggested that random lasing with a lower threshold can be achieved by using TP pumping instead of single photon excitation [110]. In a later paper, Wang et al. [111] reported a numerical analysis of the saturation effects of emitted light intensity following TP pumping. Our group has investigated, both theoretically and experimentally, the RL features around threshold of a silica gel powder containing Rhodamine 6G doped silica nanoparticles by pumping at one and two photons (at 532 and 800 nm), under typical diffusive conditions, i.e. by using a broad pumped area, which lead to a smooth and narrow RL emission spectrum [112]. Contrarily to the previously mentioned analytical result, in this disordered active material, the TP pumped RL threshold is 50 times larger than the onset of RL action following the conventional OP excitation. In a preliminary study, we have also experimentally demonstrated the possibility of obtaining random lasing by pumping at one and two photons in a sample based on Rhodamine B (RhB) doped di-ureasil with a large pump spot [113].

On the other hand, we have also decided to thoroughly study the random lasing by neodymium doped crystal powders in the ${}^4F_{3/2} \rightarrow {}^4 I_{11/2}$ emission band of $Nd^{3+}$ ions at 1064 µm with different concentrations and grain sizes in order to clarify some properties on the emission of these systems and their interpretation, which are not clear in literature: the dependence of the laser threshold energy with the pump spot size and wavelength, the dynamics of the emission pulses and the relation between the absorbance and the laser slope efficiency and threshold energy density. In all the samples the wavelength of the radiation is much shorter than the transport, inelastic and absorption lengths.

We believe that the outcome of our experiments will help the RL community to deepen the understanding of fundamental and intriguing aspects of DRLs such as their spatiotemporal behaviour.

# Chapter 2

# Aims of the work

In this dissertation we study the random lasing emission of different diffusive random lasers doped with organic dyes and rare-earth ions to address the main unanswered questions in literature. The aims of the study are:

- First, to analyse the emission under one-photon picosecond pumping of a diffusive random laser based on a Rhodamine B doped di-ureasil dU(600) host in order to deepen the understanding of its modal dynamics. This can be found in chapter 3, where we develop a spatial filtering method to allow for mode selection. This method provides the necessary conditions to perform an analysis of the modal dynamics of individual lasing modes and the degree of coherence of the sample emission.

- To extend the study of the spectral dynamics of the same powder crystal under two-photon (TP) pumping, which provides anti-Stokes emission. TP induced random lasing has been the subject of just a few works despite the advantages multiphoton excitation presents, like the absence of the phase matching requirement, and the potential applications in the near-infrared. The results are discussed in Part I, chapter 4.

- To characterise the emission of several $Nd^{3+}$ stoichiometric and low-doped powders under nanosecond pumping and explore the relation between the laser slope, the absorption, the emission and pump wavelengths and the threshold energy (Part II, chapters 5 and 6). In addition, we study the dynamics of the emitted pulses.

- In Part III we explore two applications of the studied phenomena. First, in chapter 7, we study the emission of a $Nd^{3+}$ doped sample as a NIR source for speckle-free imaging and compare it with a traditional laser source. Finally, in chapter 8 the thermal response of different $Nd^{3+}$ doped oxysulfide powders is analysed and the cooling of discrete regions by means of anti-Stokes processes is studied.

# Part I

# DYE-BASED SOLID STATE RANDOM LASERS

# Chapter 3

# Analysis of the one-photon pumped random laser emission of an organic-inorganic hybrid compound based on a Rhodamine B-doped di-ureasil host (RhB-dU)

## 3.1 Introduction

We investigate the spatiotemporal dynamics under one-photon pumping of a dye-doped diffusive random laser (DRL) based on an organic-inorganic hybrid ground powder, a Rhodamine B doped di-ureasil host, and analyse the modal oscillation dynamics, lasing mode structure and evaluate the coherence of this compound. We develop a spatial filtering method to study the modal and spectral dynamics of the explored powder and characterise spatially and temporally individual modes. Additionally, we evaluate the coherence of the RL emission of our doped hybrid sample.

The interest of these doped hybrid compounds in solid state dye random lasers relies not only in its static configuration, with defined and fixed diffusors but also on the synergy between the spectroscopic properties of the organic dyes and the characteristics of sol-gel derived hybrid hosts. These hybrid hosts are easily processed by sol-gel route, which enables the incorporation of large amounts of dye molecules into the hybrid matrix isolated from each other and protected by the hybrid host [114].

Organic dyes have been thoroughly studied and implemented as gain medium for conventional lasers (i.e. dye lasers), consisting typically of a solution of organic fluorescent molecules in water or an organic solvent. These compounds present large emission and absorption cross sections, high fluorescence quantum efficiency, and

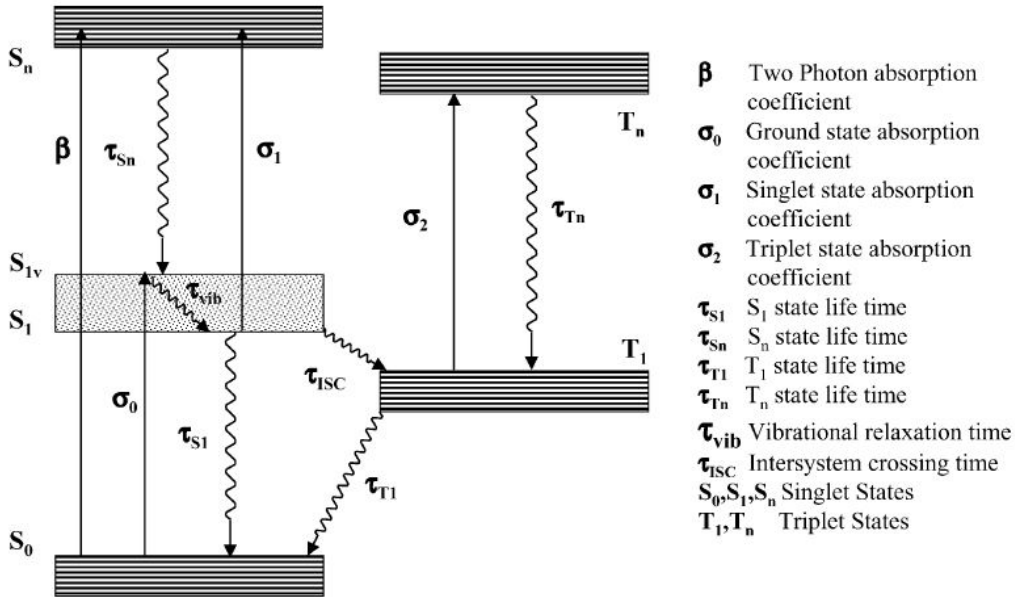


**Figure 3.1:** Energy levels of a Rhodamine B molecule. [Image from Venugopal Rao [116]]

broad emission and absorption bands which allow a good tunability. The development of material hosts for solid-state dye lasers has been intensively studied for the last three decades due to the advantages they present comparing to liquid dye lasers: non-flammable, non-toxic, more compact and mechanically stable.

Dye molecules have singlet and triplet electronic states, composed of several vibrational and rotational states, creating a broad continuous band of energy levels, which translates on their capability of being able to absorb and emit over a range of wavelengths [115]. These molecules have a four-level system (figure 3.1), which minimizes absorption and makes the population inversion possible. When the molecules are excited by the pump light, higher vibrational levels of the $S_1$ and $S_2$ are populated from levels of $S_0$ and relax to the lowest vibrational level of $S_1$. Later, it decays to a high level of $S_0$ and finally relaxes to the ground state. Under certain pumping conditions, the population inversion can be also achieved between the lowest level of $S_1$ and a high vibronic level of $S_0$. Under one-photon (OP) pumping of our RhB-dU sample, at 532 nm, the molecule is directly excited to the lowest state of the $S_1$.

In our sample, Rhodamine B is incorporated into a sol-gel derived poly(oxyethylene)/-siloxane hybrid matrix named di-ureasil (dU(600)), which is known for its optimized optical properties [117–119]. The host hybrid matrix is composed by a siliceous framework to which polyether chains containing oxyethylene are covalently bonded through urea linkages, which increases the efficiency comparing to the one of hybrid materials based on silica gels where the dye is entangled in the porous silica network. The matrix contains $1.23 \times 10^{19}$ RhBmolecules/cm$^3$.

The synthesis, developed and described by Pecoraro et al. [114], consists of

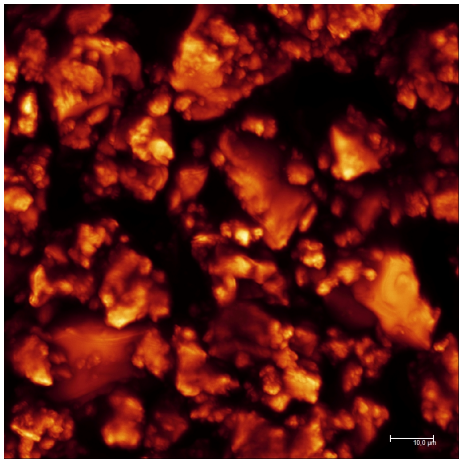

**Figure 3.2:** Confocal microscope image of the RhB-dU(600) sample

the following process: The reagents O, O′-Bis(2-aminopropyl) polypropylene glycol-block-polyethylene glycol-block-polypropylene glycol (Fluka), commercially known as Jeffamine - ED600®, average molecular weight 600 g · mol$^{-1}$, 3- isocyanatepropyltriethoxysilane (ICPTES) (Aldrich 95 %, ethyl alcohol absolute P.A. (Carlo Erba), tetrahydrofuran P.A. (stabilized- Riedel-de Han), HCl (ACS Reagent 37 % - Sigma-Aldrich) and Rhodamine B were used as received. The di-ureasil host, termed as d-U(600), contains 8.5 ($OCH_2CH_2$) polymer chains with both ends grafted to a siliceous network by means of urea linkages. The cross-links between the organic and the inorganic components were formed by reacting the $NH_2$ groups of Jeffamine-ED600®with the -N=C=O group of ICPTES, in THF, under magnetic stirring and reflux at 80 °C for 18 h. The non-hydrolyzed d-U(600) precursor was isolated after complete THF evaporation at 45 °C in a rotary bench evaporator. A solution of RhB chloride in 1 mL of ethanol was incorporated into the di-ureasil host, under magnetic stirring. The RhB solutions were added to 3 g of d-UPTES after 15 min. The suspensions were kept under magnetic stirring for 15 min at room temperature, and were then cast into a polystyrene mould (1× 1× 3 cm) and left to gel, which happened within 3 min. After gelation, the mould was covered by Parafilm®and kept at room temperature for 24 h. Then the cover was removed and a three-step heat treatment at 40 °C (72 h), 50 °C (24 h) and 60 °C (24 h) was performed to eliminate residual solvents (including ethanol and water produced by polycondensation). The final volume of the sample was not significantly affected by shrinkage process (less than 5 %).

The material was ground using a mixer mill (Retsch MM200) during 4 minutes. A confocal microscope (Leica TCS SP5) is used to measure the polydespersity of the ground powder. As a result, an average powder size of 6.6 µm is found.

Figure 3.2 shows one of the recorded images. We create a histogram of the size of the grains and fit it to a log-normal function. As can be observed in the micrograph, there are particles larger than 10 µm but there are more particles with a smaller

size. The powder is compacted in a cylindrical cell 6 mm high and with a 5 mm diameter, open at the top, and a volume filling factor $f = 0.55$. The estimated transport mean free path in a similar sample [120] was $14 \pm 2$ µm at 630 nm, which confirms the diffusive scattering regime of our random laser.

## 3.2 Experimental

The set-up used to perform these study with subnanosecond time-resolved images is shown in figure 3.3. The excitation source is a frequency-doubled mode-locked Nd:YAG laser (EKSPLA, PL2251B) with a pulse duration of 30 ps and repetition rate 20 Hz. The laser energy is measured with an energy meter after attenuation with a half-wave plate and a polariser. The signal is divided with a beam splitter; a reflected 5 % of the excitation beam is diverted to an optical line to provide a reference signal and the transmitted light is focused into a 500 µm spot on the doped powder for most of the measurements; the photon counting measurements are performed with a 50 µm focus diameter. Both optical paths are equally long; we verify it collecting with the a reflection of a paper placed on the surface sample and the reference signal coming from the other optical line camera at the same time. Adjusting the mirrors allows us to reduce the delay between both pulses to zero, thus asserting the identical length of both optical paths and providing a proper time reference to the random laser emission. The emission from the pumped surface of the sample is collected with a lens (f = 5 cm) placed at twice the focal length distance ($S_1 = 2f$) and imaged on a pinhole positioned on a translation stage at the same distance behind the lens ($S_2 = S_1$). A long-pass filter (Semrock LP532) is placed after this lens to remove the pumping light diffusively reflected by the sample surface. Finally, another lens focuses the signal from the two optical paths to the slit of the image spectrograph (Chromex A6365-01) coupled to the streak camera (Hamamatsu, C5680). The lateral magnification is one, granting the collection of the emission from an area equal to the pinhole aperture.

The experimental set-up allows for a detailed study of the RL emission dynamics as the signal can be recorded in single shot measurements with a resolution of 2 ps along with the pump pulse. The images taken with the streak camera are resolved in time and wavelength. The time is represented in the vertical axis, with a time window set at 1 ns, and the wavelength corresponds with the horizontal axis. Temporal and spectral profiles of the images can be extracted for any selected area.

#### Spectrograph - Streak camera

The study of the dynamics of the RL emission of our doped hybrid powder is possible thanks to the spectrograph Chromex-A6365 coupled to a Hamamatsu C5680 streak camera. The combination of these devices allows for time resolved spectroscopy. The streak camera is an imaging device that spatially and spectrally analyses the

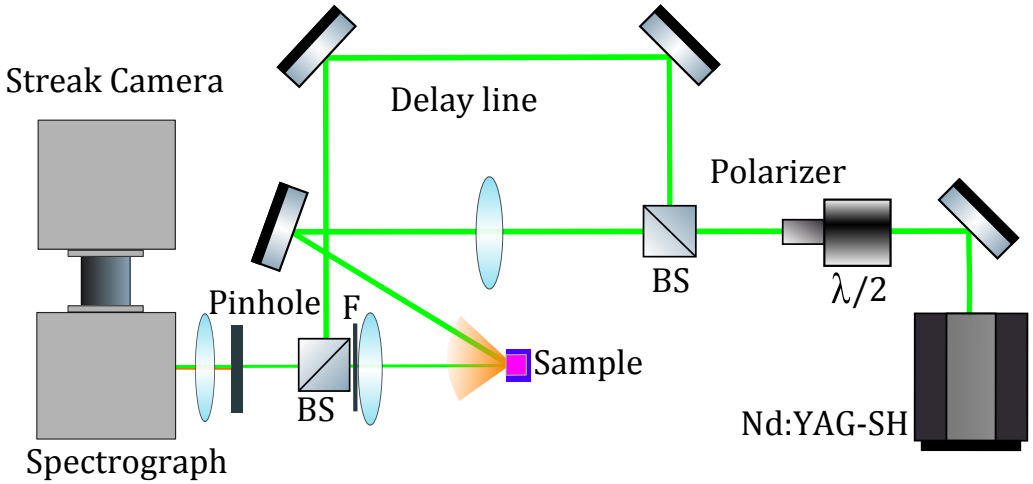


**Figure 3.3:** Set-up for the ps time-resolved study under OP pumping. F is a long-pass filter and BS are beam splitters.

receiving radiation. In combination with the spectrograph it can measure time variation of the incident light intensity with respect to wavelength. Its working range is between 200 nm and 900 nm, and it is capable of measuring a wavelength window 87 nm wide. For the temporal analysis it can operate with different modules. To study the emission of this sample we use the fast single sweep unit, which can evaluate a time range up to 50 ns with a 2 ps resolution. The operating principle of the streak tube is shown in figure 3.4. The light passes through the spectroscope, which directs it to the photocathode. An image with the spatial information in the horizontal axis forms on the photocathode, which converts the light into electrons. The electrons are accelerated by a pair of electrodes towards a phosphor screen, while the electrons are swept towards a micro-channel plate (MCP) and amplified. The phosphor screen converts the electrons back into light and the optical image is produced. Finally, the attached digital CCD camera (C4742-95-12ER) reads the image from the phosphor screen and displays it.

We export the streak images from the camera software (Hamamatsu, HPD-TA 6.4) as data files DAT. We use the OriginPro software to analyse the measurement. The files are then converted into a $512 \times 512$ matrix by setting the dimensions with the values of the time and spectral limits of the image, which the software automatically interpolates using a constant step in both axis to set the spectral and time coordinates of every pixel element of the matrix -. However, the pixels are not equally spaced on the time axis, so we have to correct the shift with respect to the linear interpolation, within the time range of interest. Figure 3.5 shows the non-linearity of the steps displaying the difference between the real points of the time axis and the ones obtained using a constant step, as a function of the real time values of the elements of the matrix.

The time shift due to the non-linearity of the time steps can reach up to 0.022 ns in the operating time window. Nevertheless, the temporal range of interest when

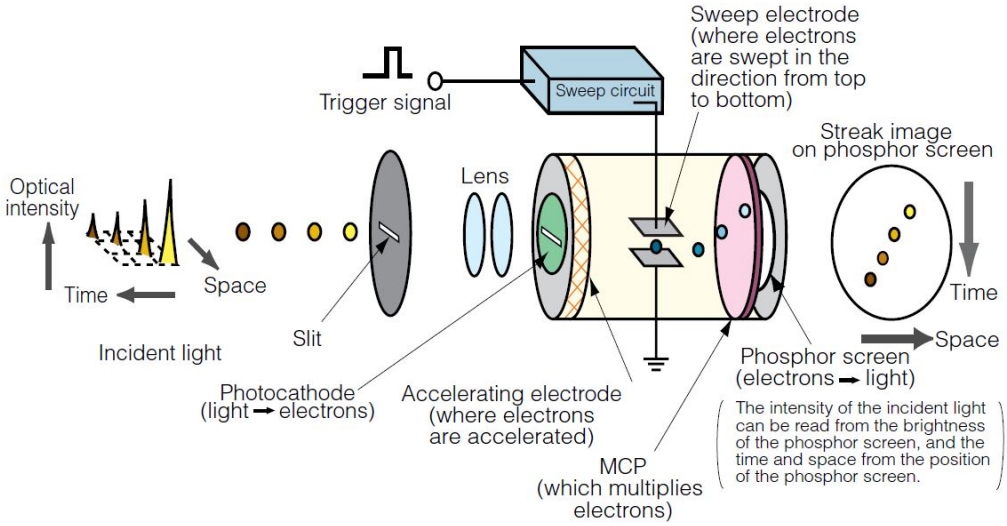


**Figure 3.4:** Operating principle of the streak camera. (Image from Hamamatsu)

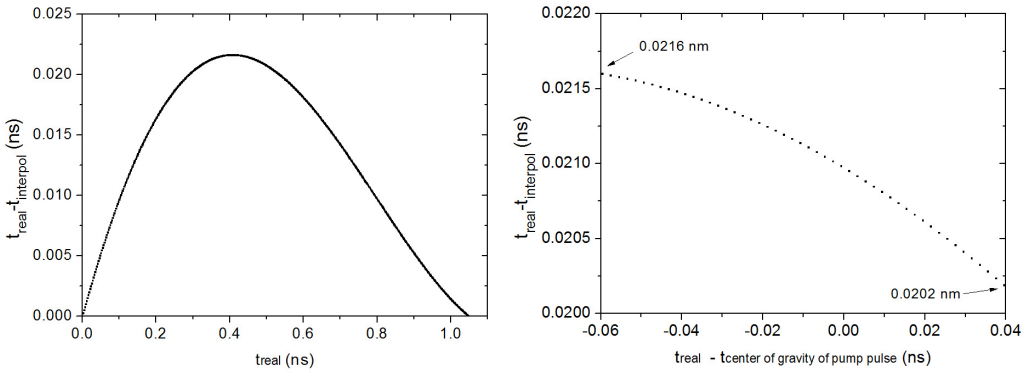


**Figure 3.5:** Difference between the real and interpolated times plotted as a function of the real image time values (left) and time difference in the time range of interest (right).

analysing the emission, at around 0.49 ns, is 0.01 ns wide 3.5 (right). Within that time range, the time difference caused by the interpolation is 1.4 ps, within our time resolution of 2 ps, and has a value of 0.021 ns. Hence, we can assume that within the examined time range, $\Delta t = 0.021$ ns. The difference between the real wavelength values and those obtained from the interpolation are also explored and not significant effect is found.

The streak camera has different data acquisition modes. The live mode allows viewing the streak image in real-time, which is very useful for aligning and setting the measuring parameters. As the system is synchronized with the pumping laser, we can either acquire individual shots or accumulate them.

On the other hand, the photon counting mode let us perform photon counting measurements. The use of this mode is limited to extremely weak signals. In order to avoid counting errors in the recorded image, the probability of a "two-photon event" – the probability that the photon spot areas of two photons overlap at the same image on the CCD being recognized as only one photon event – should be low. A good indication of this probability is the percentage of a previously selected region of interest (ROI) which exceeds the threshold. The smaller this percentage, the smaller is the probability that a new photon hits an already recorded one. This value should not exceed a few percent – 5 - 7 % – in the specified ROI. If the signal under study is not weak enough the "Warning: saturated pixels/photon #" appears. In this mode, both single shot and integration images are possible.

## 3.3 Mode selection and spatial filtering

In order to study the modal behaviour of our DRL it is necessary to develop a method which allows the spatial filtering of the sample emission. The random lasing emission in normal conditions is composed of many overlapped modes. Under conditions that minimise overlapping individual modes can be identified in the emission spectrum by the spikes We develop a method to differentiate between lasing modes using spatial filters.

The threshold of RL action, the energy density at which the pump required to overcome losses and the system starts lasing, is determined by the spectral collapse of the emission and the temporal shortening. For our experimental conditions the threshold is at around 1.6 µJ/pulse.

The spot size of the pumping beam on the surface of the sample is $\varnothing_{pump} = 500$ µm. The spatial filters control the size of the emission area selected for the analysis, reducing the amount of supported lasing modes. Once they are differentiated the dynamics and structure can be easily studied. Single shot images of both the pump and the emission are recorded with a streak camera. Three pinholes with apertures of 15 µm, 30 µm and 50 µm diameter are used at a single position. Images without a pinhole are also obtained. The pinholes are mounted on a translation stage, offering

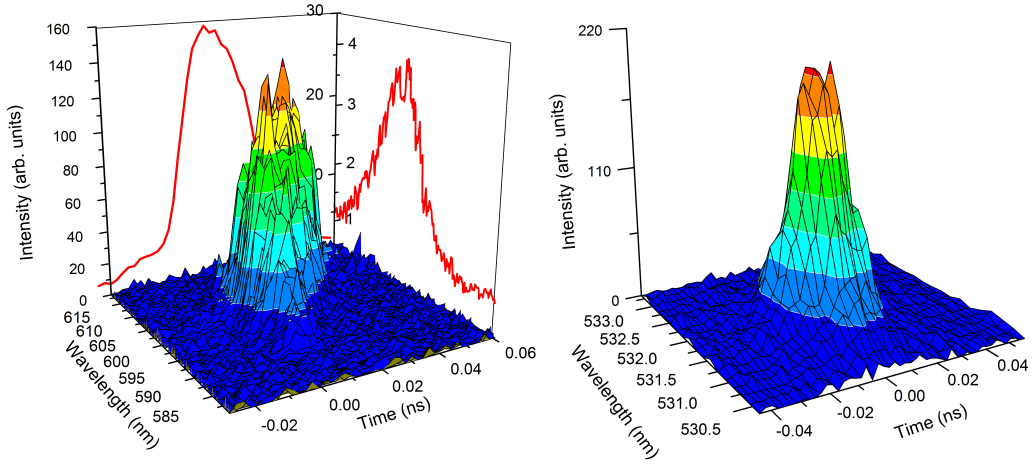


**Figure 3.6:** Surface map of the RL (left) and pump (right) pulses at 5.5 µJ/pulse detected without a pinhole. Spectral and temporal profiles are depicted in the XZ and YZ planes of the RL emission.

great flexibility to select the size and position of the studied emission area. The effect of the spatial filter size can be observed in the laser spike distribution.

A single image of the excitation pulse and the RL emission taken without any spatial filters is shown in figure 3.6. The barycentre of the pumping pulse serves as a time reference. The temporal profile and the spectral profile integrated in time of the emission are also presented, projected in the YZ and the XZ planes respectively. The spectrum exhibits a smooth band with a fine structure. Individual spikes of the lasing modes are spatially overlapped; the spacing between modes is smaller than their spectral widths, averaging the discrete lasing modes.

However, if spatial filtering is used as shown in figure 3.7 with a pinhole a finer structure appears in the RL emission. The temporal profiles become smoother as the size of the area which image at the pinhole is analysed increases, and the 3D map also shows a more uniform structure. Figures 3.7(b) and 3.7(c) show multiple individual spikes instead. On the other hand, the shape of all excitation pulses remains similar, which confirms the stability and monomode condition of the pump source.

Thanks to the spatial filters it is easier to observe spectrally separated lasing spikes. The linewidth of these sharp peaks is around 0.35 nm. It is clear from the temporal analysis of spikes uncoupled from mode competition that, for every pulse, they appear at different wavelengths and start at different times.

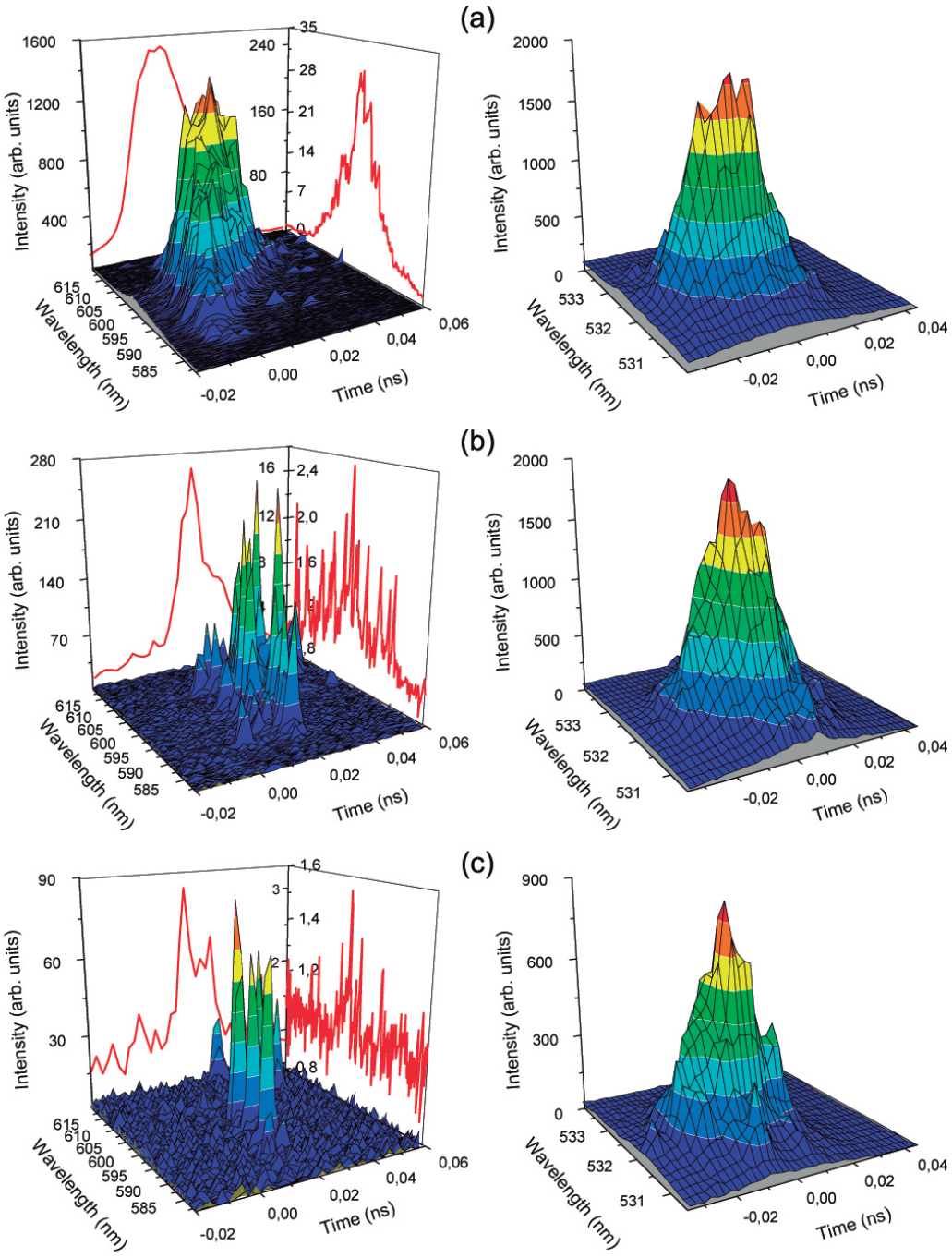


**Figure 3.7:** Surface map of the RL and pump pulses at 5.5 µJ/pulse with a $\varnothing_{pinhole}$ = 50 µm (a), $\varnothing_{pinhole}$ = 30 µm (b), $\varnothing_{pinhole}$ = 15 µm (c). Spectral and temporal profiles are depicted in the XZ and YZ planes of the RL emission.

## 3.4 Stochastic nature of the random laser emission in both spectral and temporal domains

The study of the spatiotemporal coherence of random lasing can provide some insight on the processes that contribute to the behaviour of these systems. The spatial coherence provides information about the phase difference of the wavefront of the radiation field. The emission of random lasers presents a low degree of spatial coherence due to the scattering the light suffers in the media and the uncorrelated and multiple modes that can simultaneously lase [93]. On the other hand, the temporal coherence of a radiation field is a measure of the correlation of the wave's phase along the direction of propagation. The temporal coherence can be determined by the probability distribution of photon counts, by analysing the photon statistics to see whether the distribution follows a Poisson or a Bose-Einstein distribution, as explained in chapter 1. We discuss the coherence nature of the random laser emission of the sample from the statistics of the light emission within a rather small sample window.

Several shots have been taken and analysed to explore the origin of some of the particularities of the spikes. Due to the static configuration of the studied sample and the constant experimental conditions, different shots can give us some insights into the nature of the spikes. Figure 3.8 shows some shots taken from the same sequence of those of figure 3.7 with the three different spatial filters. The spikes change their frequency from one excitation pulse to another and no frequency dominates the others. The emission peaks in the shots of 3.7 appear at different wavelengths to the ones of 3.8 whereas the excitation pulses show no significant variations between shots. Therefore, these fluctuations are neither caused by instabilities in the pump, nor dependent on the spatial distribution of the dielectric constant, but are an intrinsic characteristic of the random lasing itself.

These measurements not only reveal the sample lases in different modes for every excitation pulse but also the temporal behaviour of these modes. In order to explore the modal oscillation dynamics and modal structure of discrete lasing spikes, we extract (see figure 3.9) temporal profiles from several streak camera images by placing vertical sampling windows with a spectral width of 0.5 nm in the spectral range between 594 nm and 610 nm. One can here more clearly observe that lasing spikes appear at different wavelengths and start at different times in both cases. This evidences again the chaotic RL behaviour previously mentioned. On the other hand, it is also clear that laser modes at larger wavelengths start later. In addition, we estimate that at those wavelengths where more than one discrete peak is observed, the temporal delay between them is around 8 - 22 ps whereas their FWHM is between 4 - 8 ps.

We observe the same effect with a greater laser beam focusing of $\varnothing_{pump} = 50\,\mu m$. The threshold is at 0.6 µJ/pulse under this conditions. Reducing the pump beam diameter on the sample the number of overlapping modes decreases and therefore so does the spike density. In figure 3.10 two emission pulses, one without pinhole

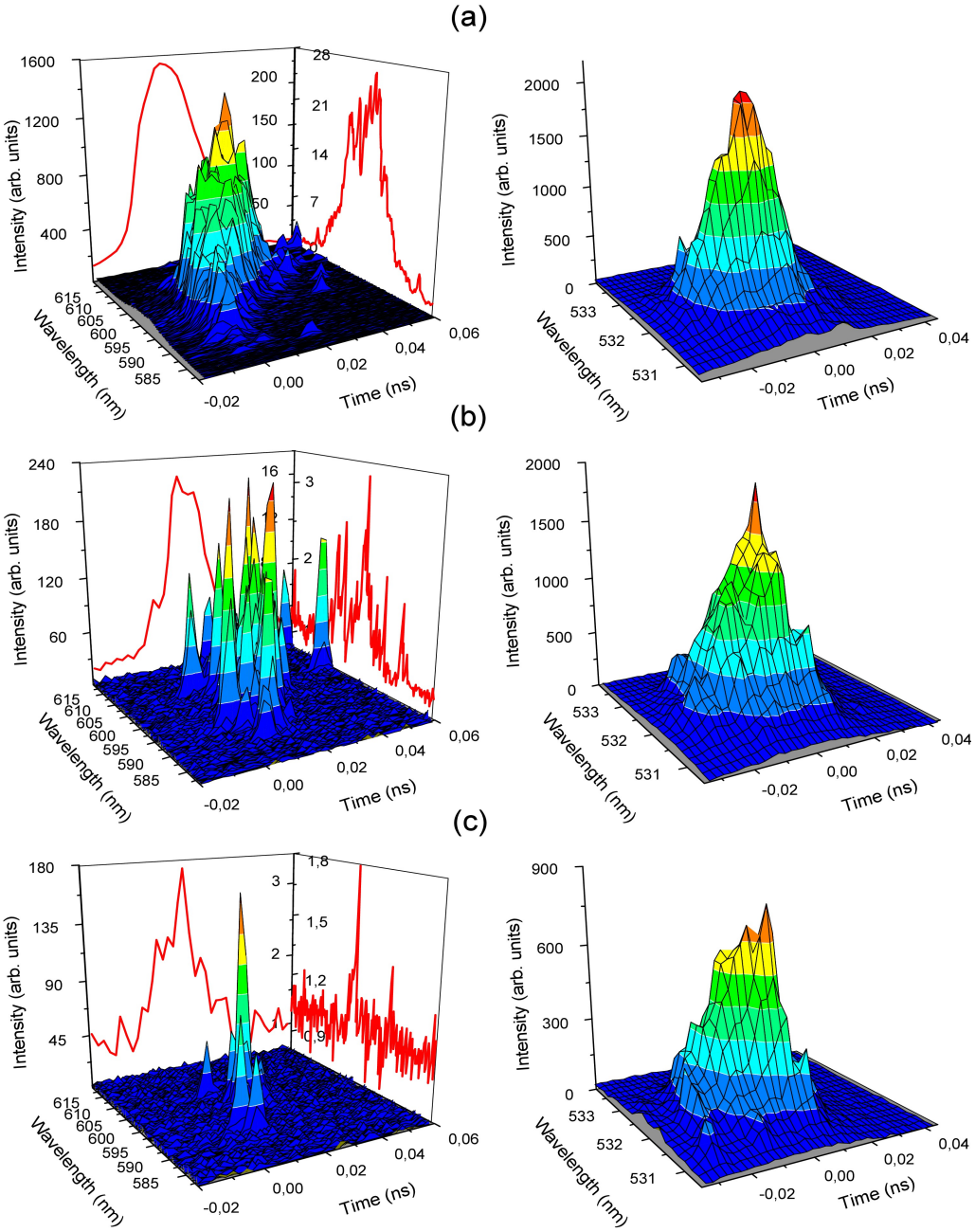


**Figure 3.8:** Surface map of the RL and pump pulses at 5.5 µJ/pulse with a $\varnothing_{pinhole}$ = 50 µJ/pulse (a), $\varnothing_{pinhole}$ = 30 µJ/pulse (b), $\varnothing_{pinhole}$ = 15 µJ/pulse (c) at different shots than those of figure 3.7. Spectral and temporal profiles are depicted in the XZ and YZ planes of the RL emission. [121]

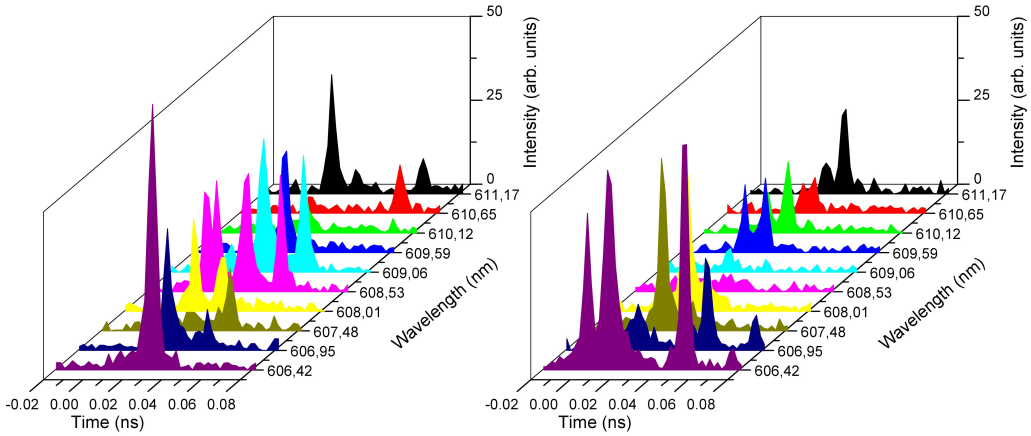


**Figure 3.9:** RL modes series of two different shots at 5.5 µJ/pulse with a $\varnothing_{pinhole}$ = 30 µJ/pulse.[121]

and another of a filtered area of 15 µm are displayed. As seen in 3.3, measuring the radiation without a spatial filter the modes overlap and the spectrum shows a narrowed emission band with almost no individual spikes. Since we are measuring the radiation from an area close to the coherence area, we can assume a high degree of spatial coherence.

### 3.4.1 Photon statistics

Photon statistics provides information on the temporal coherence of a light source. The experimental set-up for the the coherence analysis is an adaptation of the one described in section 3.3. This time we choose the small pinhole ($\varnothing_{pinhole}$ = 15 µm) - with an aperture close to the transport length -, a much smaller excitation spot of 50 µm and the photon counting mode of the streak camera. The spatial filter allows to collect the emission of a portion of the emitting area, providing a high spatial coherence, which is necessary to measure the temporal coherence, and also a small intensity of the light signal, necessary to verify the photon counting condition (see 3.2). We perform the measurements at 3 µJ/pulse above the 0.6 µJ/pulse threshold, focusing conditions $\varnothing_{pump}$ = 50 µm and within small time and wavelength intervals to determine the photon-number probability distribution and the second-order correlation coefficient. By doing so, the number of measured modes as well as the time interval are decreased as much as possible. The analysed time interval is smaller than the relaxation oscillation periods ($t_{rel.osc.}$ = 8 - 38 ps). For every analysed window, we make a photon number histogram and photon probability distribution, and fit the distribution to a linear combination of a coherent and a non-coherent emission function to measure the degree of coherence. We repeat the measurement moving the analysed window in time and wavelength to explore the coherence dependence on time and wavelength. The normalised second-order correlation coefficient, $g^{(2)}(\tau)$, is also calculated to characterise the coherence properties.

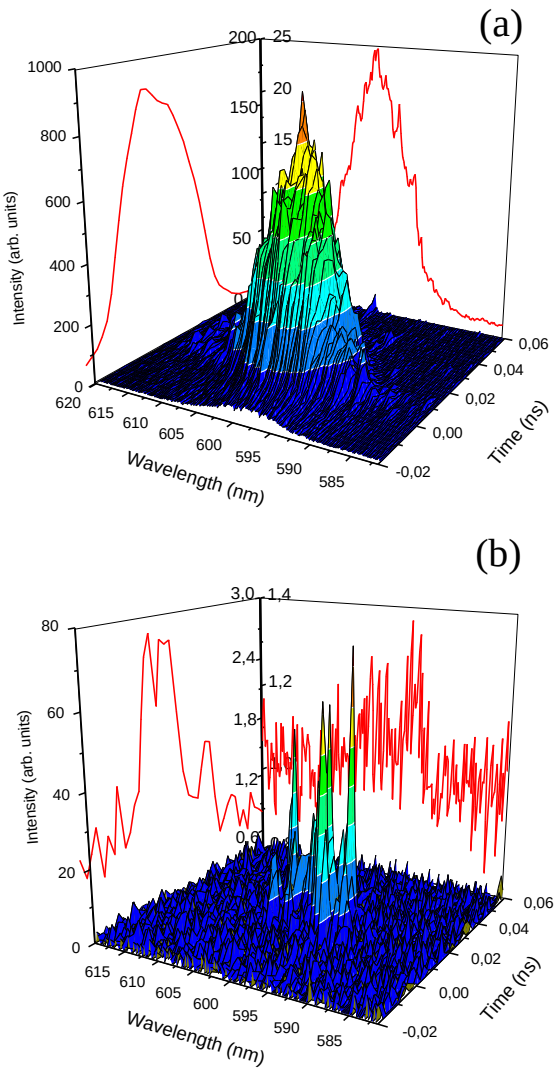


**Figure 3.10:** Surface map of the RL emission pulses without pinhole (a) and with a $\varnothing_{pinhole} = 15$ µm (b) with a pumping spot size $\varnothing_{pump} = 50$ µm.

The photon-number distribution, $P(n)$ of single-mode radiation with constant intensity follows a Poisson distribution if it is coherent and a Bose-Einstein distribution if it is chaotic [122].

$$P(n) = \frac{\langle n\rangle^n exp(-\langle n\rangle)}{n!} \quad \text{Poisson distribution} \tag{3.1}$$

$$P(n) = \frac{\langle n\rangle^n}{[1+\langle n\rangle]^{n+1}} \quad \text{Bose-Einstein distribution} \tag{3.2}$$

where $\langle n\rangle = \sum nP(n)$ is the average photon number.

The measured time interval must be smaller than the coherence time of the source, $\tau < \tau_c$, to guarantee a single-mode electric field within the time interval. The coherence time, which is the inverse of the bandwidth, can be determined by observing the characteristic fluctuation time of the signal. In chaotic light, the photon flux is not constant due to fluctuations in the intensity of the light on time scales of the order of the coherence time.

We estimate the coherent and incoherent components of the emission by fitting the probability distribution of photons to the linear combination of the Poisson and Bose-Einstein distributions:

$$P(n) = \alpha\frac{\langle n\rangle^n exp(-\langle n\rangle)}{n!} + (1-\alpha)\frac{\langle n\rangle^n}{[1+\langle n\rangle]^{n+1}} \tag{3.3}$$

The average photon number $\langle n\rangle = \sum nP(n)$ is first obtained from the measured data. The $\alpha$ corresponds to the weight of the coherent component.

In addition, we have calculated the value of the second-order correlation coefficient, $g^{(2)}(0)$, for the measured photon count distributions. For a spatially coherent – monochromatic – source $g^{(2)}(\tau) = 1$ for all $\tau$. For an incoherent source $g^{(2)}(0)$ depends on $\tau$; $g^{(2)}(0) = 2$ for small $\tau$ and decreasing $g^{(2)}(0) = 1$ for $\tau > \tau_c$. In our configuration the fluctuations of the optical intensities at times $t$ and $\tau$ are correlated. For a single mode field and a zero time delay $\tau = 0$ [123]:

$$g^{(2)}(0) = 1 + \frac{\langle(\Delta n)^2\rangle - \langle n\rangle}{\langle n\rangle^n} \tag{3.4}$$

so,

$$g^{(2)}(0) = 1 + \frac{[\Sigma n^2P(n) - (\Sigma n^2P(n))^2 - \Sigma nP(n)]}{(\Sigma n^2P(n))^2} = \frac{\Sigma n^2P(n) - \Sigma nP(n)]}{(\Sigma n^2P(n))^2} \tag{3.5}$$

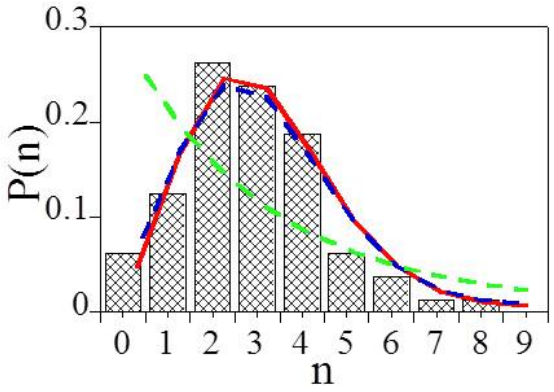


**Figure 3.11:** Photon number distribution of the pump laser at the time of maximum intensity together with the best fit to equation 3.3 (solid red line). Dashed blue and green lines represent the Poisson and the Bose-Einstein distributions for the measured count mean. [124]

In order to test the reliability of the procedure we measure the photon statistics of the coherent pump laser. The sampled window has a width $\Delta\lambda = 0.9$ nm and time $\Delta t = 32.8$ ps. The measured photon count probability centred at the barycentre is displayed in the histogram of figure 3.11.

The green line shows the Poisson distribution for the same count mean, the blue line the one of the Bose-Einstein distribution and the solid red line the fitting to the linear combination of a Poisson and a Bose-Einstein function (equation 3.3). The weight of the poissonian - coherent - contribution to the best fit is 1.08. We evaluate the normalized second-order correlation coefficient with the values of $P(n)$ and we get a $g^{(2)}(0) = 0.97$. Both the $g^{(2)}(0)$ and the photon-number distribution indicate the pump radiation source emits a coherent radiation.

Once we have checked the reliability of the procedure we proceed with the analysis of the coherence of the RL emission collecting 5000 exposures. The same width of the window is used ($\Delta t = 32.8ps$, $\Delta\lambda = 0.9nm$) – the relaxation oscillations are between 8 and 38 ps –. The complete streak images measure both the emission and the pump to set the pump barycentre as a time reference for the emission for every shot. Figure 3.12 shows the histograms of the photon distribution of the RL emission at two different times, 1.2 ps and 27.9 ps. The emission at a short delay, 1.2 ps, is temporally coherent, while the one at a longer delay, 27.9 ps, is incoherent.

We also explore the coherence properties as a function of time and wavelength. Figure 3.13 shows the regions examined to study the distributions and the corresponding coherence percentage $\alpha$, and the normalized second-order coefficient, $g^{(2)}(0)$.

The results of the coherence parameters in function of the time and centred at 601.2 nm is depicted in figure 3.14. The coherent contribution (red) decreases at times more distant to the pump barycentre, while the correlation coefficient (blue)

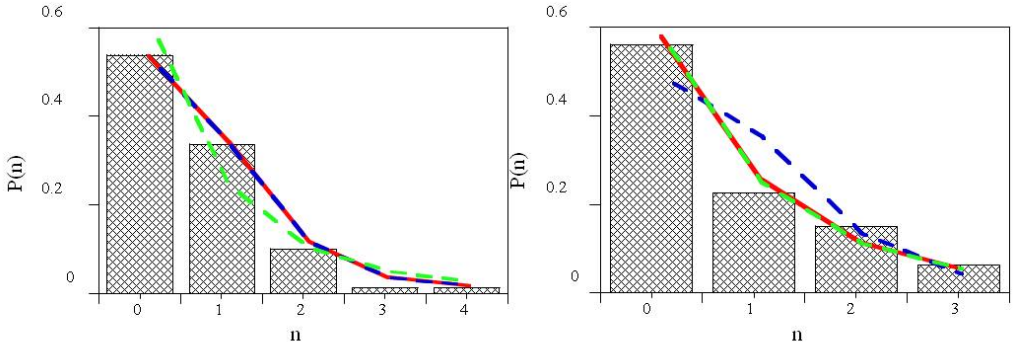


**Figure 3.12:** Photon count probability distributions of the RL emission at 1.2 ps (a) and 27.9 ps (b) time delays. Solid red lines represent the best fits to equation 3.3. Dashed blue and green lines correspond to the Poisson and Bose-Einstein distributions for the measured count mean. The best fit line at 1.2 ps in (a) is superimposed on the Poisson distribution (blue line) whereas at 27.9 ps (b) it matches the Bose-Einstein distribution (green line) [124]

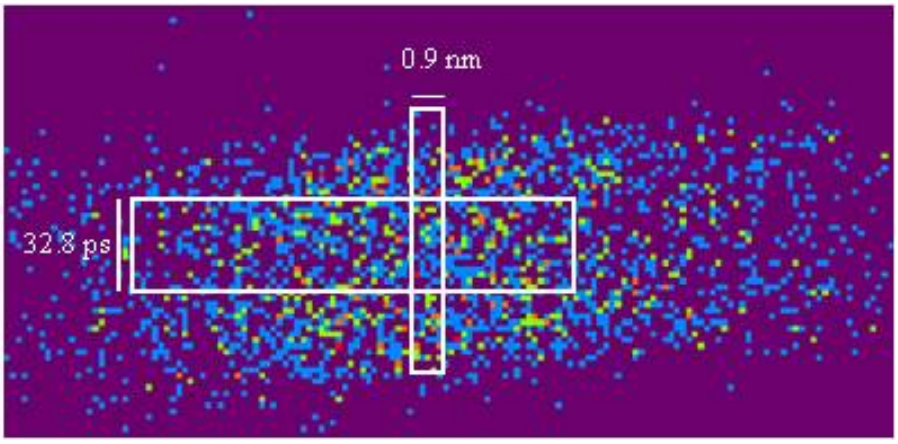


**Figure 3.13:** Streak image of the RL emission of the powder sample under 3 µJ/pulse pumping. The vertical and horizontal white rectangles represent the regions under examination when the coherence properties of the RL emission are explored as a function of the delay time and wavelength, respectively. The vertical rectangle is centered at 601.3 nm whereas the horizontal one is centered at a 1.2 ps delay time. [124]

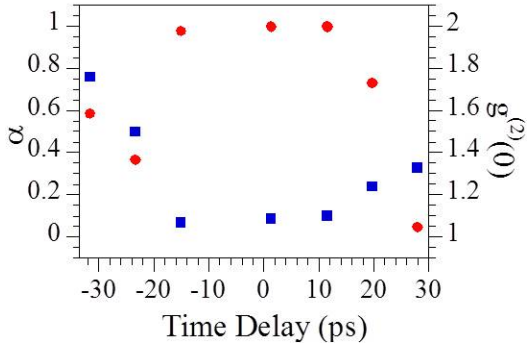


**Figure 3.14:** Dependence of the coherent percentage $\alpha$ (red dots) and of the coefficient $g^2(0)$ (blue squares) on the time delay, obtained by using $\Delta\lambda = 0.9$ nm and $\Delta\lambda = 32.8$ ps from the RL emission shown in figure 3.13. The time origin was set at the excitation pulse center. [124]

increases. The coherent component of the emission is the main contribution in a time range of about 40 ps. On figure 3.15 the parameters at 1.2 ps delay time is shown, from 597 nm to 611 nm. The photon statistics reveal a Poisson distribution of the photon number and hence, the coherent nature of the RL emission.

## 3.5 Influence of pump pulse energy on the modal distribution

Single shot images at different pumping energies, all above threshold, are recorded with the spatial filters. The changes in the modal density and distribution, and the build-up time, the time interval between the peak of the pumping and that of the RL pulse, are studied. To explore the change of the RL build-up time, we record an image sequence of 10 shots with the 50 µm pinhole and measure the delay between the centre of gravity of the pumping pulse and the one of the RL emission. The sequences are performed at different energies: 5.5 µJ/pulse, 27 µJ/pulse, 40 µJ/pulse, 65 µJ/pulse and 83 µJ/pulse. Averaging the time delays at each energy we get the following delays:

| $E_{pump}$ (µJ/pulse) | Delay (ps) |
|---|---|
| 5.5 | 9.9 |
| 27 | 12 |
| 40 | 13 |
| 65 | 11 |
| 83 | 12 |

These time delays show no significant change within our time resolution (2ps); a constant RL build-up time around 12 ps is observed at all excitation energies.

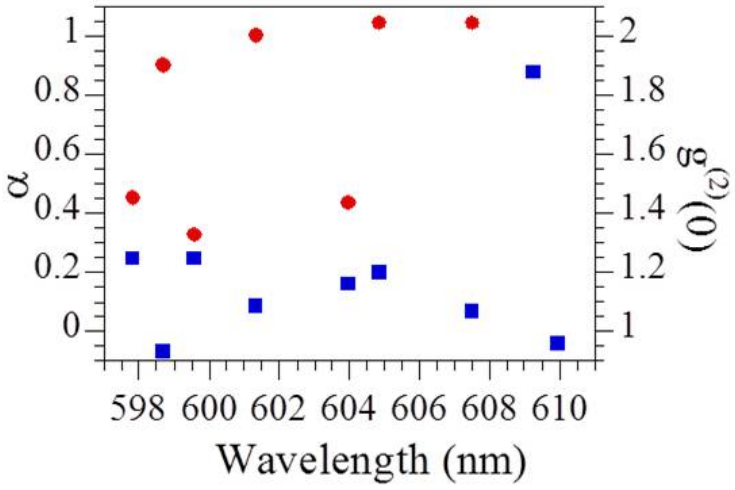


**Figure 3.15:** Dependence of the coherent percentage $\alpha$ (red dots) and of the coefficient $g^2(0)$" (blue squares) on the wavelength, obtained by using $\Delta\lambda = 0.9$ nm and $\Delta\lambda = 32.8$ ps from the RL emission shown in figure 3.13. [124]

Another sequence of shots is obtained with the 30 µm pinhole to analyse the modal oscillation dynamics. As shown in figure 3.16, the distribution of spikes in the emission changes in wavelength and in time from shot to shot, although, as we have seen in section 3.3, the pump is stable. Along with the increase in pump energy, the emission suffers several modifications: the intensity of the spikes is typically higher and more modes are activated, because the increase in the excitation energy increases the number of available laser modes, i.e. it allows the creation of lasing modes with higher thresholds.

## 3.6 Pump versus emission surface areas: The dominant role of diffusion

In this section we examine the spatial features of the RL emission. To this end, we take, for pumped areas of different sizes, images of the sample surface with a CCD analyzer. The radiation is collected with a lens, and after filtering the pumping or the emission wavelengths, projected onto the CCD with a lateral magnification of one. This way, we can obtain a map of the intensity distribution of the pumped and emitting areas. Figure 3.17 shows the images taken with the CCD device, above and below threshold.

Upper images display the emitting surface at 0.2 µJ/pulse, below threshold, and below are the images above threshold, at 10 µJ/pulse. Images on the left are images of the pumping radiation at 532 nm and on the right the emitting area is shown. The widths at 37 % of maximal intensity of the beams presented in the figure are:

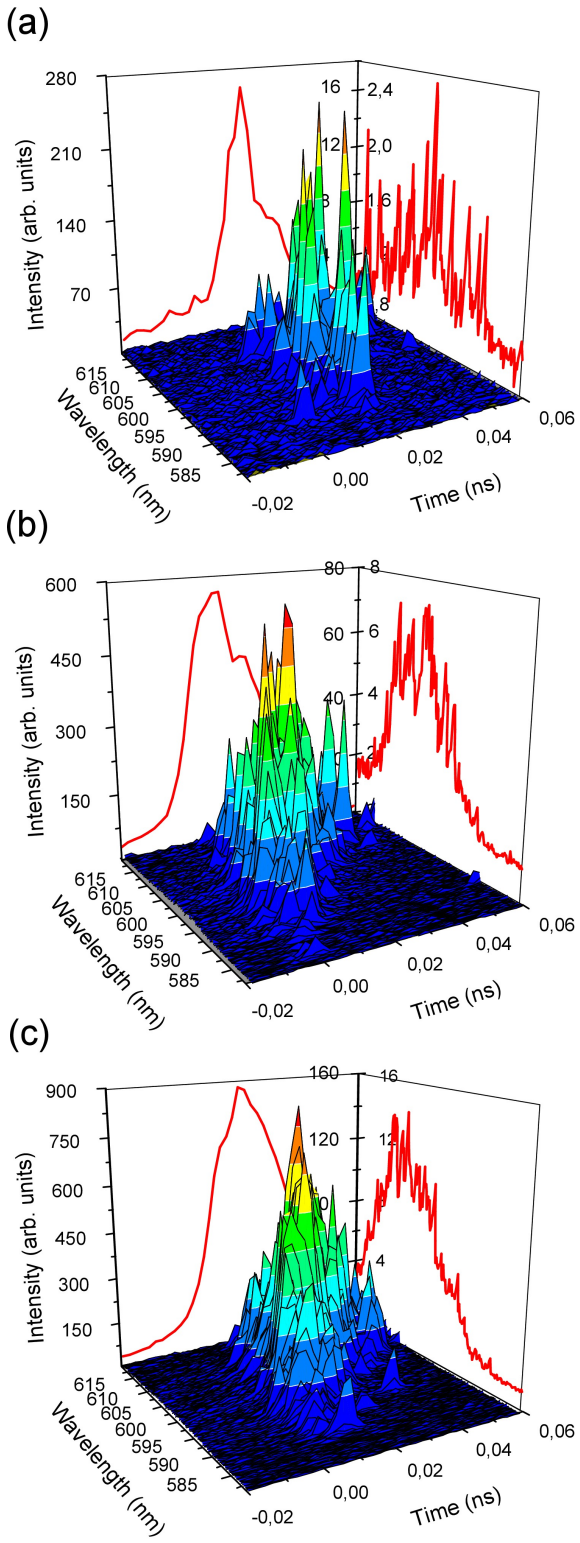


**Figure 3.16:** RL pulse measured with a $\varnothing_{pinhole}$ = 30 µm at 5.5 µJ/pulse (a), 27 µJ/pulse (b), and 83 µJ/pulse (c). Spectral and temporal profiles extracted over the whole images are presented in the XZ and YZ planes of the figures. [121]

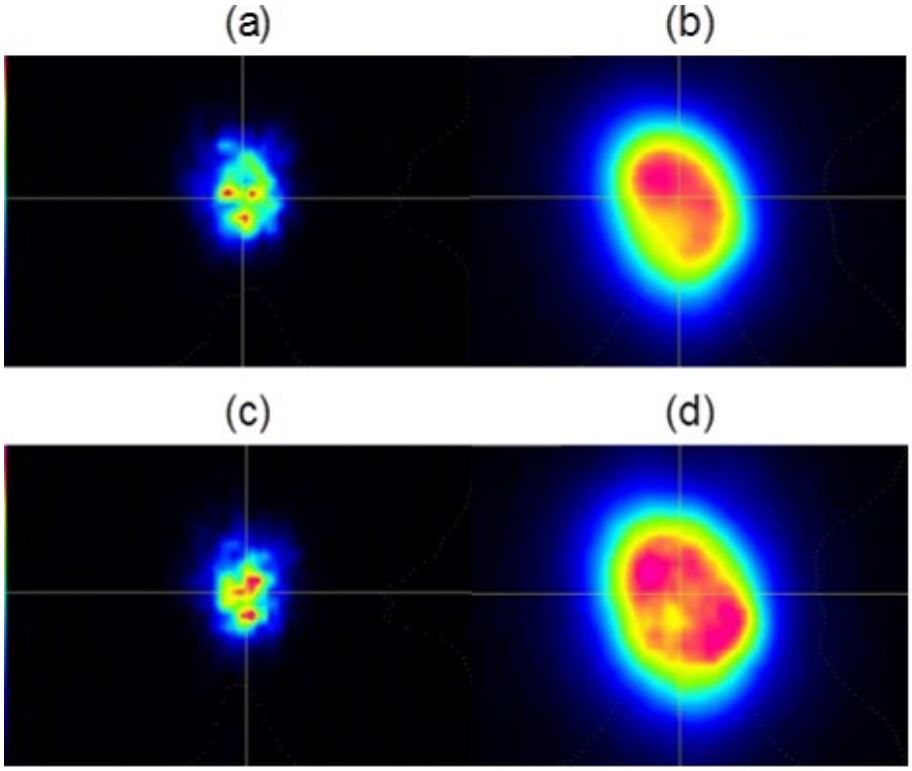


**Figure 3.17:** Images of the emitting surface of the RhB doped di-ureasil powder pumped at 0.2 µJ/pulse(upper) and 10 µJ/pulse (down), i.e. below and above RL threshold, respectively. The left hand images (a, c) are images of the pumped area, since sample emission has been removed by filtering. Those to the right (b, d) are images of the emission area, since the reflected or re-emitted pumping has been removed by filtering. Widths of beams at 37% of maximal intensity are: a) 126 × 137 µm, b) 264 × 294 µm, c) 105 × 132 µm and d) 301 × 329 µm. [121]

a) 126 x 137 µm, b) 264 x 294 µm, c) 105 x 132 µm, d) 301 x 329 µm. At both energies we observe the same effect, the emitted light extends over a larger region than the pumped area, which evidences the dominant role of diffusion processes over amplification or spontaneous emission in the powder.

## 3.7 Summary and conclusions

This work provides a unique spectro-temporal insight into the modal dynamics of a diffusive random laser based on a solid-state disordered gain medium, rarely addressed in the literature. Most researchers investigate the steady-state properties for the sake of simplicity, but for a full understanding of the intricate behaviour and mode competition of these disordered active media, it is essential to shed light on this fundamental issue.

First of all, we have developed a spatial filtering method that allows to study the dynamics of individual modes of a DRL, in particular, of a Rhodamine B doped di-ureasil hybrid ground powder. We have observed that the pumping energy and size of emitting area change the structure of the RL emission as they can increase mode coupling. When the size of the emitting area changes we observe several effects on the modal behaviour of the emission. The reduction of the spatial filter aperture used to control the size of the detected emitting surface area, reduces the number of spatially overlapping random laser modes while maintaining the size of the gain medium. This enables the observation of discrete lasing spikes originated from non overlapping cavities. If no pinhole is used, the number of supported lasing modes is so large that the fine structure of the emission line shape is partially washed out, resembling the smooth emission profile of a diffusive random laser. On the other hand, decreasing the pump beam diameter reduces the spike density, and an enhancement of the modal density appears with the intensification of the excitation energy as the creation of lasing modes with larger thresholds becomes then permitted. No mode suppression within our pumping energy range is observed.

Image sequences of several pumping shots recorded under the same experimental conditions unambiguously show an intrinsically stochastic behaviour not only in the spectral but also in the temporal response of the random lasing of our sample with static disorder. The spectral position of spikes, which is thus not related to the realization of disorder, differs individually from shot-to-shot although almost no pulse-to-pulse variation of the pumping pulse occurs. This gives direct experimental evidence of how the system lases in different modes in successive excitation events. Note that our results agree with some previous experimental works where time-integrated data are recorded but are not in accordance with the behaviour predicted by the time-independent constant-flux theory where uniformly spaced frequency spectra are expected. Moreover, the comparison of time traces extracted at the same spectral position reveals that lasing modes are turned on at different times in different shots, which suggests they are from different cavities. We have measured a

constant build-up time of 12 ps between 5.5 and 83 µJ/pulse. The average FWHM of the temporal profiles of uncoupled lasing modes is around 6 ps, with relaxation oscillation periods in the range of 8 - 38 ps.

Imaging results show the dominance of diffusion over amplification processes on the spatial features of the powder random laser emission. The emitted light is extended over a larger area than the pump domain, so contrarily to what some authors assert, no spatial restriction of the random laser modes to the excited region is found in our case.

We have also been able to control the spatial coherence by limiting the detected region on the explored sample surface to nearly the spatial coherence area of its laser-like emission using a spatial filter with an aperture close to the transport length of the sample. We have performed single photon counting measurements above threshold, and assessed the photon probability distributions obtained within a wavelength interval $\Delta\lambda = 0.9$ nm and sampling windows $\Delta t = 32.8$ ps. Account taken of the relaxation oscillation periods, just few lasing modes might thus be supported which is a crucial requirement to evaluate the coherent nature of a light beam from its photon statistics. The dependence of the photon statistics on time delay and wavelength shows values of the coherent percentage and of the second-order correlation coefficient close to 1, both at the time of maximum pump intensity and around the gain maximum of the Rhodamine B dye in the employed hybrid host. This result is an experimental evidence of the high degree of temporal coherence that can be achieved in our DRL.

# Chapter 4

# Spectrotemporal dynamics of RhB-dU random laser under two photon pumping

## 4.1 Introduction

We now explore the spectral dynamics of the Rhodamine B doped di-ureasil host under two-photon excitation. The two-photon excitation, at 1064 nm, requires, as other multi-photon excitations, no phase matching, and provides an anti-Stokes visible emission in the explored powder. The main interest of this process relies on the advantages of NIR for the RLs applications in bio sensing and medical diagnostic purposes [6, 24, 88], as we have presented in chapter 1. Light has its maximum of tissue penetration depth on the NIR, which increases the excited volume and allows working with thicker biological samples. Organic dyes, which can be compatible with the biological material and have a large two-photon absorption coefficient, are therefore interesting dopants of RLs for these applications. The OP absorption cross-section (OPA) of RhB is $\sigma_{OPA} = 2.4 \times 10^{-16}$ cm$^2$ [125]. Under two-photon (TP) excitation either an excited molecule absorbs additional photons or the molecule absorbs several al the same time. The TP absorption cross-section (TPA) in methanol is $\sigma_{TPA} = 31 \times 10^{-48}$ cm$^2$s/photon [126]. Due to the lower absorption of the radiation by the molecule under TP pumping, light can penetrate deeper into the material and the excited volume is higher.

Using the same sample as for OP pumping analysis and the set-up described in chapter 3 with small adaptations and the spatial filtering method, we have characterises the sample RL emission features and its modal dynamics and compare them to the ones obtained under one-photon pumping.

In addition, images obtained in the multiphoton microscope pumping at 840 nm are analysed. At this wavelength, the RhB has the largest two-photon absorp-

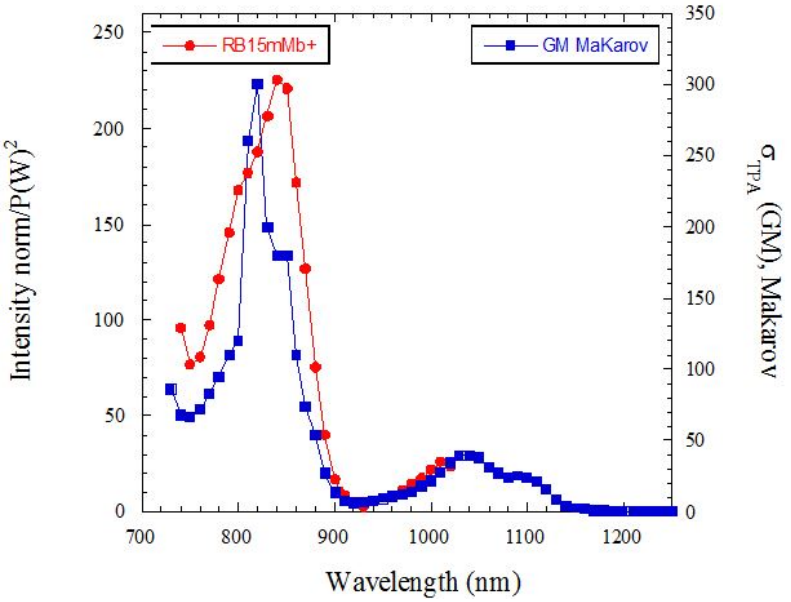


**Figure 4.1:** Two-photon excitation spectra of the RB15Mb+ powder sample monitoring the RhB at 600 nm.

tion (TPA) cross-section within the tuning range of the Ti:sapphire. Figure 4.1 shows the two-photon excitation spectra (TPE) of a less concentrated powder sample denoted by RB15mMb+ ($6.31 \times 10^{18}$ RhBmolecules/cm$^3$, whereas our sample has $12.3 \times 10^{18}$ RhBmolecules/cm$^3$). In this figure the absolute TPA cross-section of the RhB dye given by Makarov et al. [126] is also presented. As can be observed, a good agreement with literature in observed.

## 4.2 Experimental

Subnanosecond time-resolved measurements performed under two-photon excitation are carried out at room temperature using the experimental set-up shown in figure 4.2. The sample is pumped at 1064 nm, the fundamental wavelength of a mode locked Nd:YAG laser (PL2250 EKSPLA). The pump pulse has a duration of 30 ps and a repetition rate of 20 Hz. The laser output is attenuated with a half-wave plate and a polariser. The polariser is also employed as a beam splitter as the laser beam coming out at 90° is reflected to an optical delay line to provide a time reference signal.

Due to dispersion of our imaging spectrograph grating, the maximum width of the sampling windows of 87 nm. This prevents us from taking a reflection of the laser pump as a time reference for the RL emission when working at TP excitation. In order to obtain a time reference, we work this time with the second harmonic emission of a potassium dihydrogen phosphate – KDP – compacted powder sample.

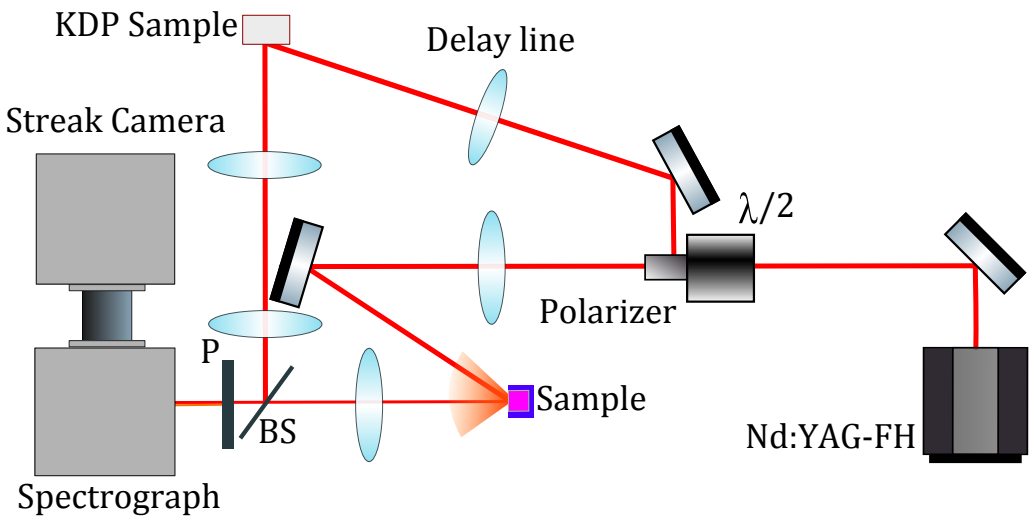


**Figure 4.2:** Set-up for the two-photon pumping analysis. BS is a beam-splitter and P a pinhole.

TP pumped RL emission of the explored sample is centred at 630 nm while the second harmonic emission pulse of the KDP appears at 532 nm. This way, both the sample signal and the delay line signal – used as a time reference – can be simultaneously detected in single shot measurements. We assume there is no delay on the second harmonic generation.

With the purpose of checking the equal lengths of the reference line and the sample path, we place one KDP sample at the delay line and the other one at the explored sample position. As can be seen in the optical delay path of figure 4.2, we use two additional lenses after the laser beam is focused on the KDP surface in order to collect its second harmonic emission. By changing the position of this sample while detecting within the same shot in real time the second harmonic emission of the two KDP samples, it is possible to reduce until zero the delay time between both signals and therefore assert that lengths of both paths are identical. After this alignment, we place the sample under study in a vertical holder so the surface can receive the pump radiation. Then, a short-pass filter (Semrock FF01-842) removes the pumping light diffusively reflected by the sample and the KDP. We record several streak images using the 1 ns time range at different pumping energies with different pinhole apertures.

The streak images display the measured time on the vertical axis and the wavelength on the horizontal axis. The streak camera software allows us to extract temporal profiles placing vertical sampling windows at the desired wavelength positions. Alternatively, by using horizontal windows, it is also possible to extract spectral profiles at various time positions and gate lengths. It is therefore a versatile tool to explore the build-up time of the TP pumped RL emission as well as to evaluate its modal oscillation dynamics, once the time reference is set at the center of gravity of the KDP second harmonic pulse coming from the optical delay line.

The transmitted laser beam is focused to a spot size of 500 µm on the sample surface in most of the measurements. Just for the study of the effect of the emitting surface area on the modal oscillation dynamics a tighter diameter of 50 µm of the pumped area is also used.

## 4.3 Two-photon pumped random laser thresholds and build-up times

A sequence of single shot streak images are recorded at different pumping energies above threshold with the aim of experimentally explore the change of the RL build-up time. No pinhole aperture is used in order to get intense signals, as the emission from the whole excited surface is collected. The pump beam is focused in the sample surface with a 500 µm diameter spot on the powder surface. Figures 4.3(a) and (b) show single shot streak images recorded pumping at 0.85 mJ/pulse and 1.5 mJ/pulse while figures 4.3(c) and (d) display the spectral and temporal profiles of the whole measurement range at both energies.

The images differ widely on time and wavelength. At both energies the emission is centred at 630 nm but while at 0.85 mJ/pulse the emission is spectrally broad, the emission linewidth is 15.6 nm at 1.5 mJ/pulse. The temporal domain also show significant differences. At 0.85 mJ/pulse the emissions presents an exponential decay with a lifetime value of 5.7 ns, which evidences the main contribution of the fluorescence to the emission. On the other hand, at 1.5 mJ/pulse the output pulse duration shows a significant shortening until 147 ps. This behaviour corresponds to the one expected close to the onset of lasing. These experimental results reveal that 1.5 mJ/pulse exceeds slightly the onset of the TP pumped random lasing under the mentioned focusing conditions, so the anti-Stokes RL onset is between 0.85 mJ/pulse and 1.5 mJ/pulse.

Under OP pumping at 532 nm, the spontaneous emission is centred at 612 nm whereas the lifetime value is around 3.4 ns. The measured emission under TP excitation undergoes a redshift and an enlargement of the lifetime. This seems to indicate a larger contribution of the re-absorption effect under TP excitation explained by the larger penetration depth of the NIR pump, and the longer propagation distances of the resulting fluorescence photons.

The same explored RhB-dU system under OP pumping and with the experimental configuration shows (chapter 3) a threshold around 1.6 µJ/pulse, i.e. three orders of magnitude lower. This behaviour is explained by the lower absorption of the dye under this two-photon pumping (section 4.1).

In order to study the RL build-up time, it is important to remark again that the maximum spectral width of a streak image is 87 nm. As can be observed in figure 4.4, by centring the spectrograph at 578 nm, the green pulse appears at the

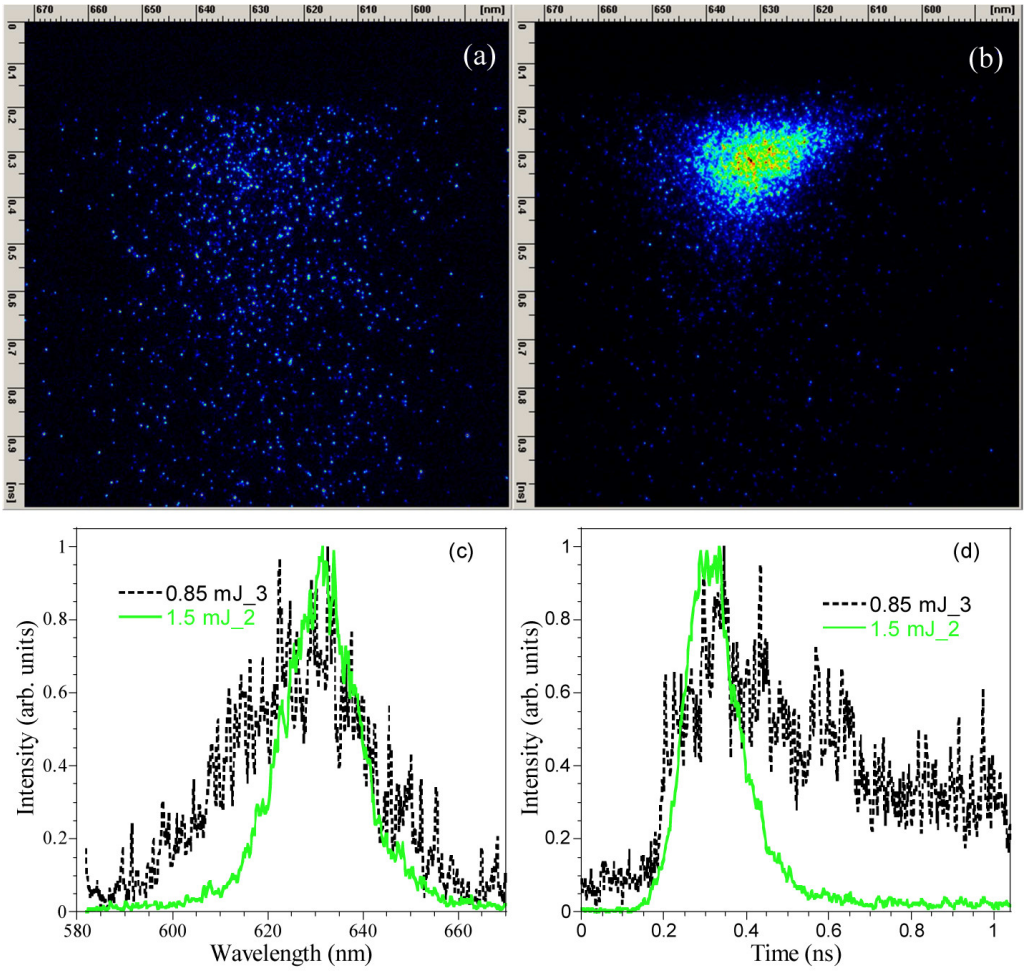


**Figure 4.3:** Anti-Stokes RL threshold: single shot images obtained at 0.85 mJ/pulse (a) and 1.5 mJ/pulse (b) with no spatial filtering. Spectral and temporal profiles of the whole measured range are displayed in the images (c) and (d) respectively. [127]

| $E_{exc}$ | $\Delta t_{Tail-Pump}$ | $\Delta t_{Tail-Sample}$ | $\Delta t_{Sample-Pump}$ |
|---|---|---|---|
| 1.5 mJ/pulse | 110 ps | 44 ps | 154 ps |
| 2.5 mJ/pulse | 88 ps | 28 ps | 116 ps |
| 3.2 mJ/pulse | 102 ps | 35 ps | 137 ps |
| 4.0 mJ/pulse | 99 ps | 28 ps | 127 ps |
| | 85 ps | 28 ps | 113 ps |

**Table 4.1:** Time delays between the centres of gravity of temporal profiles extracted within the mentioned spectral ranges centring the imaging spectrograph at 578 nm (second column) and at 630 nm (third column) at different excitation energies by focusing the laser beam to a spot size of 0.5 mm on the sample surface. Values shown in the fourth column correspond to the build-up time at each pump energy and result from the sum of the two previous column values. At 4 mJ/pulse, delay values obtained when the laser beam impinged on two different sample points are also given.

right image edge and just the short wavelength tail of the TP pumped RL emission of the di-ureasil powder sample can be simultaneously detected. It is therefore necessary to follow a two step procedure to estimate the time delay between the KDP green pulse and the TP pumped RL pulse at different excitation energies: 1.5, 2.5, 3.2 and 4 mJ/pulse after focusing the laser beam to a spot size of 500 µm on the powder surface. First of all, an image sequence of five pumping shots is recorded at each pumping energy with a sample window range of 1 ns by centring the imaging spectrograph at 578 nm as shown in figure 4.4a. Then, we estimate the time delay between the center of gravity of the temporal profiles extracted by using vertical sampling windows extended over the ranges [530.33 nm, 534.03 nm] and [612.5 nm, 620.25 nm] – corresponding to the second harmonic of the pump beam ("Pump"), and the tail of the TP pumped RL ("Tail") –, respectively. Average time delays between both profiles are collected in table 4.1. Secondly, we centre the Chromex spectrograph at 630 nm and record image sequences at the same excitation energies 4.4b. Afterwards, temporal profiles are extracted in both ranges; i.e. [612.5 nm, 620.25 nm]( "Tail") and the whole image spectral width, i.e. [581.83 nm, 671.76 nm] ("Sample"), see black and red lines in figure4.4(c)(d), respectively. In the third column of table 4.1, time delays between the center of gravity of both temporal profiles are presented. The resulting time intervals between the peak of the pumping or, in our case, of the corresponding second harmonic pulse, and that of the total RL pulse (defined as build-up time) are shown in the fourth column.

As mentioned above, for every energy we record 5 images of 5 pumping shots while the laser beam excites the same sample point. In table 4.1, average time delays are presented for each case. Note that no significant time differences were found within images of the same sequence (less than 5 ps). However, when changing the excitation energy, we have to change the place where the laser beam impings on the sample because the shock wave associated with the tight focused excitation removes powder from the sample surface. Therefore, different parts of the sample are explored as a function of pumping. Table 4.1 also shows the build-up times estimated for two different excited points at the same energy, i.e. at 4 mJ/pulse. Build-up times of 127 ps and 113 ps are obtained. As can be observed, the time difference between both values is larger in this case than when comparing shots

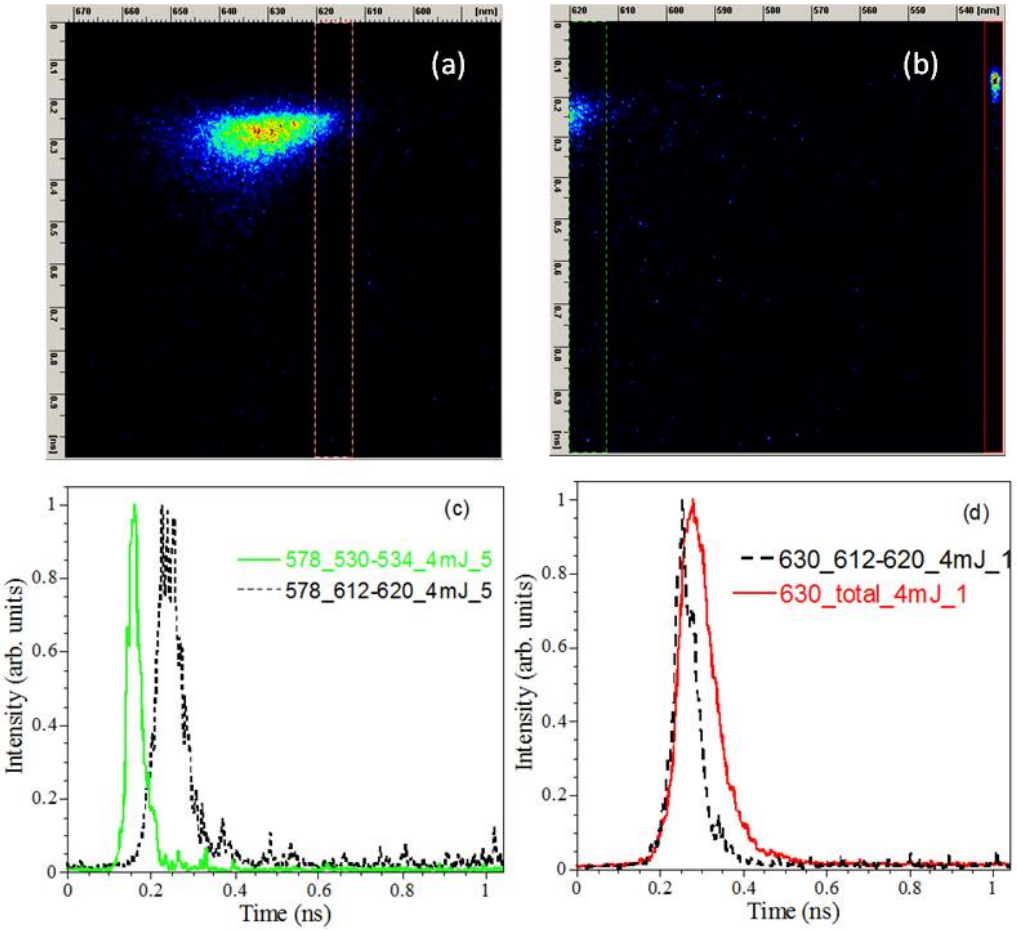


**Figure 4.4:** Single shot images and profiles at $E_{exc}$ = 4mJ/pulse with no pinhole aperture by focusing the laser beam to a spot size of 0.5 mm on the sample surface and centring the image spectrograph at 578 nm (a) and 630 nm (b). Vertical windows on the 612.62 - 620.25 nm spectral range depicted with dashed lines correspond to the tail of the TP pumped RL emission of the powder sample. Corresponding temporal profiles extracted from these sampling windows are plotted with a black dashed line in (c) and (d) respectively. The temporal profiles of the second harmonic emission of the KDP sample used as time reference (extracted from the vertical window centred at 532 nm in the upper image) as well as the temporal profile extracted over the whole spectral range of the lower image are also presented in (c) and (d) with green and a red line respectively.

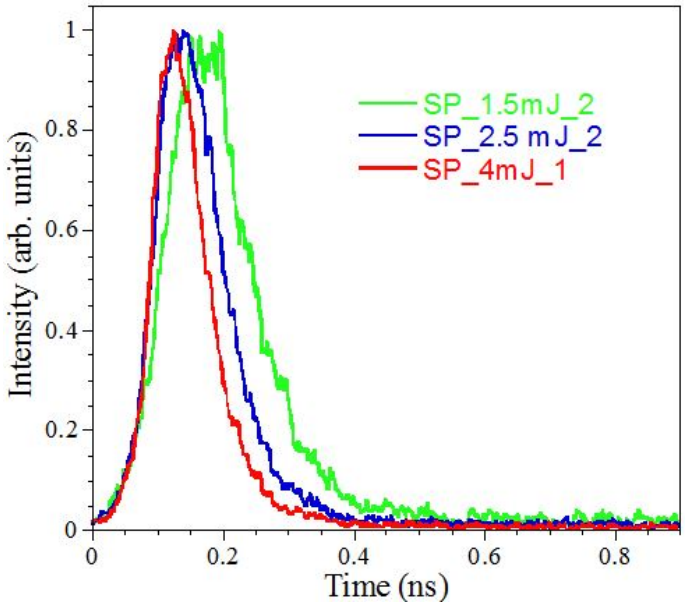


**Figure 4.5:** Temporal profiles extracted over the whole spectral range from streak images recorded at 1.5 mJ/pulse (green line), 2.5 mJ/pulse (blue line) and 4 mJ/pulse (red line) by focusing the laser beam to a spot size of 0.5 mm on the sample surface.

of the same sequence. The last value is the one we use to settle down the time origin at this energy. Time delay values collected in table 4.1 seem to indicate the expected decrease of the RL build-up time with the excitation energy. Note that apart from the build-up time reduction, figure 4.5 shows that the FWHM of the temporal profiles extracted over the whole spectral range is also reduced upon increasing energy, in particular from 147 ps at 1.5 mJ/pulse till 93 ps at 4 mJ/pulse. In this plot, the center of gravity of the KDP second harmonic pulse provides the time origin.

### 4.3.1 Comparison of one- and two- photon pumped random laser thresholds and build-up times

The study of the RL emission performed under the same experimental conditions but under OP pumping, i.e. at 532 nm, reveals that the RL threshold value pumping in the visible (VIS) range is around 1.6 µJ/pulse. Therefore, under this excitation scheme an almost 3 orders of magnitude smaller pump density is required to overcome the losses and therefore reach the onset of laser-like action than in the TP case we are currently exploring. This is caused by the weaker absorption, and the resulting larger excited volume, of the dye at this pumping wavelengths (see 4.1).

On the other hand, in the OP case RL build-up times of around 12 ps are obtained when using excitation energies within the 5 - 83 µJ/pulse range, one order of magnitude smaller, i.e. times required to achieve enough gain to reach the RL

onset are shorter under OP excitation. In the OP case not only the build-up time is shorter, but also the pulse length, which has the same duration as the laser beam, 30 ps. Under TP excitation, however, the temporal shortening of the emission is not as strong; 147 ps pulses are measured slightly above threshold, at 1.5 mJ/pulse, and this time is reduced down to 93 ps at 4 mJ/pulse. It is not possible to measure under larger pumping energy density because the pumping shock wave damages the sample.

## 4.4 Modal distribution in the spectral and temporal domains

### 4.4.1 Mode density control

To better understand the relation between temporal and spatial properties of the TP pumped RL emission of the explored samples, we employ, as in the case of OP pumping, spatial filters of different apertures which allow us to control the size of the emitting area whose radiation is collected. By imaging the emitting surface over a plane where those filters are located, we reduce the number of lasing modes which are correlated in space. In fact, the comparison of streak images recorded with a diameter of the pumped area of 500 µm, by using different pinhole apertures at the same pumping energy allows us to study the effect of the spatial filter size on the laser spikes distribution. Figure 4.6 shows single-shot streak images of these measurements without spatial filter (a) and with pinholes of 50 µm (b), 30 µm (c) and 15 µm (d) diameter. The spectral and temporal profiles extracted over the whole images are presented in the XZ and YZ planes, respectively. It is clear from this plot that if no spatial filter is used, the number of existing spatially overlapping lasing modes is so large that their average spectral and temporal widths exceed the average spacing between neighbouring modes. Therefore, spikes assigned to discrete lasing modes are averaged out leaving a smooth spectral profile. In fact, the map surface just presents a small fine structure on top of the ASE band. In contrast, when spatial filters are employed, discrete lasing peaks, not necessary located at the center of the gain curve and originated from non overlapping cavities are found.

As expected, the decrease in the pinhole aperture reduces the density of supported modes while keeping the size of the gain medium constant. With the smallest pinhole size we find just a few anti-Stokes lasing spikes independently oscillating and not necessarily located at the center of the gain curve. The time-integrated spectral profile and the sprectrally integrated temporal profile are also displayed for comparison with almost all RL reported experiments because they record integrated data. These profiles, which do not provide any information on whether different modes co-exist at the same time o appear subsequently, show an increasingly resolved fine structure as the pinhole size is decreased. We therefore use the small pinholes to analyse the mode dynamics and stability originated from non-overlapping cavities.

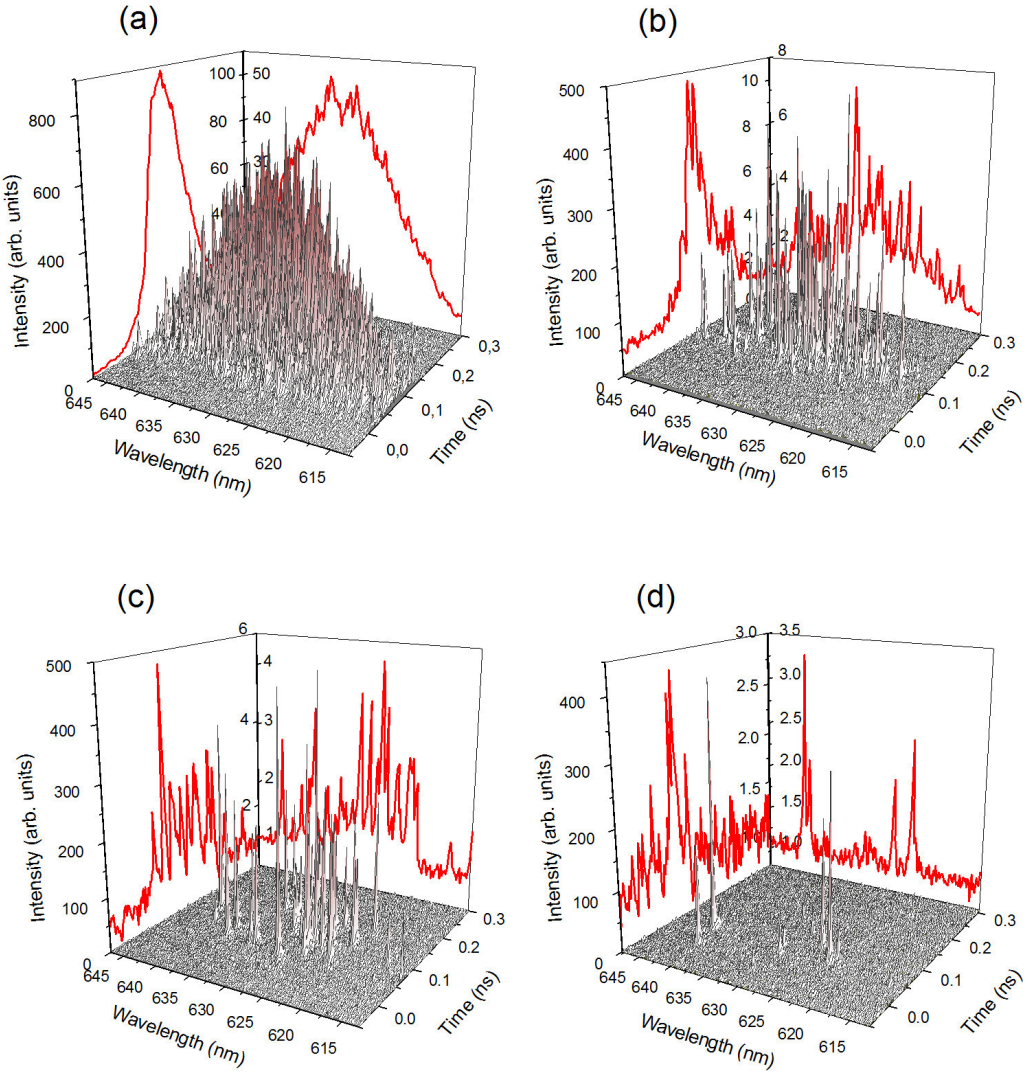


**Figure 4.6:** Single-shot surfaces from streak images of RL pulses under 4 mJ/pulse pumping with no pinhole (a), $\varnothing_{pinhole}$ = 15 µm (b), 30 µm (c) and 50 µm. Spectral and temporal profiles over the whole range are projected on the XZ and YZ planes, respectively. [127]

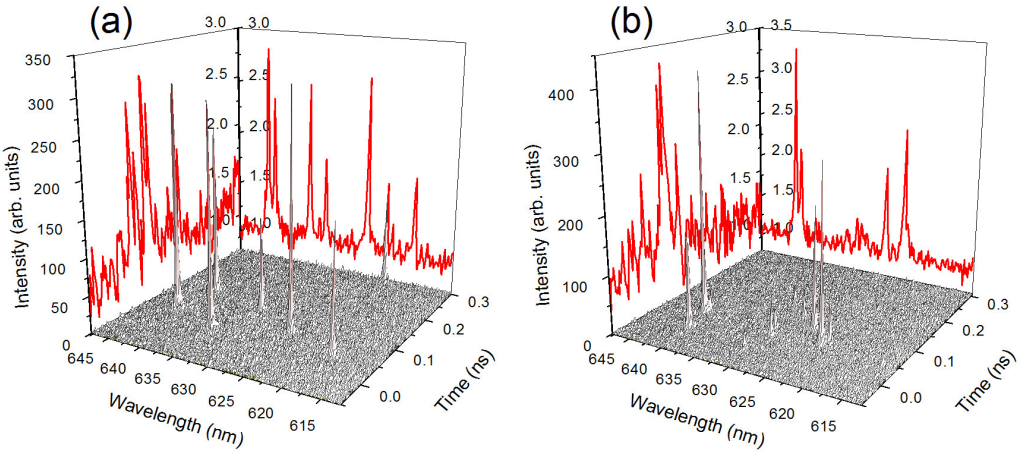


**Figure 4.7:** Single-shot surfaces from streak images of two consecutive RL pulses under 4 mJ/pulse pumping with $\varnothing_{pinhole} = 15$ µm. Spectral and temporal profiles over the whole range are projected on the XZ and YZ planes, respectively.[127]

### 4.4.2 Shot-to-shot analysis

To compare the dynamics of consecutive emission pulses with identical experimental conditions we perform sequences of measurements with the streak camera. We pump again at 4 mJ/pulse with a beam spot size of $\varnothing_{pump} = 500$ µm, which provides the highest safe pumping energy density and using a 15 µm diameter pinhole. Figure 4.7 compares the lasing peaks distribution of two consecutive shots measured at 4 mJ/pulse around the maximum of the RhB gain curve. Map surfaces show different modal distributions from shot to shot as lasing spikes appear at different wavelengths and times. It is worthy to notice that in these experiments, scattering particles are not moving due to the static disorder of the powder sample. Nevertheless, we observe that no specific frequency dominates the others and that spikes were distinct from pulse to pulse revealing an intrinsically stochastic behaviour in the temporal and spectral response of the TP pumped random lasing. This different mode competition could be related to tiny intensity fluctuations. Modes of similar wavelengths are activated at different times in consecutive pulses, which suggest they are originated in different cavities due to the stochasticity of the spontaneous emission.

In order to further study the modal oscillation dynamics of our powder system under NIR excitation we extract temporal profiles of several streak camera by placing vertical sampling windows with a spectral width of 0.5 nm over the spectral range in which the TP pumped RL emission is spread. The comparison of temporal profiles extracted from different shots and measured under the same experimental conditions confirms the above mentioned chaotic RL behaviour. The individual modes have a duration around 6 ps and linewidths of 0.35 nm. Figure 4.8 shows as an example the profiles of the emission of an area of 30 µm diameter under 4 mJ/pulse pumping over the central region of the RhB gain curve. Modes of this figure have varying relaxation oscillations periods. These oscillations are easy to observe as the lasing

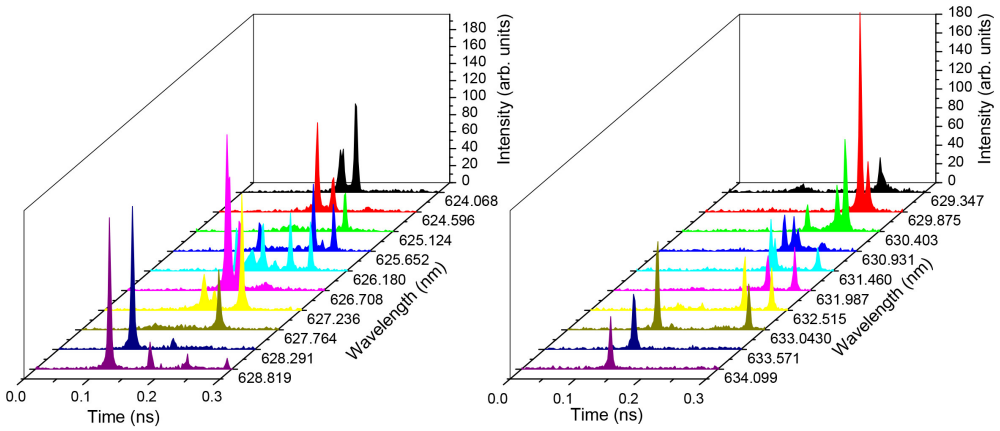


**Figure 4.8:** Detailed mode analysis of an RL pulse under 4 mJ/pulse pumping with a $\varnothing_{pinhole} = 30$ µm.[127]

modes are uncoupled. The periods vary from 12 to 70 ps for different lasing modes.

### 4.4.3 Effect of the pump energy on the modal oscillation dynamics

The increase of the excitation energy allows the creation of lasing modes with larger thresholds. We thus expect an enhancement of the mode coupling and of the overlap between lasing spikes with the pumping energy density. However, we do not see a smoother spectral profile. Figure 4.9 shows two shots of an emitting area $\varnothing_{pump} = 50$ µm under 4 mJ/pulse and 2.5 mJ/pulse pumping. In order to explain this result we must bear in mind that due to strong modal interactions, the number of lasing modes can saturate with increasing pumping. This effect is related to the non-monotonic dependence of mode intensities on the pump strength and complete disappearance of some modes for pumping exceeding certain threshold. To explore more deeply this effect, larger pumping energies would be desirable. Nevertheless, within the employed focusing conditions, this was not possible due to the powder removal caused by the pumping shock wave.

## 4.5 Summary and conclusions

In this chapter we have studied the random laser build-up time and modal oscillation dynamics of a Rhodamine B doped di-ureasil powder under TP pumping at 1064 nm with a picosecond laser using the mode selection method described in chapter 3. The threshold energy for a pumping size of 500 µm, is between 0.85 and 1.5 mJ/pulse, i.e. between 433 and 764 mJ/cm$^2$. A reduction of the anti-Stokes build-

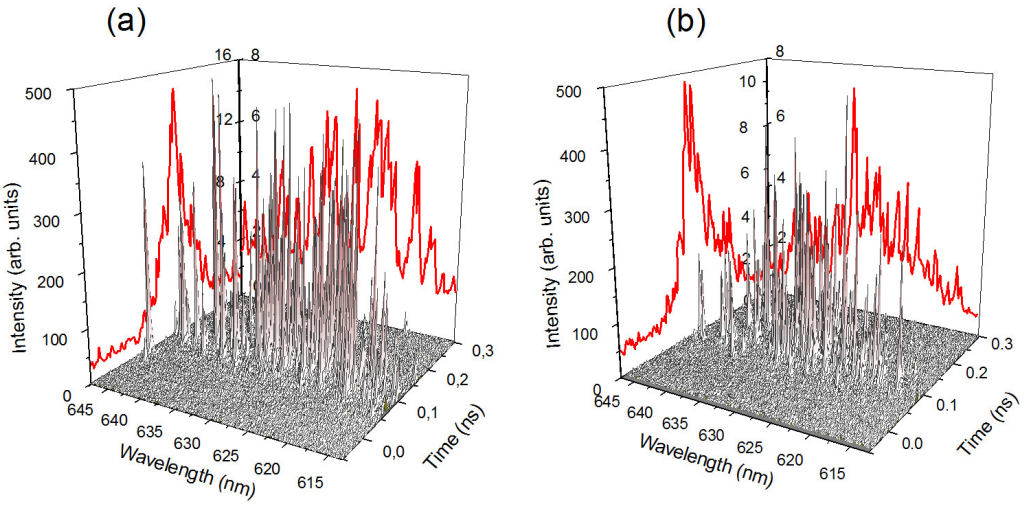


**Figure 4.9:** Single-shot surfaces from streak images of RL pulses under 2.5 mJ/pulse pumping and 4 mJ/pulse pumping with $\varnothing_{pinhole} = 50$ µm. Spectral and temporal profiles over the whole range are projected on the XZ and YZ planes, respectively.[127]

up time from 154 to 113 ps was found when increasing the pump energy from 1.5 to 4 mJ/pulse. Within the mentioned range of pump strength the output pulse duration was reduced from 147 to 93 ps. Under the same experimental conditions, the random laser threshold in the OP case is almost three orders of magnitudes smaller whereas the time delay between the barycentres of pumping and the random laser pulses was around 12 ps. Moreover, in such a case, output pulses as short as the pumping pulses were achieved above threshold. The different random laser performance found under both excitation schemes may be due to their different pumping volumes; in the TP case, light can go much deeper into the material due to the much weaker absorption which may lead to a lower effective pump density, causing an increase in the mode lasing thresholds.

By isolating the emission of the TP pumped random laser from a predetermined size area, equal to the employed pinhole aperture, we demonstrate the stochastic frequency behaviour of the anti-Stokes random laser modes of our powder sample with static disorder. This system lases in different modes upon repeated identical excitations. The lasing modes show relaxation oscillation periods from 12 to 70 ps.

# Part II

# NEODYMIUM-BASED SOLID SATE RANDOM LASERS

# Chapter 5

# Random Laser performance of stoichiometric Nd crystal powders

## 5.1 Introduction

The first detailed studies of random laser emission were performed on powders of neodymium-activated luminophosphores by Markushev et al. on 1986 [8, 9] at either liquid nitrogen or liquid helium temperature. They were the first ones to describe the pumping energy threshold and measure the pulse shortening, the intensity enhancement and the narrowing of the spectra of powders doped with $Nd^{3+}$. Although all these features are common to all RL lasers, the behaviour of some of them differ significantly comparing to the RL studied in chapters 3 and 4.

Neodymium-doped systems present a significantly different emission if compared with organic-based systems such as the one explored in Part I, showing a lifetime of a few ns or narrowing to less than a nm. Among rare-earth RL powders, those based on $Nd^{3+}$ are especially interesting due to their high efficiency and low threshold in almost every host [9, 14, 50, 128–134]. $Nd^{3+}$ is the most extensively studied ion for stimulated emission with more than one hundred crystals analyzed, thanks to the many absorption bands, which proide good optical pumping efficiency, and rapid energy cascade to the $^4F_{3/2}$ level [135]. In addition, pumping at around 800 nm can reduce lattice heating from multiphonon relaxation cascade to $^4F_{3/2}$.

The stoichiometric hosts have received the most attention for RL [6, 93, 135, 136]. In contrast to other hosts where the active ion is dispersed as a dopant in the crystalline matrix, stoichiometric hosts are pure chemical compounds of RE ions. In principle, the main variable controlling the quenching of the luminescence is the nonradiative energy transfer process between rear-earth ions. The high concentration of ions gives rise to a short-range spatial migration of energy among ND3+ ions [137], that may affect the threshold and slope efficiency for laser action. In addition, and because of the high density of optically active ions, stoichiometric laser

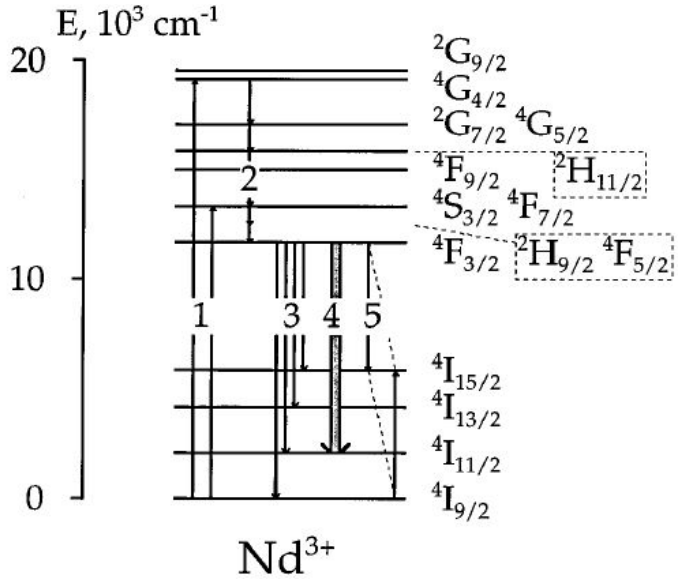


**Figure 5.1:** $Nd^{3+}$ energy level diagram and main transitions. [6]

materials are interesting for low threshold, high gain miniature solid-state oscilaltors and amplifiers, and integrated devices. Our group has previously studied the dependence of the efficiency on the concentration and we have seen that despite the concentration quenching the efficiency was very high because the build-up time of the random pulse is much lower than the lifetime of these systems [130]. Moreover, from a practical point of view, the low coherence and lonng emission wavelength [93] of $Nd^{3+}$ RL makes this type of emission source a very promising one for applications in biomedicine and high resolution bioimaging [138]. For these reasons, we have analysed the emission mean features – slope efficiency, threshold energy – of several stoichiometric Nd doped ground crystal samples working as random laser sources in the ${}^4F_{3/2} \rightarrow {}^4 I_{11/2}$ emission band of $Nd^{3+}$ ions around 1064 nm by exciting the ${}^4I_{9/2} \rightarrow {}^4 F_{5/2}$ transition. The energy level diagram in figure 5.1 shows the $Nd^{3+}$ main transitions.

## 5.2 Experimental

All studied samples – $NdAl_3(BO_3)_4$, $NdVO_4$, $NdPO_4$, $NdP_4O_{12}Li$ and $NdGa_5O_{12}$ – present a high absorption and a similar transport length of about 10 µm. $NdVO_4$ has the highest absorption and emission cross-sections among vanadates [139]; $NdAl_3(BO_3)_4$ has been previously by our group and presents a high efficiency [92]; $NdP_4O_{12}Li$ and $NdAl_3(BO_3)_4$ have a large distance between $Nd^{3+}$ ions which reduces the concentration quenching of fluorescence resulting in a limitation of cross relaxation processes. The samples were prepared by different research groups. $NdP_4O_{12}Li$ was provided and prepared by Strek et al. following their synthesis method as explained in a previous work [140]; $NdGa_5O_{12}$ garnet crystal has been grown by Lavn, Rodriguez-

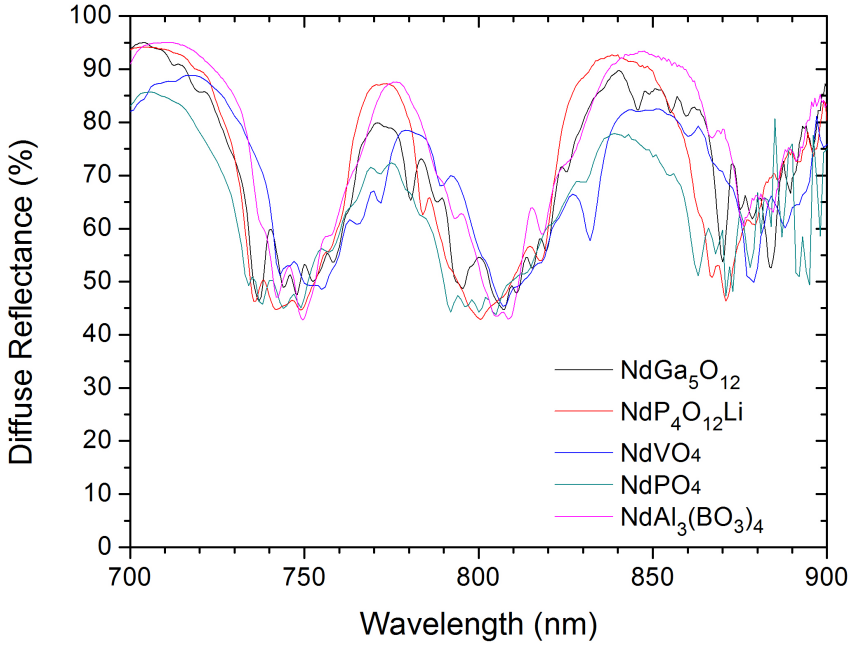


**Figure 5.2:** Spectral diffuse reflectance for $NdAl_3(BO_3)_4$, $NdVO_4$, $NdPO_4$, $NdP_4O_{12}Li$ and $NdGa_5O_{12}$.

Mendoza, Kamada and Yoshikawa as described in our publication by Iparraguirre et al. of 2016 [141]; $NdAl_3(BO_3)_4$ was prepared by citrate precursos obtained by soft chemistry procedures by Cascales [16] and $NdVO_4$ and $NdPO_4$ samples were grown by BEttinelli and Cavalli [136].

The experimental set-up for the RL emission analysis is shown in the inset of figure 5.3. The pumping source is a tunable Ti:sapphire pulsed laser with a 10 ns pulse. Maximum pumping energy is about 35 mJ; a variable attenuator by reflection (Lotis, VA-R) controls it to avoid changes in the size of the pump beam when the energy is modified. The pump beam is focused on the samples with a 40 cm focal lens placed in a movable holder to control the size of the pumped area. The absolute value of the intensity of the pump beam is obtained from the calibration of the measurement of the radiation diffused by a folder mirror in the pump path by an energy meter (Newport 818-BB-21). The sample is pumped with a 20° angle to prevent any damage in the optics. The emission is collected with no lens. An optic fiber of 0.5 mm diameter at 25 cm distance above the sample collects part of the emission; a filter removes the pump radiation reflected by the sample when necessary. The detection system has been calibrated in order to know in every moment the pumping and stimulated emission energies and the absolute value of the slope efficiency. Given the spatial incoherence of the RL emission, its angular distribution can be assumed to be Lambertian [134, 142] allowing for a calibration to obtain the absolute emitted energy by the sample. The measured energy per unit

area at a distance $r$ and at an angle $\theta$ with respect to the normal is given by:

$$M(r,\theta) = \frac{E_{em}\cos\theta}{\pi r^2}, \tag{5.1}$$

where $E_{em}$ is the total energy of the RL emission. Placing a calibrated energy meter of area $S$ at a much smaller distance $r$ and angle $\theta$, we obtain the relation between the emitted and the measured energies:

$$E_{mea} = \frac{Scos\theta}{\pi r^2} E_{em}, \tag{5.2}$$

Hence, measuring the RL emission with the energy meter and the collected by the optical fibre coupled to a detector (Thorlabs, SIR5)connected to an oscilloscope (Tektronix, TDS 7104, 10 Gs/s) at the same time we obtain the calibration between the absolute emitted energy and the area under the curve of RL emission intensity registered by the oscilloscope.

## 5.3 Laser slopes and thresholds of $NdAl_3(BO_3)_4$, $NdVO_4$, $NdPO_4$, $NdP_4O_{12}Li$ and $NdGa_5O_{12}$

In order to characterise the powders and set the pump wavelength we first measure the diffuse reflectance of the sample with an integrating sphere coupled to a spectrophotometer (Varian Cary 5) with 0.5 nm resolution; the resulting absorbance is shown in figure 5.2. The pump wavelength for the study of the RL emission is set at the minimal diffuse reflectance – maximal absorbance – wavelength, which is at 810 nm for $NdAl_3(BO_3)_4$, 808 nm for $NdVO_4$, 795 nm for $NdPO_4$, 797 nm for $NdP_4O_{12}Li$ and 807 nm for $NdGa_5O_{12}$ because it gives the minimal input threshold energy and tha maximum laser slope efficiency [134, 136].

The emission of all samples shows a typical threshold behaviour above a certain pump energy; the emission spectrum narrows greatly to a single peak of a width smaller than our spectral resolution (0.3 nm), the intensity increases by some orders of magnitude and the pulse duration shortens from two hundred microseconds – the spontaneous emission decay time – to a few nanoseconds. In order to study the temporal behaviour of the RL emission of these materials we simultaneously measure the intensity of the pumping and laser emission as a function of time. First, we calibrate the time delay between the signals caused by the different path lengths – lengths of the cables, optic fibres and optic paths – filtering the sample emission and observing the pump pulse in both detectors at the same time. We estimate the error of this calibration due to the modal dispersion of multimode fibers and the chromatic dispersion in 10 ps, which is acceptable considering that pump pulses are

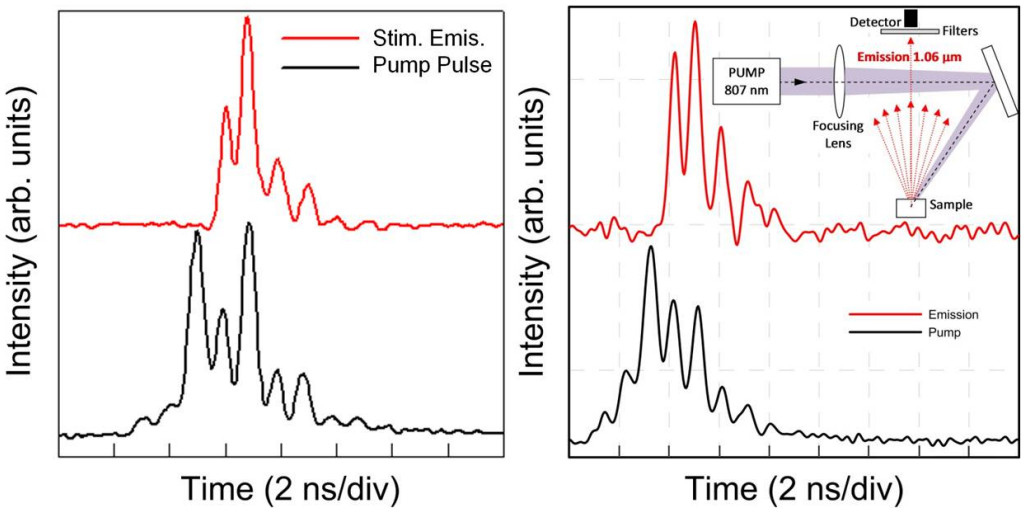


**Figure 5.3:** Intensity as a function of time of the pump pulse (below) with its corresponding RL emission pulse (above) of the sample $NdGa_5O_{12}$ (left) and $NdP_4O_{12}Li$ (right).

10 ns long and the temporal widening of the measuring system is around 200 - 300 ps.

Figure 5.3 shows the temporal profile of the pulses, of two highly concentrated neodymium stoichiometric samples. We have collected the radiation from all the surface to perform this analysis. It can be seen that the emission takes a time to reach the threshold after absorbing the pump pulse – the build up time – but after that time, the signals are nearly synchronous. The observed oscillations in the emission are caused by the pump pulse and are not relaxation oscillations. All analysed samples show identical behaviour.

Laser slope efficiency is measured for $NdAl_3(BO_3)_4$, $NdVO_4$, $NdPO_4$, $NdP_4O_{12}Li$ and $NdGa_5O_{12}$ crystal powders pumping around 800 nm ($^4I_{9/2} \rightarrow ^4F_{5/2}$). We set the pump wavelength at the maximum absorbance wavelength. The absorbances of the sample powders are all about 50 % at this wavelength. We measure the laser output energy as a function of the incident energy for all samples with the experimental set-up described in 5.2 and a pump area of 0.4 $mm^2$. The error is $\pm$ 0.05. The results of the measurements can be seen in figure 5.4. The maximum pumping energy is lower for the $NdVO_4$ because its damage threshold is lower.

A previous work by Iparraguirre et al. [134] proposed the following expression for the slope efficiency of the stimulated emission energy versus incident pumping energy in oxysulfide crystal powders doped with Nd:

$$slope = \eta(\lambda_p)\frac{\lambda_p}{\lambda_{em}} \tag{5.3}$$

where $\eta$ is the absorbance of the doped powder at the pump wavelength, $\lambda_p$ the pump wavelength and $\lambda_{em}$ the emission wavelength. This implies that all pumping

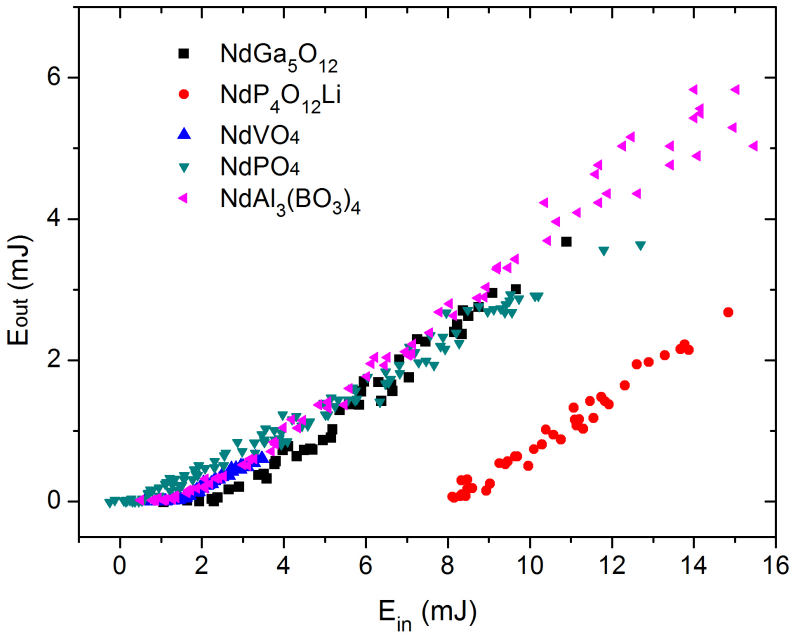


**Figure 5.4:** Laser output energy as a function of pump energy for $NdAl_3(BO_3)_4$, $NdVO_4$, $NdPO_4$, $NdP_4O_{12}Li$ and $NdGa_5O_{12}$.

photons absorbed above the threshold are later re-emitted as stimulated emission. The experimental slope efficiencies and the ones obtained from the absorbances and equation 5.3 are in good agreement when pumping to $^4F_{5/2}$ level. In addition, we perform the slope measurements for three of the samples, $NdAl_3(BO_3)_4$, $NdVO_4$ and $NdPO_4$ , with different pump beam sizes. We find that the slope efficiency $m$ is essentially independent of the pump beam area. Nevertheless, when the size of the pump area is too small – less than 0.5 mm of diameter – the reproducibility of the results is bad: the directionality changes, the slope sometimes increases, some subsidence of the surface appears. The increase in slope is due to a larger absorbance and the other effects are probably caused by the irregularities the pump beam causes on the surface for small pumped areas.

In order to further test the accuracy of equation 5.3 when pumping at different wavelengths, we also measure the slope efficiency dependence on the pump wavelength for the $NdPO_4$ sample. The experimental slope efficiency is shown in figure 5.5 along with the predicted slope by equation 5.3. The measured values fit very well the predicted values, suggesting that all absorbed photons above threshold are later re-emitted.

To explore the slope efficiency when exciting other levels, we perform the slope measurements for the $NdAl_3(BO_3)_4$ exciting the $^4F_{3/2}$ level, pumping at 876 nm. The absorbance at this wavelength is 27 %, lower than the one measured under

| **Sample** | $\lambda_p$ | $\lambda_{em}$ | $\eta(\lambda_p)(\%)$ | **Slope (%)** | $E_{th}$ **(mJ/mm$^2$)** |
|---|---|---|---|---|---|
| $\mathbf{NdPO_4}$ | 797 nm | 1059 nm | 0.52 | 0.36 | 8 |
| $\mathbf{NdAl_3(BO_3)_4}$ | 810 nm | 1063 nm | 0.47 | 0.33 | 4 |
| | 876 nm | 1063 nm | 0.27 | 0.20 | 6.5 |
| $\mathbf{Nd_3Ga_5O_{12}}$ | 807 nm | 1062 nm | 0.56 | 0.42 | 6.5 |
| $\mathbf{NdP_4O_{12}Li}$ | 800 nm | 1048 nm | 0.48 | 0.33 | 13 |
| $\mathbf{NdVO_4}$ | 808 nm | 1061 nm | 0.54 | 0.30 | 4 |

**Table 5.1:** Experimental values of the diffuse absorbance, laser slope efficiency and threshold energy per unit area for different stoichiometric powdered samples. The estimated error in the measurements is 10 %.

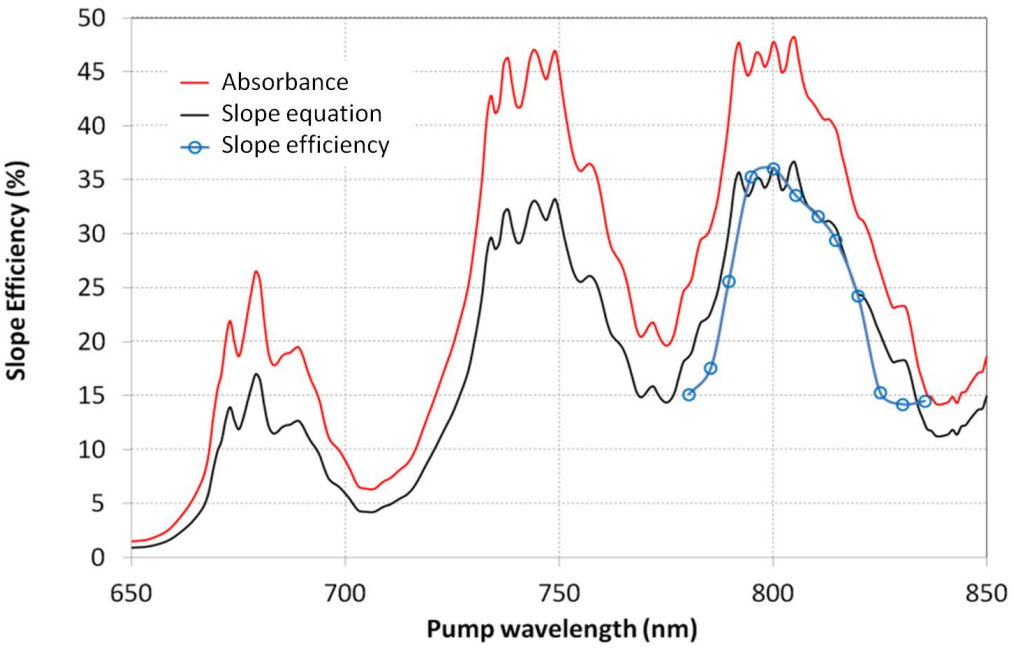


**Figure 5.5:** Slope efficiency of the RL emission of the $NdPO_4$ powder predicted by equation 5.3 (black line), experimental slope efficiencies and absorbance spectrum (red line).

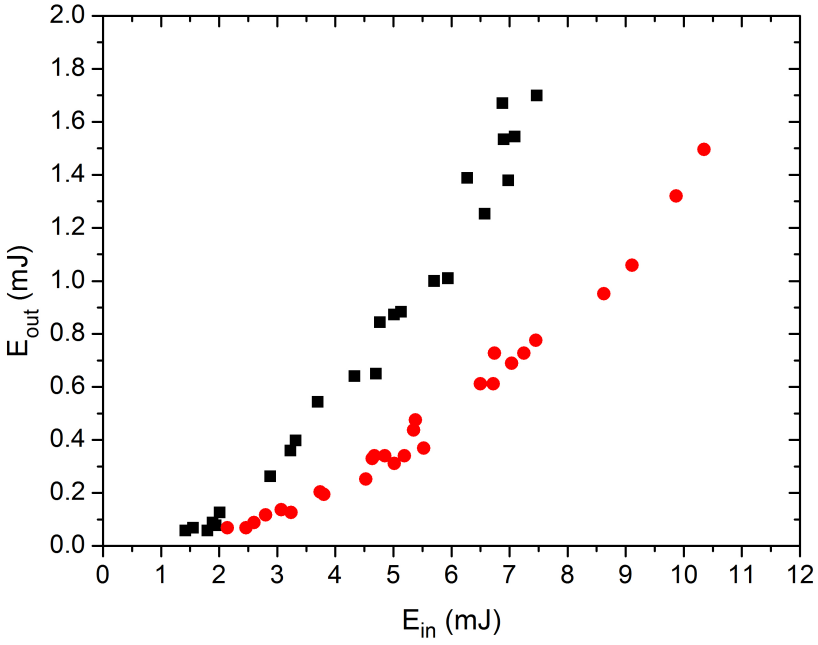


**Figure 5.6:** Output laser energy as a function of pumping energy for powdered $NdAl_3(BO_3)_4$ for two different pump wavelengths: 810 nm (black squares) and 876 nm (red dots).

pumping at 810 nm, 47 %. Slope efficiency under 810 nm pump (exciting the ${}^4F_{5/2}$ level) is 33% and 20% under pumping at 876 nm (exciting the ${}^4F_{3/2}$ level). The measured slopes for both pumping wavelengths are shown in figure 5.6. Equation 5.3 is also satisfied exciting the ${}^4F_{3/2}$ levels for our powder sample.

The threshold energy $E_{th}$ of the samples vary from 4 mJ/mm$^2$ to 6.5 mJ/mm$^2$, as can be seen in figure 5.4; all the values are displayed on table 5.1. The threshold energy per unit area remains constant for areas with a diameter above 0.5 mm and it increases below that size. The energy threshold expression (equation 1.7) proposed by the RL one-dimensional theory depends on the pumping area, the stimulated emission cross-section, the transport length, the inelastic length, which depends on the absorption cross-section, the concentration and the filling factor. Nonetheless, while studying a sample the threshold energy per unit area remains, for all $\lambda_p$, inversely proportional to the absorbance at the pumping wavelength. However, it is complex to compare threshold energies for different samples due to the different emission cross-section.

## 5.4 Summary and conclusions

Analysing the emission of different $Nd^{3+}$ stoichiometric powders pumped to $^4F_{3/2}$ and $^4F_{5/2}$ levels under nanosecond pumping pulses we have observed the following behaviour. The laser slope is proportional to the absorption of the material and the constant of proportionality is the quotient between the pump and emission wavelengths (equation 5.3). This result implies that almost all pump photons with energy over the threshold are converted into stimulated emission photons. This means that the probability of stimulated emission is much higher than any other transfer or loss-channel of the upper-level. In addition, neither the slope nor the threshold energy per unit area depend on the area of the pumping beam, if the pump beam diameter is much longer than the absorption length. When both lengths are comparable the threshold appears at a higher energy than expected, probably because the emission photons are more likely to be present in peripherally pumped areas.

Finally, the temporal, spatially integrated, measurements (figure 5.3) show the RL emission intensity, once the threshold energy is reached, follows the pump pulse with a delay of the order of 100 ps.

# Chapter 6

# Non stoichiometric Random Lasers. Influence of Nd concentration in the RL emission of the powders

## 6.1 Random laser action in Nd:$La_2O_2S$

Rare earth oxysulfides ($RE_2O_2S$) are among the RE-doped oxides one of the most efficient phosphores investigated for lighting applications or commercial television [143]. Lanthanum oxysulfide crystal matrix is an excellent host lattice for trivalent RE ions [144] with the lanthanum atoms coordinated by four oxygen atoms and three sulfur atoms [145]. The laser and spectroscopic properties of these crystals were investigated by Alves et al. in 1971 [144] and the stimulated emission kineticsat liquid nitrogen temperature by Markushev et al. in 1990 [146]. Iparraguirre et al. investigated in 2012 for the first time the laser action of $Nd^{3+}$ doped $La_2O_2S$ powders at room temperature [134].

In order to study the effect of dopant concentration on the threshold and slope, we analyse the emission of samples of $La_2O_2S$ doped with 9 %, 6 %, 3 % and 2 % Nd. Crystals with different concentrations of Nd have different absorption properties due to the inelastic length, but the same diffusion characteristics (transport length). In the other hand, the grain size only affects the transport length. It has been observed that smaller grain samples reflect the pump radiation more efficiently [147].

The experimental set-up used in our experiments is described in chapter 5. The system has been previously calibrated to obtain the absolute units of the energies as has been explained in chapter 5.

Table 6.1 shows a summary of the study for these oxysulfide samples. The laser

| **Sample Nd:$La_2O_2S$** | **9 % Nd** | **6 % Nd** | **3 % Nd** | **2 % Nd** |
|---|---|---|---|---|
| **Absorbance at 819 nm** | 0.23 | 0.19 | 0.16 | 0.13 |
| **Laser slope** | 0.16 | 0.14 | 0.12 | 0.10 |
| **$E_{th}$ per unit area (mJ/mm$^2$)** | 2.0 | 2.3 | 2.7 | 3.0 |
| **$E_{th}$ rel. to 9% doped** | 1 | 1.15 | 1.35 | 1.50 |
| **Relative $E_{th}$ ($l_{res} \propto l_i$)** | 1 | 0.97 | 0.95 | 0.94 |
| **Relative $E_{th}$ ($l_{res} \propto l_{abs}$)** | 1 | 1.21 | 1.44 | 1.77 |

**Table 6.1:** Absorbance, slope and threshold of the $La_2O_2S$ doped with Nd at different concentrations.

slope behaviour follows the expression 5.3, as we have already seen in chapter 5. In addition, we explore the behaviour of the threshold energy. From equation 1.7, if $l_{res} \propto l_i$:

$$\frac{E_{th}}{h\nu A} = \frac{\sqrt{l_t/l_i}}{\eta\sigma_{em}} \tag{6.1}$$

This relation, as we can see in table 6.1, is not in good agreement with the experimental measurements of the energy threshold. On the contrary, we have observed that considering $l_{res} \propto l_{abs}$, from equation 1.7, the threshold energy is proportional to the inverse of the absorbance:

$$\frac{E_{th}}{h\nu A} = \frac{1}{\eta\sigma_{em}}, \tag{6.2}$$

which seems to indicate that the changes in residence lengths compensates the changes in pumping volume.

To conclude the study, we measure the output energy as a function of the pump energy for different pump beam diameters for the 9 % Nd doped sample, pumping at 819 nm and collecting the emission at 1076 nm. The slope efficiencies, as we can see in figure 6.1 are the same for all three pump area sizes, 15 % ($\pm$ 1 %). Considering the absorbance at the pump wavelength is 23 % and the ratio between absorbed and emitted photons is 76 % the slope-efficiency $m$ follows the expression 5.3 if the branching ratio of the excited state to the metastable state level is close to one [134].

## 6.2 A paradigmatic non stoichiometric random laser: Nd:YAG

Nd:YAG is one of the most popular and well studied crystals for stimulated emission. In this crystal, the matrix, $Y_3Al_5O_{12}$, is doped with a Neodymium ion in a concentration of a few percent. The YAG garnet crystal has very interesting properties for its use as a host matrix for $RE^{3+}$ ions, such a good thermal conductivity

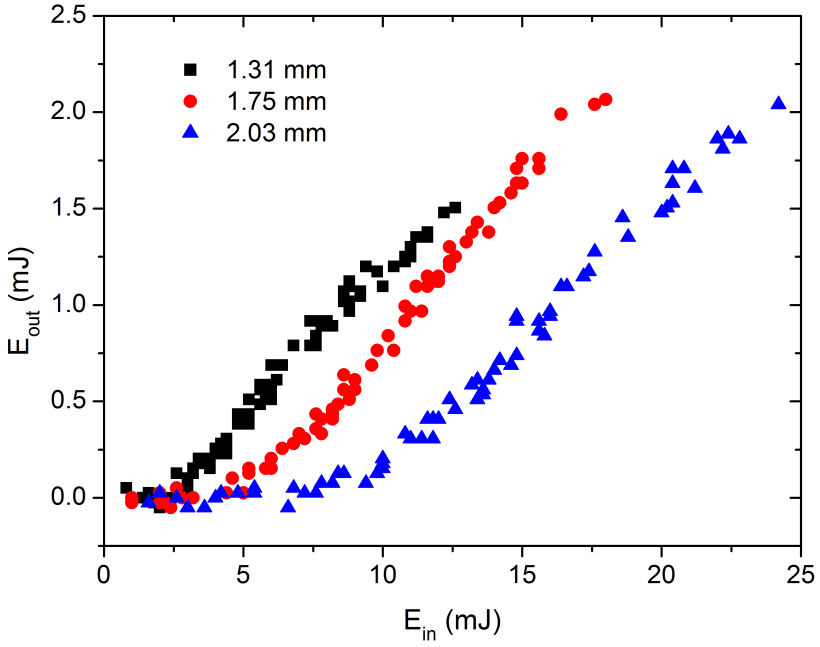


**Figure 6.1:** Output energy as a function of pump energy for three different pump areas, with diameters 1.31 mm, 1.75 mm and 2.03 mm, in % Nd doped sample.

and transparency, hardness, low threshold and high efficiency; it is therefore very suitable for high-power and continuous wave (CW) applications and one of the most valuable solid-state materials for commercial laser oscillators and amplifiers [148]. Although some works have studied Nd:YAG as a random laser source, its emission has not been properly characterized. Feng at al. observed RL emission in nano powders with a 250 nm grain diameter under diode pumping and a one mirror structure [149] and described the emission spectrum, the emitted energy in relative units, the threshold behaviour, the temporal behaviour in time scales of the order of 200 µs and thermal effects[150]; no lasing was detected without the mirror. They also built a hybrid microchip combining a Nd:YAG transparent ceramic and a Nd:YAG powder tablet [151].

We obtain a 1064 nm RL emission by pumping around 800 nm a 1 mol % Nd doped YAG crystal powder using a set-up with no mirrors [152]. We study its emission and measure absolute emission energy versus pump energy – the slope efficiency –, the pump threshold energy as a function of the pumped area and pump wavelength, and laser intensity is a function of time.

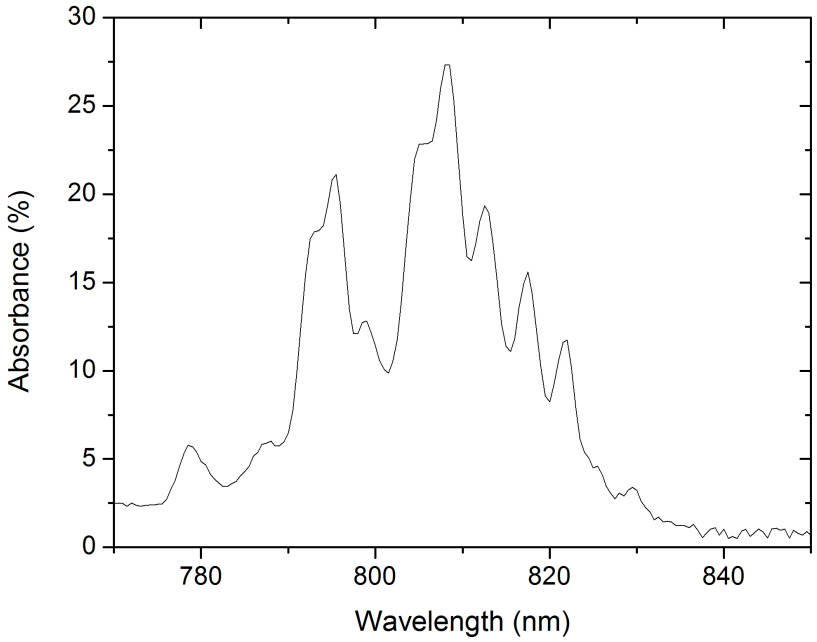


**Figure 6.2:** Absorbance spectrum of Nd:YAG crystal powder.

### 6.2.1 Experimental

The studied Nd:YAG crystal powder is fabricated from a commercial Nd:YAG rod with 1 % Nd (Laser Crystal Corp), grinded in a mixer mill (Retsch MM200). We measure the grain size of the powder with a confocal microscope (Leica TCS SP5) and an average powder size of tens of microns is found. As we are pumping around 800 nm we perform a diffuse reflectance spectrum to obtain the absorbance of the powder on the pumping ${}^4I_{9/2} \rightarrow {}^4F_{5/2}$ transition and the precise absorbance maximum wavelength. Figure 6.2 shows the absorbance of the powder; a maximum value of 27 % is found at 808.5 nm. We perform the study of this sample pumping at this wavelength as it is the one with the minimum threshold energy and the maximum slope efficiency (chapter 5) [134, 136]. The experimental set-up is an adaptation to the one described in section 5.2.

### 6.2.2 Results

The sample shows again the typical threshold behaviour described for the stoichiometric samples (section 5.3. The peak of the emission wavelength is at 1064.1 nm and does not change with the pump wavelength. We measure a pump pulse and its corresponding stimulated emission pulse as a function of time as shown in figure 6.3. We observe that the stimulated emission pulse starts after the pump pulse; as

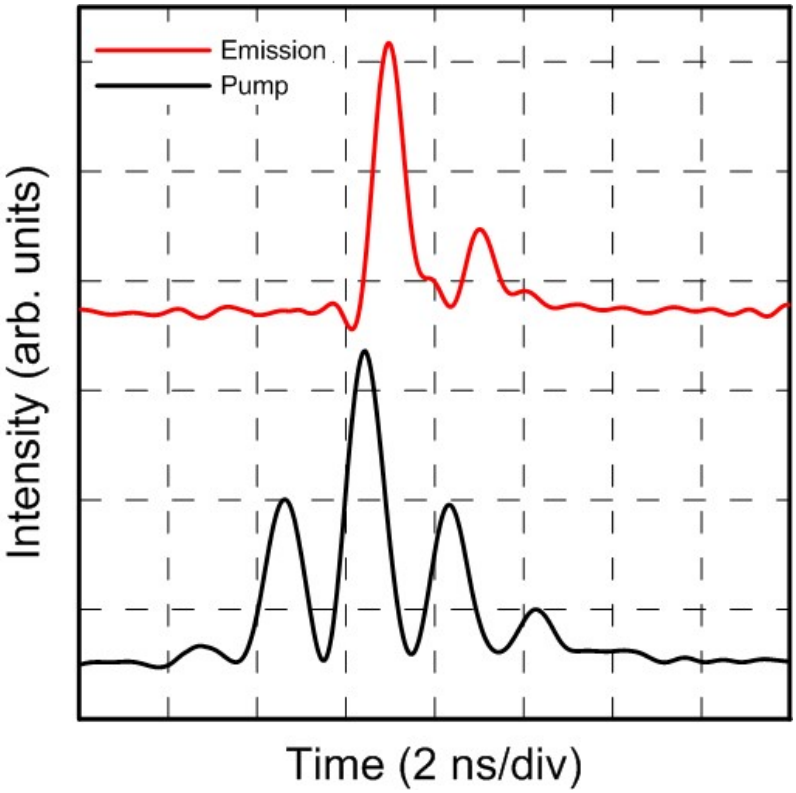


**Figure 6.3:** Pump pulse intensity (below) and the corresponding laser intensity (above) as a function of time for the Nd:YAG sample.

the optical paths are calibrated, we know that this delay is due to the time it takes to the material to absorb the pump radiation and reach the threshold level of the population inversion, the build up time. Once the RL emission appears, it presents some fluctuations which follow the pump intensity ones with a 500 ps time delay. This behaviour resembles that of the stoichiometric powders 5.3 but this time the observed delay is higher.

We also register the RL input/output slope as the absolute emission energy versus pump energy for two diameters, $\varnothing_1 = 1.04$ mm and $\varnothing_2 = 0.78$ mm. We can observe in figure 6.4 that the slope efficiency is similar for both pumped areas, 20 %. This value is in good agreement with the one predicted by equation 5.3.

The experimental RL threshold energies per unit area of figure 6.4 show both a value of 8.3 mJ/mm$^2$, i.e., the threshold energy density is constant in our experiment, at least above a certain focus area limit. We measure the threshold energy as a function of the pumped area to test the range of validity of this feature. To do so, we measure the threshold energy for different spot sizes of diameter between 0.47 mm and 1.04 mm, which we achieve moving the lens. The results are depicted in figure 6.5. We observe laser radiation for all areas in that range; for the biggest area the threshold is measured at around 7 mJ and for the smallest area at below 2 mJ. The energy threshold increases linearly with the pumped area and the threshold

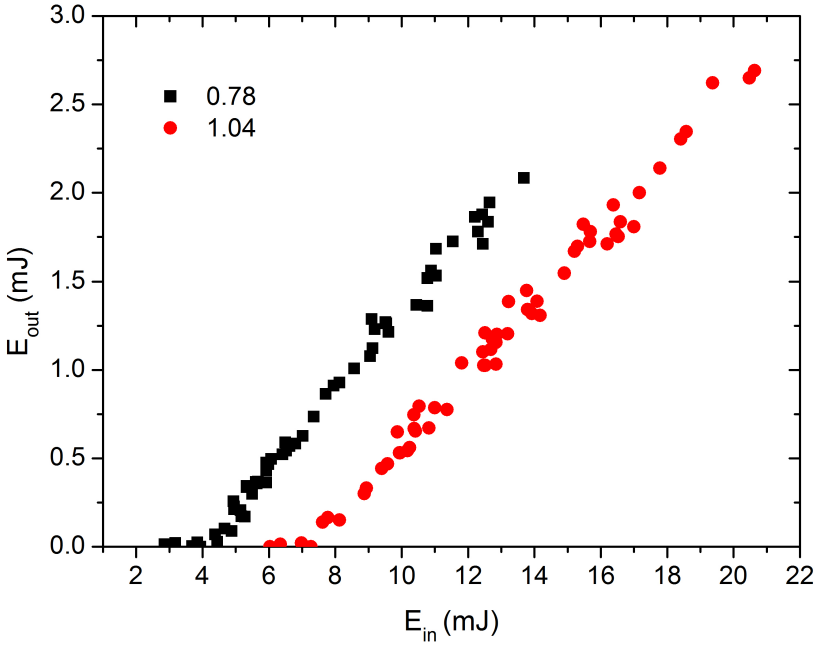


**Figure 6.4:** Input and output energy pumped at 808.5 nm for two different pumped areas of diameters 0.78 mm and 1.04 mm in the Nd:YAG sample. Thresholds are 7.1 and 4.0 mJ respectively.

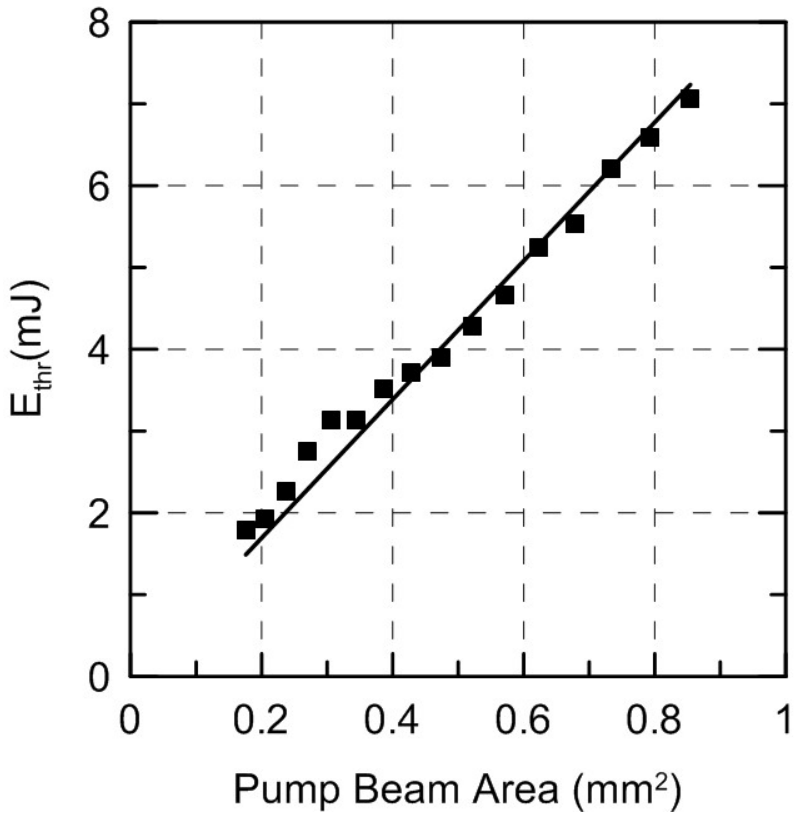


**Figure 6.5:** Threshold energy for Nd:YAG crystal powder as a function of pump beam area and threshold energy density of 8.4 mJ/mm$^2$. [152]

energy density is at 8.4 mJ/mm$^2$; however, for areas smaller than 0.4 mm$^2$ the threshold energy density presents some deviations to the linear fit, probably caused by some damage created by the pump beam on the surface. This deteriorates the linear behaviour of the threshold energy but it is difficult to determine whether this is caused by some drilling or burning of the sample. It is interesting to point out that under the maximum pumped energy density, around 30 mJ/mm$^2$ with a 0.78 mm diameter pumped area (see figure 6.4) no marks are observed in the sample surface.

Finally, we measure the threshold energy as a function of the pump wavelength for two different pump beam area with diameters $\varnothing_1 = 1.04$ mm and $\varnothing_3 = 0.89$ mm. Figure 6.6 shows the results of these measurement the ratio between both curves and the beam area ratio. The shape of both threshold curves is similar to the one of the absorbance (figure6.2) and their ratio is close to the constant ratio of the pumped areas (1.37). We observe that the threshold energy density remains constant for different area sizes, not excessively focused, and pump wavelengths.

Finally, we explore the spatial properties of the emitting surface by projecting the image of the surface on a CCD analyzer for both the RL emission and the reflected pumping with appropriate filters. The projection is made using a lens, obtaining an

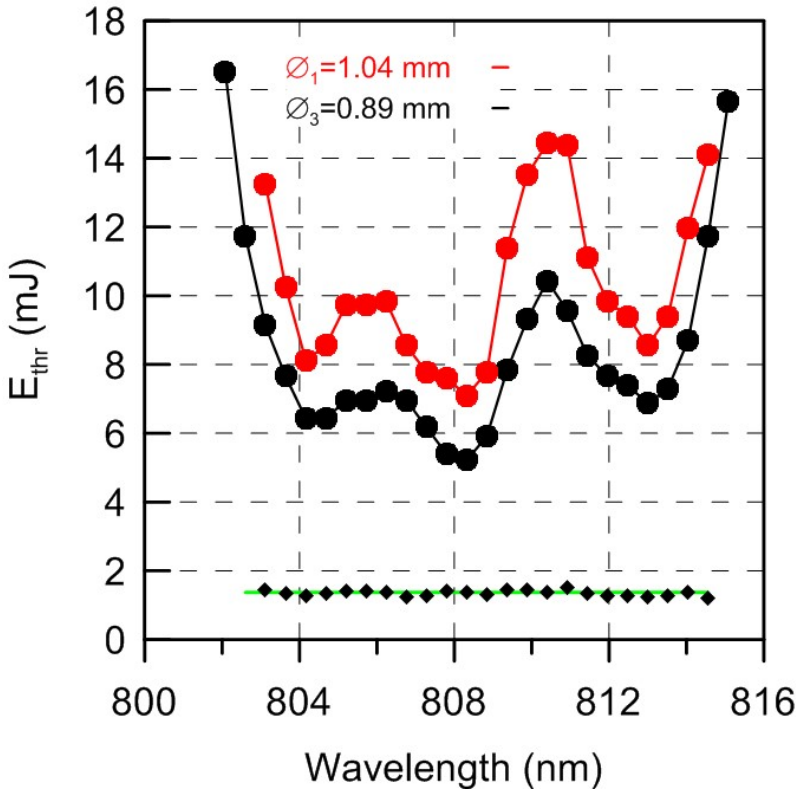


**Figure 6.6:** Threshold energy as a function of pump wavelength for two different pumped areas of diameters 1.04 and 0.89 mm. The ratio (black diamonds) is nearly constant and equal to the beam area ratio (green line). [152]

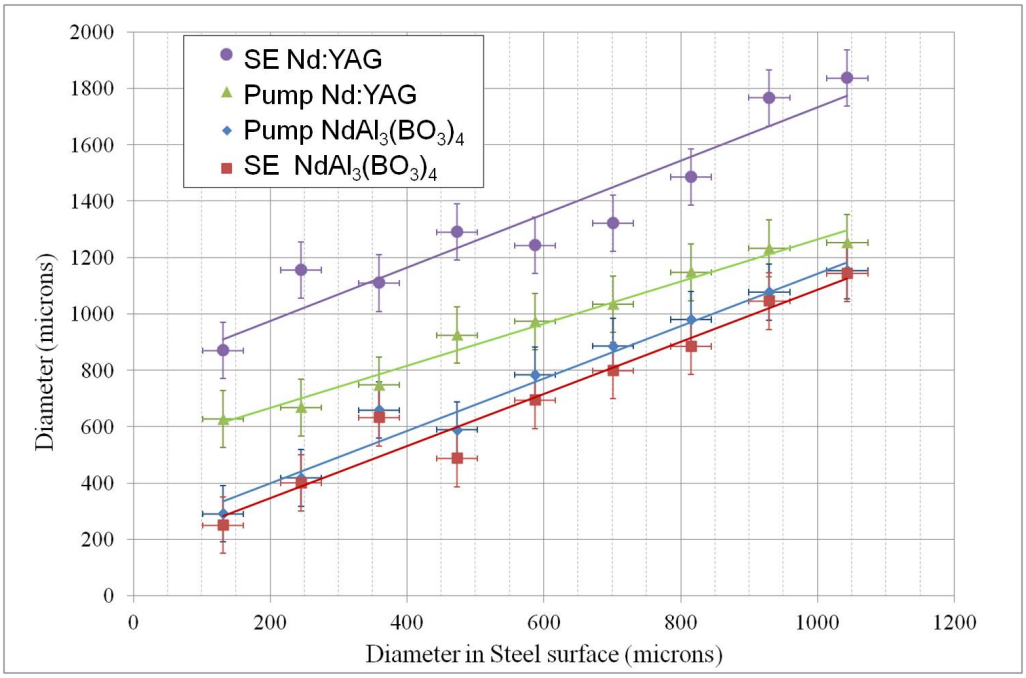


**Figure 6.7:** Diameters of the RL emission and reflected pump at the surface of the stoichiometric powder $NdAl_3(BO_3)_4$ and the Nd:YAG samples as a function of the pumping beam diameter measured in a non-scattering steel surface.

image of lateral magnification one. This way it is possible to explore the interaction between diffusion and amplifications of these materials. Thanks to these images we can also measure the size of the pump beams and therefore estimate the pumped energy per unit of area.

We simultaneously measure the size of the RL emission and the reflected pump beam, which also include its scattering in the powder, for every beam size. As a reference, we also measure the size of the reflected pump beam in a steel surface, with very low scattering. Using this set-up the shapes and sizes of the borate and the Nd:YAG samples, under different focusing or pumping energy conditions, are measured. In figure 6.7 we can see the diameters of RL emission and reflected pumping zones as a function of the pumping beam diameter measured in a non scattering steel surface for our Nd:YAG sample and the stoichiometric $NdAl_3(BO_3)_4$ sample pumped at 810 nm studied in chapter 5.

In the stoichiometric material, sizes of the pump beam (on a steel surface), reflected pump beam on the sample and RL emission area are similar considering the experimental error. However, the measured diameters with the Nd:YAG sample exhibits a moderate expansion of the reflected pumping respect to the incident beam at all measured beam sizes, and the RL emission is even "compressed" respect to the reflected pumping, surely due to effect of more gain in central zones. For the smallest incident beams, the results show higher dispersions.

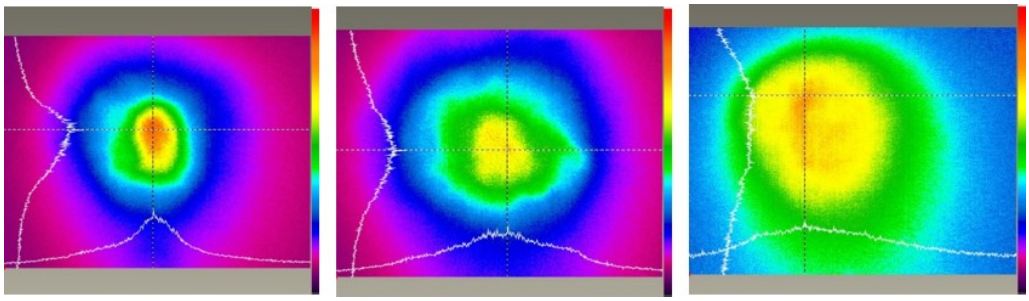

**Figure 6.8:** Emission zones for Nd:YAG (1% doped) for a pump beam of diameter 1.2 mm. Pumping at 808 nm wavelength (left), on a sample with larger grain size (center), and pumping at 810 nm wavelength.

The effect of changes in grain size (transport length) and pump wavelength (inelastic length) are shown in figure 6.8 under a pumping energy of twice the threshold. The sample on the left, pumped al 808 nm, has an inelastic length of 1 mm and a scattering length of 20 µm. The one depicted on the center, pumped also at 808 nm, has a larger grain size, with an inelastic length of 1 mm and transport length of 60 µm. On the right, we see a sample pumped at 810 nm, with an inelastic length of 3 mm and transport length 20 µm. The resulting emitting areas have a diameter of 1.2 mm, 1.9 mm and 2.4 mm. The expansion of the emission area is directly affected by both lengths, and when this emission area is clearly larger than the incident pump area, the rules obtained for threshold could not work well. The threshold energy per unit of area tends to be higher due to the dispersion of stimulated emission photons towards zones of low gain.

As an example, in figure 6.8, the absorbance is 0.18 (eft), 0.26 (center) and 0.09 (right). The experimental threshold energy is 9 mJ in the first case; the expected threshold energies from the RL one-dimensional theory proposed energy threshold expression (equation 6.2) for the cases on the center and right would be 6 and 18 mJ respectively, but the experimental thresholds are 9 mJ and more than 25 mJ respectively. Note that the absorption lengths are about 80 µm (left) and 140 µm in the other two cases. The rise of the threshold energy with respect to the expected value when the absorption length increases either by diffusion (center) or absorption (right) is clearly shown.

## 6.3 Summary and conclusions

Analysing the emission of different $Nd^{3+}$ doped powders pumped to $^4F_{3/2}$ and $^4F_{5/2}$ levels under nanosecond pumping pulses we have observed that the laser slope, as in the case of stoichiometric powders, is proportional to the absorption of the material and the constant of proportionality is the quotient between the pump and emission wavelengths (equation 5.3), which means that almost all pump photons over the energy threshold are converted into stimulated emission photons; i.e., the probability

of stimulated emission is much higher than any other transfer or loss-channel of the upper-level. On the other hand, the pumping threshold energy per unit area is inversely proportional to the absorption. This indicates that the changes in pumping volume and therefore the population inversion are compensated by changes in the residence length, and not by the inelastic length. The observed expansion of the emission surface with respect to the incident pump beam and the reflected pump beam also suggests this behaviour. Neither the slope nor the threshold energy per unit area depend on the area of the pumping beam, if the pump beam diameter is much longer than the absorption length; this is also observed in the stoichiometric powders (Chapter 5).

Finally, the temporal, spatially integrated, measurements show the RL emission intensity, above threshold, follows the pump pulse with a delay of the order of 10 ps, one order of magnitude lower that in the case of low-doped samples.

# Part III

# APPLICATIONS

# Chapter 7

# Speckle-free near-infrared imaging using a $Nd^{3+}$ random laser source

In recent years, the use of Random Lasers as speckle-free sources has attracted significant attention [24–27, 93, 99, 153, 154]. Although other speckle-free lighting sources like LEDs and ASE sources have been investigated for this purpose, RL sources offer interesting features such as a narrow spectra, short pulse duration and high emitted power, offering good image quality, sensitivity and temporal resolution [93, 99, 153]. RL sources for imaging are based on organic dyes and Raman devices and their emission is in the visible spectrum. We have tested different RLs based on Nd-doped powders as a source of bright and low coherence illumination for near infrared (NIR) speckle-fee single-shot imaging.

## 7.1 Experimental

The experimental set-up is shown in figure 7.1. The pump laser is again a Ti:sapphire pulsed laser and the beam is focused by a lens, $L1$, on a 0.5 mm diameter spot on the sample surface. The pump wavelength for each sample is set at its maximum absorbance peak, whereas the pump energy is always three times the threshold energy.

The chosen powder sample due to its low threshold and relatively high slope is made of $NdAl_3(BO_3)_4$ (see chapter 5). The other tested RL samples are $NdPO_4$, $NdGa_5O_{12}$, described also in chapter 5, and the non-stoichiometric samples Nd:$La_2O_2S$ and Nd:YAG of chapter 6.

After the pump beam irradiates the sample surface we place a lens to collect the reflected pump radiation and the RL emission and couple them into a 0.5 mm core diameter multi-mode optical fibre of 1 m length and NA 0.5. In order to optimize the amount of radiation collected by the fibre, the distances between of the sample

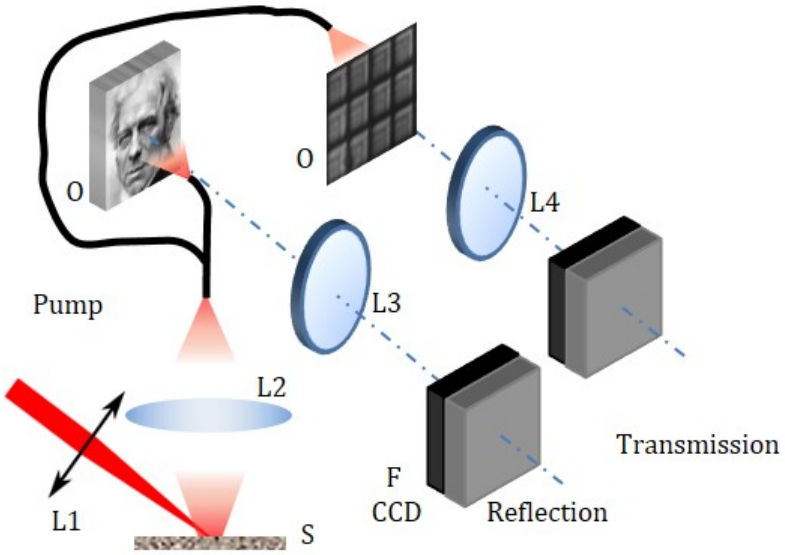


**Figure 7.1:** Set-up used for the infrared imaging. L1, lens for focusing pump beam; S, RL powder; L2, collecting lens; O, object for imaging, L3-L4, imaging lenses, F, Optical filters to remove pumping radiation or RL emission; CCD camera. [155]

and the fibre to the lens are set at twice the focal length, so the lateral magnification is one. Assuming a Lambertian emission from the sample surface, from equation 5.1, the energy collected by a lens with a circumference subtending an angle $\theta_0$ with respect to the normal to the surface is given by equation

$$E(r,\theta_0) = \int_0^{2\pi} d\varphi \int_0^{\theta_0} Mr^2 \sin\theta d\theta = E_{em}(1-\cos^2\theta_0) \tag{7.1}$$

where $\tan\theta_0 \simeq \varphi/2r$, $r$ is the distance between the sample surface and lens and $\varphi$ the lens diameter.

The collecting lens has a 32 mm focal length and 46 mm diameter. Under these conditions the energy captured by the fibre is around 10 % of the total emitted energy from the powder surface. After the fibre, the output radiation illuminates our object O – fibre head distance to the object is 50 mm – with an infrared single-shot and then this image is projected by a lens onto the surface of a CCD camera (LBP-3; Newport) with a sensitive area of 4.83 x 6.47 $mm^2$ by a lens. Before the CCD, optical filters are placed to remove either the pump or the RL radiation. By using this configuration, we obtain both transmitted and reflected images illuminated by the pump pulse and the RL pulse. It is important to remark that no spatial filters are used and that the fibre directly illuminates the object, without any diffuser [93]. All images are taken by illuminating with a single shot.

The size of the objects used for the reflected images is 25 mm and the lateral magnification is 0.2, fitting its image on the size of the CCD. The first image for the reflection study is a low-contrast printed portrait. Images of the portrait under the

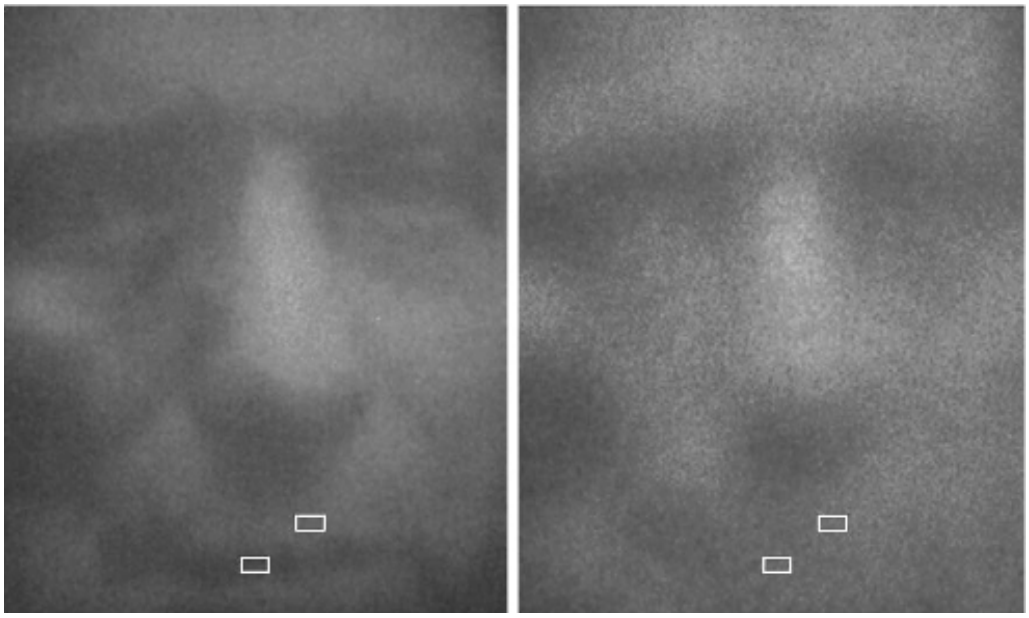

**Figure 7.2:** Single shot reflection images of a low contrast portrait obtained using the set-up in figure 7.1. Left: lighting up with RL emission. Right: Lighting up with the reflected pumping. The ROIs used for the CNR calculations are indicated. [155]

pump radiation lighting and RL lighting for different samples are shown in figures 7.2. It is evident the effect the speckle has on the quality of the images.

We measure the relative contrast between same sized regions of interests (ROIs), which gives information on the capability to clearly distinguish different features of an object. Hence,we can compare the quality of the images under different lighting. This relative contrast can be quantified by the contrast-to-noise ratio (CNR) as defined by Redding et al. [93] by

$$CNR = 2\frac{\langle I_{R1}\rangle - \langle I_{R2}\rangle}{\sigma_{R1} + \sigma_{R2}} \tag{7.2}$$

where $\langle I_{Ri}\rangle$ and $\sigma_{Ri}$ are the average intensities and standard deviations of the two selected ROIs.

We evaluate the CNR of the images with the ROIs in figure 7.2. The CNR of the image under RL illumination is 6 and 2 under the illumination with the reflected pump radiation. It is worth noticing that the later presents less speckle than expected because of the multimode fibre which decreases the spatial coherence of the radiation. Another set of images are taken with a different object, a pattern of white regions on a dark background. The magnification and lighting conditions are the same as in figure 7.2 for the borate powder. Figure 7.3 shows part of two images of this object under RL and reflected pump lighting. The CNR for the RL source image is 20 and 10 for the reflected pumping one. Finally, we take single-

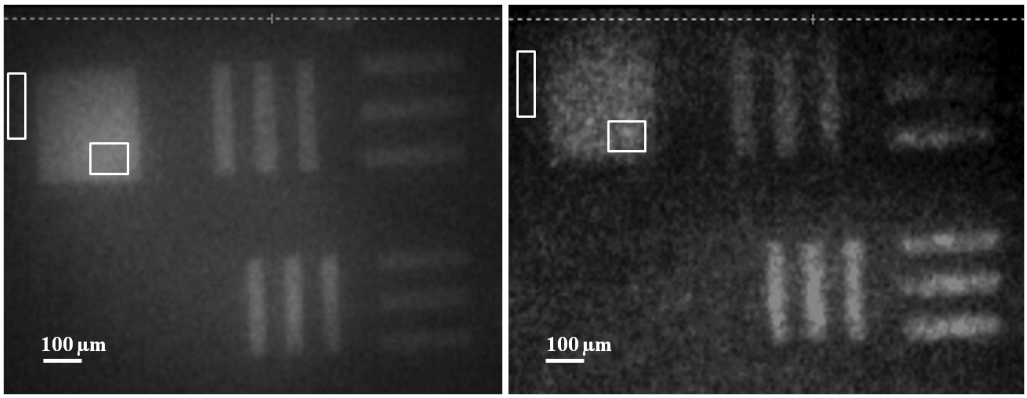


**Figure 7.3:** Single shot reflection images of a pattern obtained using the set-up in figure 7.1. Left: lighting up with RL emission. Right: Lighting up with the reflected pumping. The ROIs used for the CNR calculations are indicated. [155]

shot transmission images a slide of a grating smaller than 1 $mm^2$. The lateral magnification is 3. Figure 7.4 shows three images taken with the reflected pump light that exhibit a random speckle pattern whereas the image taken with an RL pulse presents a uniform pattern.

## 7.2 Summary and conclusions

We have experimentally proved the reliability of Nd doped RL lighting sources for speckle-free transmission and reflection infrared imaging, which is of great interest to perform high resolution imaging for optoelectronics and biomedical applications.

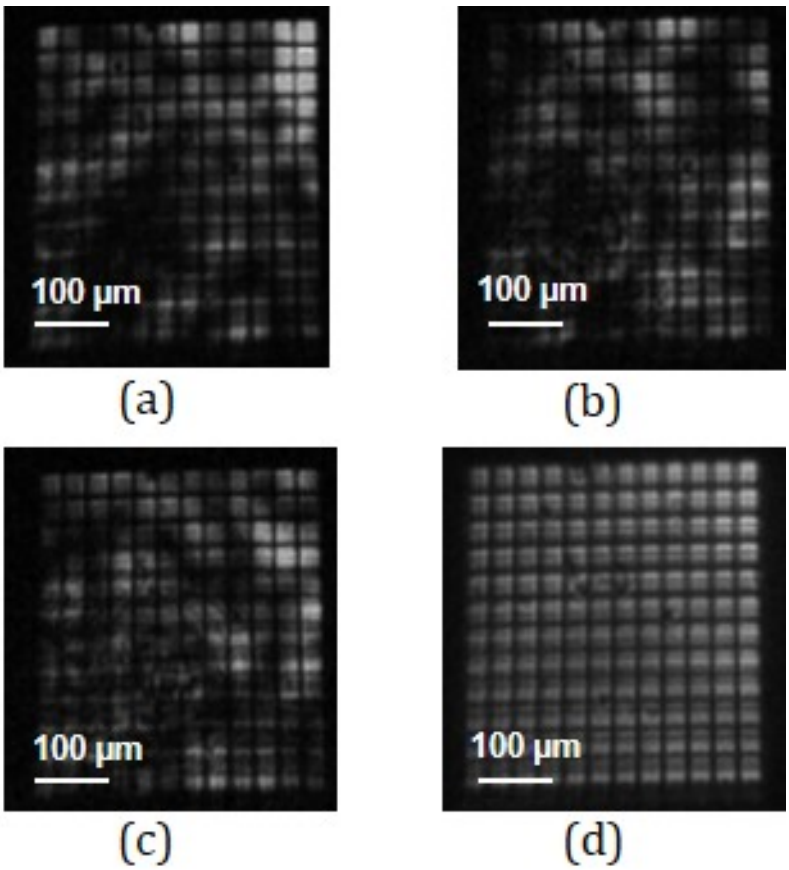


**Figure 7.4:** Single shot transmission images of a grid obtained using the set-up in figure 7.1. (a-c) Lighting up with the reflected pumping. (d) Lighting up with RL emission.[155]

# Chapter 8

# Optically induced inhomogeneous thermal behaviour of Er-doped oxysulfide powders

## 8.1 Introduction

We have analysed the thermal response of $Er^{3+}$-doped $La_2O_2S$ and $Gd_2O_2S$ crystal powders by exciting the $^4I_{9/2}$ level. After a transcient heating induced by the background absorption, cooling of discrete regions by means of anti-Stokes processes can be observed.

The possibility of cooling a material by anti-Stokes fluorescence was first described in 1929 by Pringsheim [156] and in 1950 Kastler [157] suggested that solid-state cooling by anti-Stokes emission (CASE) could be obteined in rare-earth crystals. Since the first solid-state CASE was demonstrated in 1995 in an $Yb^{3+}$ doped glass this phenomenon has been observed in many crystals, liquids and semiconductors. The interest on this effect lies on the potential applications: high power solid lasers in which no excess heat is generated and cryocoolers for aerospatial applications. Our group has been working on investigating host materials with rare-earth ions with low phonon energies to overcome the main limitations of the cooling efficiency, i.e., the nonradiative transitions between the energy level of the RE ion and the presence of impurities in the host matrix that gives rise to parasitic absorption generating heat [158]. Previous studies [159, 160] have shown that the cooling of these systems presents, due to its inhomogeneous nature, dependencies on the grain size and its spatial distribution; the diffusion of the pumping light in the sample by multiple scattering processes may create regions of localized energy where a cooling or heating effect can appear [158].

## 8.2 Thermal study of Er-doped $La_2O_2S$ and $Gd_2O_2S$ crystal powders

We first investigate the spectroscopic properties of the samples exciting them with a continuous wave (cw) Ti:sapphire laser (0.4 cm$^-$1 linewidth) in the 770-920 nm range to obtain the excitation spectra. The fluorescence is analysed with a 0.25 m monochromator and the signal detected by a photomultiplier (Hamamatsu R636) and amplified by a standard lock-in technique. We observe a weak peak at around 842 nm for both samples in the upconversion excitation spectrum of the green emission at 546 nm which does not appear neither in the infrared spectrum nor in the one-photon ground state absorption spectrum. The energy difference between the maximum of the spectrum and this peak corresponds to the energy carried out by one phonon of the host matrix, i.e., $\sim$ 400 cm$^-$1. Figure 8.1 shows the excitation spectra from levels $^4S_{3/2}$ (546 nm) and $^4F_{9/2}$ (665 nm) of the $La_2O_2S$ sample.

In addition, in order to explore the relation between $\lambda_{exc}$ and the sample temperature, we obtain the emission spectra by exciting in the low (842 nm) and the high (790 nm) energy sides of the excitation spectra of the $La_2O_2S$ sample. At these wavelengths, the pump power absorption is the same. The measurements show that the emission from level $^2H_{11/2}$ (842 nm) slightly increases with respect to the $^4S_{3/2}$ level by exiting at 790 nm at the high energy side of the $^4I_{15/2} \rightarrow^4 I_{9/2}$ absorption band. The sample temperature under 790 nm excitation is 4.1 K higher than under excitation at 842 nm, what suggests the possibility to obtain laser cooling under anti-Stokes excitation at 842 nm aided by upconversion processes. Therefore, we analyse the thermal response of the powders by pumping with a tunable femtosecond laser at 80 MHz (750 mW pump power at 842 nm) and recording with an infrared thermal camera (FLIR SC7500-MB) in the 2-5 - 5.1 µmeter spectral range with a 20 mK and scanning at 5 Hz. The powders are compacted in a cylindrical quartz cell 6 mm high and with a 6 mm diameter; the top of the cell is uncovered for the analysis. The average grain size is around 3 µm, although it is composed by smaller particulates of around 100 nm. The volume filling factor of the cell if $f = 0.15$.

The samples are placed in low vacuum inside a cryostat chamber with a wide NIR transparent window; the camera is focused on the sample surface. The absolute temperature of the sample is calibrated with a thermocouple. Figure 8.2 and figure 8.5 show video frames of the $La_2O_2S$ and $Gd_2O_2S$ samples, respectively, after irradiation. As can be seen, the temperature distribution is rather inhomogeneous showing a sharp distribution of hot spots. Although the excitation beam profile is Gaussian, due to the inhomogeneous nature of crystal powders, the light diffusion of the pumping light inside the sample, induced by multiple scattering processes, may produce localized-like energy regions inside the sample and, as a consequence, subsequent cooling or heating discrete zones. Some of the heated areas appear far away from the pumped zone showing that light diffusion operates both for the pumping and radiated thermal light. The thermal pattern remains quite the same all along

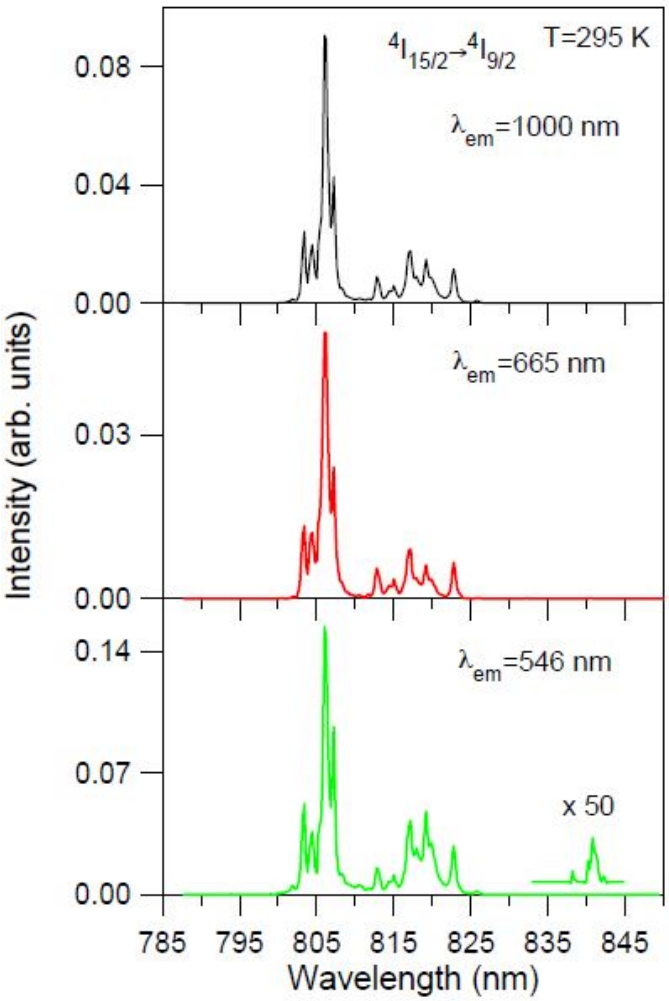


**Figure 8.1:** Excitation spectra of the upconverted emission from levels $^4S_{3/2}$ (546 nm) and $^4F_{9/2}$ (665 nm) of the $La_2O_2S$ sample, corrected for the spectral variation of the laser intensity. The ground state excitation spectrum corresponding to $^4I_{11/2} \rightarrow ^4 I_{15/2}$ transition is also included for comparison. [158]

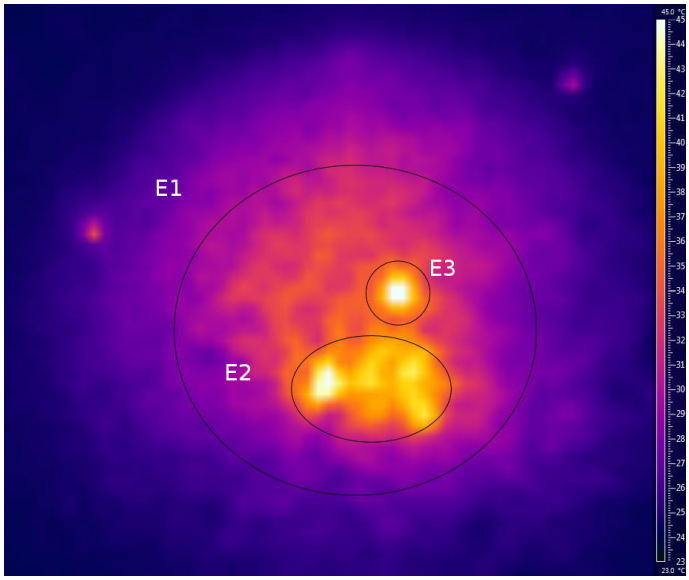


**Figure 8.2:** Thermal camera frame showing discrete zone after pumping at 842 nm with 300 mW in a 2 mol% $Er^{3+}$ doped $La_2O_2S$ sample.[158]

the experiment. Figure 8.3 displays the average temperature as a function of time measured in the three areas of the $La_2O_2S$ sample. Initially, the temperature of the sample rises in all these areas from room temperature (24°C) until it reaches a stationary regime when the thermal load deposited on the material is compensated by the fluorescent losses. In the hot zone, E2, the temperature falls by 2°C in 40 minutes, whereas in the wider one, E1, the average temperature drops about 0.5°C in the same period. These results are in good agreement with the expected random propagation of radiation in a region with a randomly distributed dielectric constant. Moreover, the static disorder produces well defined propagation modes inside the sample, in agreement with the discrete static heating observed at the sample surface. It is worthy to point out that the average temperature of the sample may cool after the initial transient heating, induced by the background absorption, due to the infrared-to-visible up-conversion processes that can offset the heat load deposited in the doped powder.

As we have already mentioned, by using the obtained relation between the integrated fluorescence intensity ratio of transitions ${}^2H_{11/2} \rightarrow {}^4 I_{15/2}$ and ${}^4S_{3/2} \rightarrow {}^4 I_{15/2}$ and temperature, the sample temperature when exciting at 790 nm is 4.1 K higher than under excitation at 842 nm. A similar temperature difference is observed in the thermal response of the sample under excitation in the Stokes (790 nm) and anti-Stokes (842 nm) side of the absorption band. Figure 8.4 shows the comparison of the thermal response of the $La_2O_2S$ sample when excited at 790 nm, in the Stokes side (black line) of the absorption spectrum, and in the cooling region, at 842 nm (red line), under the same experimental conditions with a pump power of 700mW. The figure clearly shows the different thermal behaviour of the sample in the heating and cooling regions.

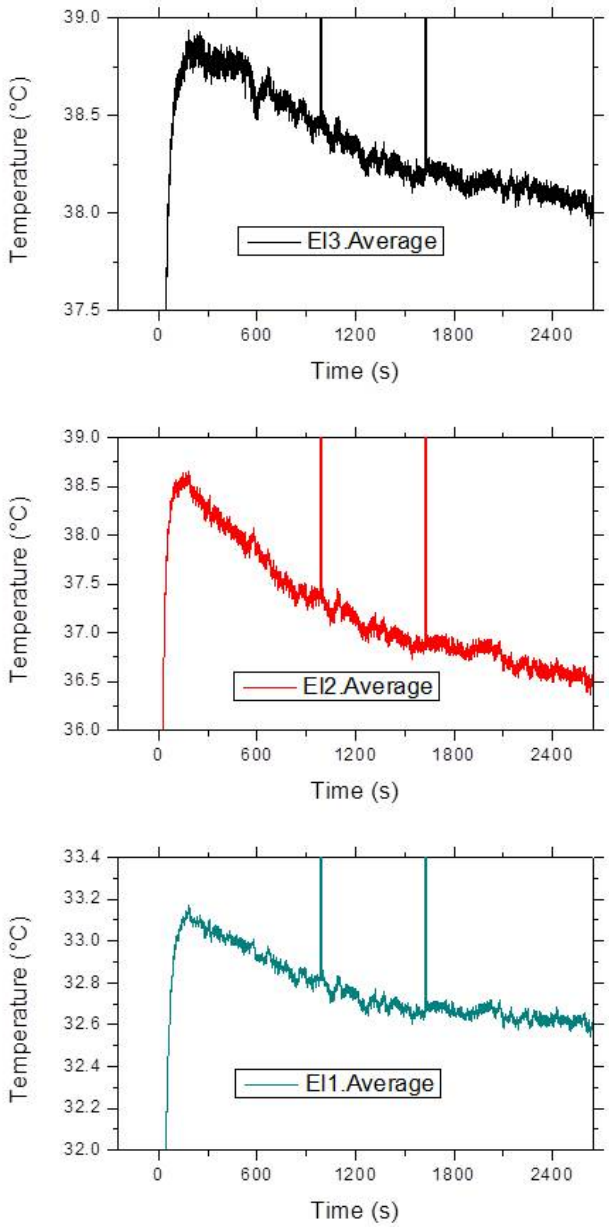


**Figure 8.3:** Average temperature as a function of time measured in the three shown zones. [158]

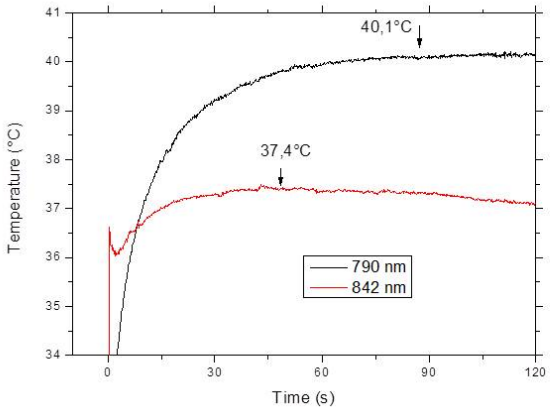


**Figure 8.4:** Comparison of the thermal response of the sample when excited at 790 nm, in the Stokes side (black line) of the absorption spectrum and in the cooling region, at 842 nm (red line), under the same experimental conditions with 700mW. [158]

From the point of view of potential applications, it is worth noticing that although the relative cooling in these regions is small, the cooling processes involved in the rare earth-doped samples may be enough to avoid the burning of the sample at high excitation fluencies, as has been experimentally proved by comparing the behaviour of doped and undoped samples.

Figure 8.6 shows the temperature increase of the $Gd_2O_2S$ powders, above the initial temperature of the cell (24°C), of $Ge_2O_2S$ oxysulfide powders doped with different amounts of erbium (0, 1, 2, 3 mol%) pumped at 100, 200 and 300 mW. As can be seen, no net cooling is detected at long term when the Er-doped samples attain equilibrium. However, it is worthy to mention that the final temperature increase in the doped samples is about half the temperature of the undoped one. Moreover, it is also remarkable that pumping at 300 mW, the lowest equilibrium temperature, corresponds to the heaviest doped sample. For comparison, Fig. 8.6(e-f) show the behaviour of a 3 mol% Er-doped lanthanum oxysulfide powder. As can be observed, it is quite similar to the one of the corresponding gadolinium oxysulfide sample, though the equilibrium temperature is a little higher.

Bulk thermal measurements performed on the powder samples by using a thermal infra-red camera show a very inhomogeneous heat distribution at the sample surface due to the random distribution of the pumping energy inside the sample as well as to the random propagation of the emitted thermal field. The analysis of both spectroscopic and thermal measurements shows that after a transient heating induced by the background absorption, a reduced heating can be attained by means of anti-Stokes processes in the erbium-doped samples.

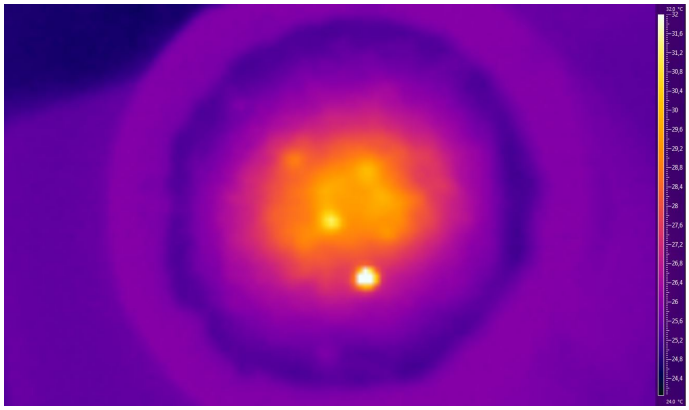

**Figure 8.5:** Thermal camera frame showing discrete zone after pumping at 842 nm with 750 mW in a 2 mol% $Er^{3+}$ doped $Gd_2O_2S$ sample. [161]

## 8.3 Summary and conclusions

We have performed thermal measurements in Er-doped powder samples with a thermal camera that exhibits a very inhomogeneous heat distribution at the sample surfaces. These inhomogeneities are caused by the random distribution of the pumping energy inside the powder sample and the random propagation of the emitted thermal field. In addition, the thermal measurements show local cooling and a reduced heating by means of anti-Stokes processes after a transient heating induced by the background absorption. Although the relative cooling of these regions is small this effect may be enough to avoid the burning of the samples at high excitation fluencies, as we have shown by comparing the behaviour of doped and undoped samples.

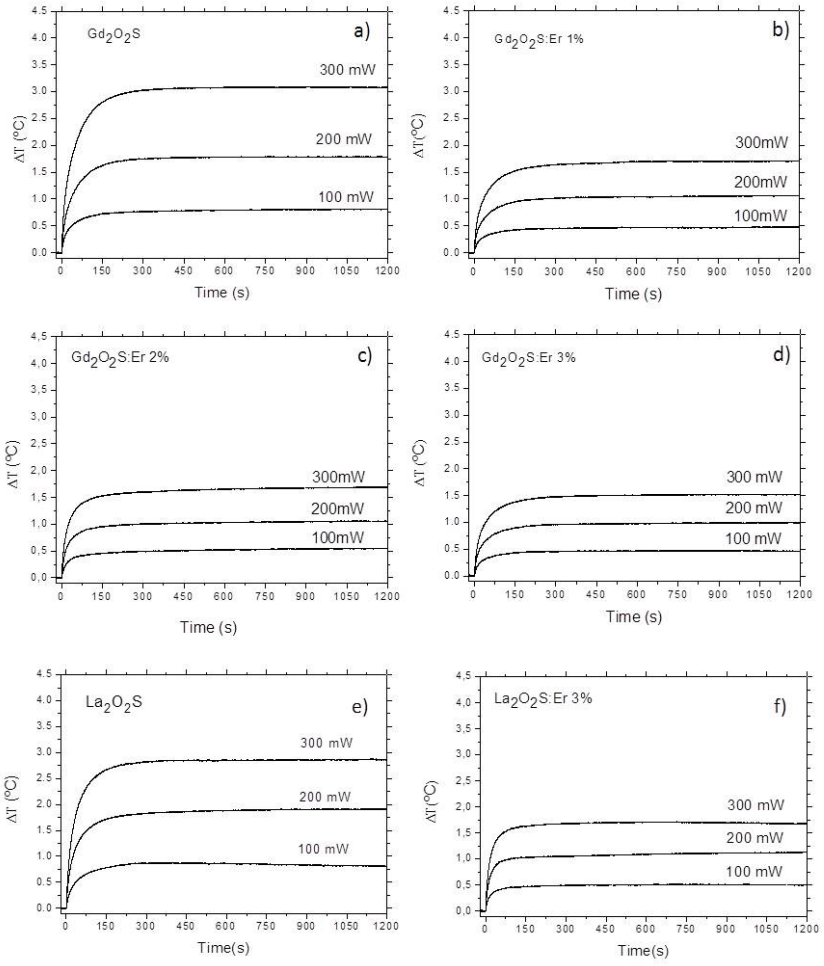


**Figure 8.6:** (a-d) Temperature increase of $Gd_2O_2S$ oxysulfide powders doped with different amounts of Er (0, 1, 2, 3 mol%) pumped at 100, 200 and 300 mW. (e-f) Temperature increase of $La_2O_2S$ oxysulfide powders doped with 0 and 3mol% Er pumped at 100, 200 and 300 mW. [161]

# Summary and conclusions

In Part I, thanks to the developing of a spatial filtering we have been able to study the modal dynamics and the spatial coherence of a diffusive random laser with static disorder based on a di-ureasil hybrid powder doped with Rhodamine B. Several features have been observed:

- Changes in the pump energy and the size of the emitting area can increase mode coupling, changing the structure of the emission.
- Discrete lasing spikes from non overlapping cavities appear after reducing the spatially overlapping modes by decreasing the area of the detected emitting surface while keeping the size of the gain medium constant.
- When no spatial filter is used the emission shows a smooth profile even in a single shot measurement and for our 30 ps Nd:YAG excitation laser.
- Reducing the focusing diameter of the pump beam decreases the spike density, while an intensification of the excitation energy activates lasing modes with larger thresholds, thus enhancing the modal density.
- Both the temporal and the spectral emission of the sample show a stochastic behaviour. The modes appear to form in different cavities as they are turned on at different times in successive shots.
- Under OP pumping the build-up time (12 ps) is one order of magnitude lower than the one under TP pumping, while the threshold is three orders of magnitude lower for the OP case. In addition, the pulses under OP pumping can be as short as the pump pulse but under TP pumping they get longer (93 - 147 ps). These differences can be explained by the lower TP effective pump density which increases the mode lasing thresholds.
- The diffusion processes dominate over the amplification ones on the spatial emission. Hence, the emitting area is larger than the pumped surface; teh laser modes are not restricted to the excited region.
- A high degree of temporal coherence of the system has been found.

Analysing the emission of different inorganic powders doped with Nd under nanosecond pumping we observe the following behaviour

- The laser slope is proportional to the absorption of the material and the constant of proportionality is the quotient between the pump and the emission wavelengths. This means that almost all pump photons with an energy over the threshold are converted into stimulated emission photons.
- If the pump diameter is much longer than the absorption length neither the slope nor the threshold energy density depend on the pump diameter.
- The emission intensity above threshold follows the pump pulse with a delay of the order of 100 ps in the case of low-doped samples and one order of magnitud lower for the non-stoichiometric samples.
- Changes in the pumped volume, i.e., in the population inversion, are compensated by changes in the residence length and not by the inelastic length.
- We have assessed the reliability of these RL sources for speckle-free infrared imaging.

# Publications

This thesis has contributed to the following publications and communications.

## Refereed Contributions

1. J. Azkargorta, I. Iparraguirre, M. Bettinelli, E. Cavalli, **M. Barredo-Zuriarrain**, S. García-Revilla, R. Balda, and J. Fernández, "Effects of pumping wavelength and pump density on the random laser performance of stoichiometric Nd crystal powders," *Opt. Express*, vol. 22, no. 22, p. 27365, 2014.

2. S. García-Revilla, J. Fernández, **M. Barredo-Zuriarrain**, L. D. Carlos, E. Pecoraro, I. Iparraguirre, J. Azkargorta, and R. Balda, "Diffusive random laser modes under a spatiotemporal scope," *Opt. Express*, vol. 23, no. 2, p. 1456, 2015.

3. S. García-Revilla, J. Fernández, **M. Barredo-Zuriarrain**, L. D. Carlos, E. Pecoraro, I. Iparraguirre, J. Azkargorta, and R. Balda, "Spectral dynamics of a diffusive random laser under two photon pumping," *Adv. Device Mater.*, vol. 1, pp. 3845, 2015.

4. S. García-Revilla, J. Fernández, **M. Barredo-Zuriarrain**, and E. Pecoraro, "Coherence characteristics of random lasing in a dye doped hybrid powder," *J. Lumin.*, vol. 169, pp. 472477, 2016.

5. I. Iparraguirre, J. Azkargorta, K. Kamada, A. Yoshikawa, U. R. Rodríguez-Mendoza, V. Lavín, **M. Barredo-Zuriarrain**, R. Balda, and J. Fernández, "Random laser action in stoichiometric $Nd_3Ga_5O_{12}$ garnet crystal powder," *Laser Phys. Lett.*, vol. 13, p. 035402, 2016.

6. J. Azkargorta, I. Iparraguirre, **M. Barredo-Zuriarrain**, S. García-Revilla, R. Balda, and J. Fernández, "Random Laser Action in Nd:YAG Crystal Powder," *Materials (Basel).*, vol. 9, no. 5, p. 369, 2016.

7. J. Azkargorta, L. Marciniak, I. Iparraguirre, R. Balda, W. Strek, **M. Barredo-Zuriarrain**, S. García-Revilla, and J. Fernández, "Influence of grain size and

$Nd^{3+}$ concentration on the stimulated emission of $LiLa_{1-x}Nd_xP_4O_{12}$ crystal powders," *Opt. Mater. (Amst).*, pp. 38, 2016.

8. R. Balda, N. Hakmeh, **M. Barredo-Zuriarrain**, O. Merdrignac-Conanec, S. García-Revilla, M. A. Arriandiaga, and J. Fernández, "Influence of Upconversion Processes in the Optically-Induced Inhomogeneous Thermal Behavior of Erbium-Doped Lanthanum Oxysulfide Powders," *Materials (Basel).*, vol. 9, no. 353, p. 13, 2016.

9. **M. Barredo-Zuriarrain**, I. Iparraguirre, J. Fernández, R. M. Balachandran, and R. Balda, "Speckle-free near-infrared imaging using a $Nd^{3+}$ random laser source," *Laser Phys. Lett.* Accepted.

## Non-Refereed Contributions

1. J. Fernández, R. Balda, **M. Barredo-Zuriarrain**, O. Merdrignac-Conanec, N. Hakmeh, S. García-Revilla, and M. A. Arriandiaga, "Spectroscopic and thermal study of Er-doped oxysulfide crystal powders," in *Proceedings of SPIE*, 2015, vol. 9380, pp. 110.

2. J. Azkargorta, L. Marciniak, I. Iparraguirre, R. Balda, W. Strek, **M. Barredo-Zuriarrain**, S. García-Revilla, and J. Fernández, "Random lasing of $LiLa_{1-x}Nd_xP_4O_{12}$ crystal powders," in *ICTON*, 2016.

3. J. Fernández, R. Balda, **M. Barredo-Zuriarrain**, O. Merdrignac-Conanec, N. Hakmeh, and S. García-Revilla, "Progress in the spectroscopic and thermal studies of Er-doped oxysulfide crystal powders," in *Proceedings of SPIE*, 2016, vol. 9765, pp. 111.

# Bibliography


[1] J. Andreasen, N. Bachelard, S. B. N. Bhaktha, H. Cao, P. Sebbah, and C. Vanneste, "Partially Pumped Random Lasers", *International Journal of Modern Physics B*, vol. 28, no. 05, p. 1 430 001, Feb. 2014. DOI: 10.1142/S0217979214300011.

[2] R. V. Ambartsumyan, N. G. Basov, P. G. Kryukov, and V. S. Letokhov, "Laser with nonresonant feedback", *JETP Letters*, vol. 3, pp. 167–169, 1966.

[3] R. V. Ambartsumyan, B. N. G, P. G. Kryukov, and V. S. Letokhov, "Nonresonant feedback in lasers", in *Progress in Quantum Electronics, Vol. 1*, J. H. Sanders and S. K. W. H, Eds., New York: Pergamon, 1970, pp. 107–185.

[4] V. S. Letokhov, "Stimulated emission of an ensemble of scattering particles with negative absorption", *JETP Letters*, no. 8, pp. 212–215, 1967.

[5] ——, "Generation of light by a scattering medium with negative resonance absorption", *Soviet Physics JETP*, vol. 26, no. 4, pp. 835–840, 1968.

[6] M. A. Noginov, *Solid-State Random Lasers*, Springer, Ed. New York, 2005.

[7] F. Varsanyi, "Surface lasers", *Applied Physics Letters*, vol. 19, no. 1971, pp. 169–171, 1971. DOI: 10.1063/1.1653870.

[8] V. M. Markushev, V. F. Zolin, and C. M. Briskina, "Powder Laser", *Zhurnal Prikladnoi Spektroskopii*, vol. 45, pp. 847–850, 1986.

[9] V. M. Markushev, V. F. Zolin, and C. M. Briskina, "Luminescence and stimulated emission of neodymium in sodium lanthanum molybdate powders", *Soviet Journal of Quantum Electronics*, vol. 16, no. 2, pp. 281–283, 1986. DOI: 10.1070/QE1986v016n02ABEH005792.

[10] V. F. Zolin, "The nature of plaser-powdered laser", *Journal of Alloys and Compounds*, vol. 300, pp. 214–217, 2000. DOI: 10.1016/S0925-8388(99)00772-0.

[11] H. Cao, Y. G. Zhao, H. C. Ong, S. T. Ho, J. Y. Dai, J. Y. Wu, and R. P. H. Chang, "Ultraviolet lasing in resonators formed by scattering in semiconductor polycrystalline films", *Applied Physics Letters*, vol. 73, no. 25, pp. 3656–3658, 1998. DOI: 10.1063/1.122853.

[12] H. Cao, "Random Lasers with Coherent Feedback", *Topics in Applied Physics*, vol. 82, pp. 303–330, 2002.

[13] H. Cao, J. Y. Xu, Y. Ling, A. L. Burin, E. W. Seeling, X. Liu, and R. P. H. Chang, "Random lasers with coherent feedback", *IEEE Journal on Selected Topics in Quantum Electronics*, vol. 9, no. 1, pp. 111–119, 2003. DOI: 10.1109/JSTQE.2002.807975.

[14] C. Gouedard, D. Husson, C. Sauteret, F. Auzel, and A. Migus, "Generation of spatially incoherent short pulses in laser-pumped neodymium stoichiometric crystals and powders", *Journal of the Optical Society of America B*, vol. 10, no. 12, p. 2358, Dec. 1993. DOI: 10.1364/JOSAB.10.002358.

[15] M. A. Noginov, N. Noginova, S. U. Egarievwe, H. J. Caulfield, C. Cochrane, J. C. Wang, M. R. Kokta, and J. Paitz, "Study of the pumping regimes in Ti-sapphire and Nd0.5La0.5Al3(BO3)4 powders", *Optical Materials*, vol. 10, no. September, pp. 297–303, 1998.

[16] M. A. Illarramendi, C. Cascales, I. Aramburu, R. Balda, V. Orera, and J. Fernández, "Characterization of light propagation in $Nd_xY_{1-x}Al(BO_3)_4$ laser crystal powders", *Optical Materials*, vol. 30, no. 1, pp. 126–128, 2007. DOI: 10.1016/j.optmat.2006.11.038.

[17] N. M. Lawandy, R. M. Balachandran, A. S. L. Gomes, and E. Sauvai, "Laser action in strongly scattering media", *Nature*, 1994.

[18] L. Cerdán, A. Costela, E. Enciso, and I. García-Moreno, "Random Lasing in Self-Assembled Dye-Doped Latex Nanoparticles: Packing Density Effects", *Advanced Functional Materials*, vol. 23, no. 31, pp. 3916–3924, Aug. 2013. DOI: 10.1002/adfm.201202616.

[19] A. Yadav, L. Zhong, J. Sun, L. Jiang, G. J. Cheng, and L. Chi, "Tunable random lasing behavior in plasmonic nanostructures", *Nano Convergence*, vol. 4, no. 1, p. 1, 2017. DOI: 10.1186/s40580-016-0095-5.

[20] V. V. Ursaki, A. Burlacu, E. V. Rusu, V. Postolake, and I. M. Tiginyanu, "Whispering gallery modes and random lasing in ZnO microstructures", *Journal of Optics A: Pure and Applied Optics*, vol. 11, p. 075 001, 2009. DOI: 10.1088/1464-4258/11/7/075001.

[21] S. K. Turitsyn, S. A. Babin, D. V. Churkin, I. D. Vatnik, M. Nikulin, and E. V. Podivilov, "Random distributed feedback fibre lasers", *Nature Photonics*, 2010. DOI: 10.1016/j.physrep.2014.02.011.

[22] C. J. S. De Matos, L. De S. Menezes, A. M. Brito-Silva, M. A. Martinez Gomez, A. S. L. Gomes, and C. B. De Araujo, "Random fiber laser", *Physical Review Letters*, vol. 99, no. 15, pp. 1–4, 2007. DOI: 10.1103/PhysRevLett.99.153903. arXiv: 0706.4445.

[23] H. Wu, Z. Wang, Q. He, M. Fan, Y. Li, and W. Sun, "Polarization-modulated random fiber laser", *Laser Physics Letters*, vol. 055101, pp. 0–4, 2016. DOI: 10.1088/1612-2011/13/5/055101.

[24] R. C. Polson and Z. V. Vardeny, "Random lasing in human tissues", *Applied Physics Letters*, vol. 85, no. 7, pp. 1289–1291, 2004. DOI: 10.1063/1.1782259.

[25] F. Lahoz, I. R. Martín, M. Urgellés, J. Marrero-Alonso, R. Marín, C. J. Saavedra, A. Boto, and M. Díaz, "Random laser in biological tissues impregnated with a fluorescent anticancer drug", *Laser Physics Letters*, vol. 12, no. 4, p. 045 805, 2015. DOI: 10.1088/1612-2011/12/4/045805.

[26] A. Smuk, E. Lazaro, L. P. Olson, and N. M. Lawandy, "Random laser action in bovine semen", *Optics Communications*, vol. 284, no. 5, pp. 1257–1258, 2011. DOI: 10.1016/j.optcom.2010.11.004.

[27] D. Huang, M. Xu, X. Liu, M. Yang, T. Yi, C. Wang, T. Li, and S. Liu, "Low threshold random lasing actions in natural biological membranes", *Laser Physics Letters*, vol. 13, no. 3, p. 065 603, 2016. DOI: 10.1088/1612-2011/13/6/065603.

[28] Y.-C. Chen, Q. Chen, and X. Fan, "Lasing in blood", *Optica*, vol. 3, no. 8, p. 809, 2016. DOI: 10.1364/OPTICA.3.000809.

[29] X. Liu, T. Li, T. Yi, C. Wang, J. Li, M. Xu, D. Huang, S. Liu, S. Jiang, and Y. Ding, "Random laser action from a natural flexible biomembrane-based device", *Journal of Modern Optics*, vol. 0340, no. January, pp. 1–6, 2016. DOI: 10.1080/09500340.2015.1136002.

[30] L. M. G. Abegão, A. A. C. Pagani, S. C. Zílio, M. A.R. C. Alencar, and J. J. Rodrigues, "Measuring milk fat content by random laser emission.", *Scientific reports*, vol. 6, p. 35 119, 2016. DOI: 10.1038/srep35119.

[31] J. Lü, T. Fan, and G. Chen, "Random laser action in dye doped nanoporous polymeric film", *Optics Communications*, vol. 356, pp. 17–20, 2015. DOI: 10.1016/j.optcom.2015.07.041.

[32] A. Consoli, D. Mariano, N. U. Wetter, and C. López, "Large area resonant feedback random lasers based on dye-doped biopolymer films", *Optics Express*, vol. 23, no. 23, pp. 303–310, 2015. DOI: 10.1364/OE.23.029954.

[33] L. Sznitko, A. Szukalski, K. Cyprych, P. Karpinski, A. Miniewicz, and J. Mysliwiec, "Surface roughness induced random lasing in bio-polymeric dye doped film", *Chemical Physics Letters*, vol. 576, pp. 31–34, 2013. DOI: 10.1016/j.cplett.2013.05.018.

[34] I. Viola, N. Ghofraniha, A. Zacheo, V. Arima, C. Conti, and G. Gigli, "Random laser emission from a paper-based device", *Journal of Materials Chemistry C*, vol. 1, no. 48, pp. 8128–8133, 2013. DOI: 10.1039/c3tc31860e.

[35] A. S. Kwok, A. Serpenguzel, W. F. Hsieh, R. K. Chang, and J. B. Gillespie, "Two-photon-pumped lasing in microdroplets.", *Optics letters*, vol. 17, no. 20, p. 1435, 1992. DOI: 10.1364/OL.17.001435.

[36] A. K. Tiwari, R. Uppu, and S. Mujumdar, "Aerosol-based coherent random laser", *Optics Letters*, vol. 37, no. 6, p. 1053, 2012.

[37] M. A. Noginov, H. J. Caulfield, N. E. Noginova, and P. Venkateswarlu, "Line narrowing in the dye solution with scattering centers", *Optics Communications*, vol. 118, no. 3-4, pp. 430–437, 1995. DOI: 10.1016/0030-4018(95)00177-A.

[38] B. He, Q. Liao, and Y. Huang, "Random lasing in a dye doped cholesteric liquid crystal polymer solution", *Optical Materials*, vol. 31, no. 2, pp. 375–379, 2008. DOI: 10.1016/j.optmat.2008.05.014.

[39] C.-R. Lee, J.-D. Lin, B.-Y. Huang, S.-H. Lin, T.-S. Mo, S.-Y. Huang, C.-T. Kuo, and H.-C. Yeh, "Electrically controllable liquid crystal random lasers below the Fréedericksz transition threshold.", *Optics express*, vol. 19, no. 3, pp. 2391–400, 2011. DOI: 10.1364/OE.19.002391.

[40] P. J. W. Hands, D. J. Gardiner, S. M. Morris, C. Mowatt, T. D. Wilkinson, and H. J. Coles, "Band-edge and random lasing in paintable liquid crystal emulsions", *Applied Physics Letters*, vol. 98, no. May, pp. 1–3, 2011. DOI: 10.1063/1.3574915.

[41] J.-L. Zhu, W.-H. Li, Y. Sun, J.-G. Lu, X.-L. Song, C.-Y. Chen, Z. Zhang, and Y. Su, "Random laser emission in a sphere-phase liquid crystal", *Applied Physics Letters*, vol. 106, no. 19, p. 191 903, 2015. DOI: 10.1063/1.4921325.

[42] G Strangi, S Ferjani, V Barna, A De Luca, C Versace, N Scaramuzza, and R Bartolino, "Random lasing and weak localization of light in dye-doped nematic liquid crystals.", *Optics express*, vol. 14, no. 17, pp. 7737–7744, 2006. DOI: 10.1364/OE.14.007737.

[43] F. Yao, H. Bian, Y. Pei, C. Hou, and X. Sun, "Behaviors of random laser in dye-doped nematic liquid crystals", *Optics Communications*, vol. 359, pp. 15–19, 2016. DOI: 10.1016/j.optcom.2015.09.053.

[44] K. L. van der Molen, A. P. Mosk, and A. Lagendijk, "Quantitative analysis of several random lasers", *Optics Communications*, vol. 278, no. 1, pp. 110–113, 2007. DOI: 10.1016/j.optcom.2007.05.047.

[45] J. Fernández, S. García-Revilla, and R. Balda, "Real-Time Spectroscopy of Solid-State Random Lasers", in *Biophotonics: Spectroscopy, Imaging, Sensing, and Manipulation*, B Di Bartolo, Ed., Springer Science, 2011, pp. 321–342. DOI: 10.1007/978-90-481-9977-8.

[46] H. Cao, "Lasing in random media", *Waves in Random Media*, vol. 13, no. 3, R1–R39, 2003.

[47] G. Berger, M. Kempe, and a. Genack, "Dynamics of stimulated emission from random media", *Physical Review E*, vol. 56, no. 5, pp. 6118–6122, 1997. DOI: 10.1103/PhysRevE.56.6118.

[48] M. A. Noginov, I. N. Fowlkes, G. Zhu, and J. Novak, "Random laser thresholds in cw and pulsed regimes", *Physical Review A - Atomic, Molecular, and Optical Physics*, vol. 70, no. 4, pp. 1–5, 2004. DOI: 10.1103/PhysRevA.70.043811.

[49] M. A. Noginov, J. Novak, and S. Williams, "Modeling of photon density dynamics in random lasers", *Physical Review A - Atomic, Molecular, and Optical Physics*, vol. 70, no. 6, pp. 1–5, 2004. DOI: 10.1103/PhysRevA.70.063810.

[50] J. Azkargorta, M. Bettinelli, I. Iparraguirre, and R. Balda, "Random lasing in Nd:$LuVO_4$ crystal powder", *Optics Express*, vol. 19, no. 20, p. 19 591, 2011. DOI: 10.1016/j.optmat.2011.03.047.C..

[51] R. M. Balachandran, N. M. Lawandy, and J. A. Moon, "Theory of laser action in scattering gain media.", *Optics letters*, vol. 22, no. 5, pp. 319–321, 1997. DOI: 10.1364/OL.22.000319.

[52] R. Uppu and S. Mujumdar, "Physical manifestation of extreme events in random lasers", *Optics Letters*, vol. 40, no. 21, pp. 5046–5049, 2015.

[53] J. Fallert, R. J. B. Dietz, J. Sartor, D. Schneider, C. Klingshirn, and H. Kalt, "Co-existence of strongly and weakly localized random laser modes", *Nature Photonics*, vol. 3, no. April, pp. 279–282, 2009. DOI: 10.1038/nphoton.2009.67.

[54] E. Ignesti, F. Tommasi, L. Fini, S. Lepri, V. Radhalakshmi, D. Wiersma, and S. Cavalieri, "Experimental and theoretical investigation of statistical regimes in random laser emission", *Physical Review A - Atomic, Molecular, and Optical Physics*, vol. 88, no. 3, pp. 1–7, 2013. DOI: 10.1103/PhysRevA.88.033820. arXiv: 1309.2412.

[55] S. John and G. Pang, "Theory of lasing in a multiple-scattering medium", *Physical Review A*, vol. 54, no. 4, pp. 3642–3652, 1996.

[56] D. Wiersma and A. Lagendijk, "Light diffusion with gain and random lasers", *Physical Review E Statistical Physics Plasmas Fluids And Related Interdisciplinary Topics*, vol. 54, no. 4, pp. 4256–4265, 1996.

[57] H. Cao, Y Zhao, S Ho, E Seelig, Q Wang, and R Chang, "Random Laser Action in Semiconductor Powder", *Physical Review Letters*, vol. 82, no. 11, pp. 2278–2281, 1999.

[58] H. Cao, Y Ling, J. Y. Xu, C. Q. Cao, and P. Kumar, "Photon statistics of random lasers with resonant feedback", *Physical Review Letters*, vol. 86, no. 20, pp. 4524–4527, May 2001. DOI: 10.1103/PhysRevLett.86.4524.

[59] H. Cao, J. Xu, D. Zhang, S Chang, S. Ho, E. Seelig, X. Liu, and R. Chang, "Spatial confinement of laser light in active random media", *Physical Review Letters*, vol. 84, no. 24, pp. 5584–7, 2000.

[60] X. Jiang and C. M. Soukoulis, "Time Dependent Theory for Random Lasers", *Physical Review Letters*, vol. 85, no. 1, p. 8, 2000.

[61] C. Vanneste and P. Sebbah, "Selective Excitation of Localized Modes in Active Random Media", *Physical Review Letters*, vol. 87, no. 18, p. 183 903, Oct. 2001. DOI: 10.1103/PhysRevLett.87.183903.

[62] R. C. Polson, A. Chipouline, and Z. V. Vardeny, "Random lasing in pi-conjugated films and infiltrated opals", *Advanced Materials*, vol. 13, no. 10, pp. 760–764, 2001.

[63] S. Mujumdar, M. Ricci, R. Torre, and D. Wiersma, "Amplified Extended Modes in Random Lasers", *Physical Review Letters*, vol. 93, no. 5, p. 053 903, Jul. 2004. DOI: 10.1103/PhysRevLett.93.053903.

[64] A. Ishimaru, *Wave propagation and scattering in random media*. IEEE Press, 1997, p. 574.

[65] V. M. Apalkov, M. E. Raikh, and B. Shapiro, "Random resonators and prelocalized modes in disordered dielectric films", *Physical Review Letters*, vol. 89, no. 1, pp. 168 021–168 024, 2002. DOI: 10.1103/PhysRevLett.89.016802. arXiv: 0111047 [cond-mat].

[66] R. C. Polson, M. E. Raikh, and Z. V. Vardeny, "Random Lasing from Weakly Scattering Media: Universality in the Emission Spectra from Pi-Conjugated Polymer Films", *Physica E*, vol. 13, pp. 1240–1242, 2002. arXiv: 0105360 [cond-mat].

[67] R. C. Polson, M. Raikh, and Z. Vardeny, "Universal properties of random lasers", *IEEE Journal of Selected Topics in Quantum Electronics*, vol. 9, no. 1, pp. 120–123, Jan. 2003. DOI: 10.1109/JSTQE.2002.807970.

[68] X. Wu, W. Fang, A. Yamilov, A. Chabanov, A. A. Asatryan, L. Botten, and H. Cao, "Random lasing in weakly scattering systems", *Physical Review A*, vol. 74, no. 5, p. 053 812, Nov. 2006. DOI: 10.1103/PhysRevA.74.053812.

[69] S. Mujumdar, V. Türck, R. Torre, and D. S. Wiersma, "Chaotic behavior of a random laser with static disorder", *Physical Review A - Atomic, Molecular, and Optical Physics*, vol. 76, no. 3, pp. 1–6, 2007. DOI: 10.1103/PhysRevA.76.033807.

[70] A. A. Chabanov, Z. Q. Zhang, and A. Z. Genack, "Breakdown of diffusion in dynamics of extended waves in mesoscopic media.", *Physical review letters*, vol. 90, no. 20, p. 203 903, 2003. DOI: 10.1103/PhysRevLett.90.203903. arXiv: 0211651 [cond-mat].

[71] H. Cao, X. Jiang, Y Ling, J. Y. Xu, and C. M. Soukoulis, "Mode repulsion and mode coupling in random lasers", *Physical Review B Condensed Matter*, vol. 67, no. 16, pp. 161 101–161 104, Apr. 2003. DOI: 10.1103/PhysRevB.67.161101.

[72] X. Jiang, S. Feng, C. Soukoulis, J. Zi, J. Joannopoulos, and H. Cao, "Coupling, competition, and stability of modes in random lasers", *Physical Review B*, vol. 69, no. 10, pp. 1–7, 2004. DOI: 10.1103/PhysRevB.69.104202.

[73] J. Andreasen, P. Sebbah, and C. Vanneste, "Nonlinear effects in random lasers", *Journal of the Optical Society of America B: Optical Physics*, vol. 28, no. 12, pp. 2947–2955, 2011. DOI: 10.1364/JOSAB.28.002947.

[74] D. Sharma, H. Ramachandran, and N Kumar, "Lévy statistics of emission from a novel random amplifying medium: an optical realization of the Arrhenius cascade.", *Optics Letters*, vol. 31, no. 12, pp. 1806–1808, 2006. DOI: 10.1364/OL.31.001806.

[75] S. Lepri, S. Cavalieri, G. L. Oppo, and D. S. Wiersma, "Statistical regimes of random laser fluctuations", *Physical Review A - Atomic, Molecular, and Optical Physics*, vol. 75, no. 6, pp. 1–7, 2007. DOI: 10.1103/PhysRevA.75.063820. arXiv: 0611059 [physics].

[76] R. Uppu, A. Tiwari, and S. Mujumdar, "Identification of statistical regimes and crossovers in coherent random laser emission", *Optics letters*, vol. 37, no. 4, pp. 662–664, 2012.

[77] R. Uppu and S. Mujumdar, "Dependence of the Gaussian-Lévy transition on the disorder strength in random lasers", *Physical Review A - Atomic, Molecular, and Optical Physics*, vol. 87, no. 1, pp. 1–8, 2013. DOI: 10.1103/PhysRevA.87.013822.

[78] O. Zaitsev and L. Deych, "Recent developments in the theory of multimode random lasers", *Journal of Optics*, vol. 12, no. 2, p. 024 001, Feb. 2010. DOI: 10.1088/2040-8978/12/2/024001.

[79] J. Andreasen, A. A. Asatryan, L. C. Botten, M. A. Byrne, H. Cao, L. Ge, L. Labonté, P. Sebbah, A. D. Stone, H. E. Türeci, and C. Vanneste, "Modes of random lasers", *Advances in Optics and Photonics*, vol. 3, no. 1, pp. 88–127, Oct. 2011. DOI: 10.1364/AOP.3.000088. arXiv: 1001.4671.

[80] H. E. Türeci, A. D. Stone, and B. Collier, "Self-consistent multimode lasing theory for complex or random lasing media", *Physical Review A - Atomic, Molecular, and Optical Physics*, vol. 74, no. 4, p. 043 822, 2006. DOI: 10.1103/PhysRevA.74.043822. arXiv: 0605673 [cond-mat].

[81] H. E. Türeci, L. Ge, S. Rotter, and A. D. Stone, "Strong interactions in multimode random lasers.", *Science*, vol. 320, no. 5876, pp. 643–6, May 2008. DOI: 10.1126/science.1155311. arXiv: 0805.4497.

[82] H. E. Türeci, A. D. Stone, L. Ge, S. Rotter, and R. J. Tandy, "Ab initio self-consistent laser theory and random lasers", *Nonlinearity*, vol. 22, no. 1, pp. C1–C18, Jan. 2009. DOI: 10.1088/0951-7715/22/1/C01.

[83] X. Wu and H. Cao, "Statistical studies of random-lasing modes and amplified spontaneous-emission spikes in weakly scattering systems", *Physical Review A - Atomic, Molecular, and Optical Physics*, vol. 77, no. 1, p. 013 832, 2008. DOI: 10.1103/PhysRevA.77.013832. arXiv: 0703255v1 [arXiv:physics].

[84] K. L. van der Molen, R. Tjerkstra, A. P. Mosk, and A. Lagendijk, "Spatial Extent of Random Laser Modes", *Physical Review Letters*, vol. 98, no. 14, p. 143 901, Apr. 2007. DOI: 10.1103/PhysRevLett.98.143901.

[85] K. L. van der Molen, A. P. Mosk, and A. Lagendijk, "Relaxation oscillations in long-pulsed random lasers", *Physical Review A*, vol. 80, no. 5, p. 055 803, Nov. 2009. DOI: 10.1103/PhysRevA.80.055803.

[86] ——, "Intrinsic intensity fluctuations in random lasers", *Physical Review A*, vol. 74, no. 5, p. 053 808, Nov. 2006. DOI: 10.1103/PhysRevA.74.053808.

[87] B. Hapke, *Theory of reflectance and emittance spectroscopy*, 2nd. Cambridge University Press, 2012, p. 513.

[88] D. S. Wiersma, "The physics and applications of random lasers", *Nature Physics*, vol. 4, no. May, 2008.

[89] M. Leonetti, C. Conti, and C. Lopez, "The mode-locking transition of random lasers", *Nature Photonics*, vol. 5, no. September, pp. 615–617, 2011. DOI: 10.1038/nphoton.2011.217. arXiv: arXiv:1304.3652v1.

[90] S. Frolov, Z. Vardeny, K. Yoshino, a. Zakhidov, and R. Baughman, "Stimulated emission in high-gain organic media", *Physical Review B*, vol. 59, no. 8, R5284–R5287, 1999. DOI: 10.1103/PhysRevB.59.R5284.

[91] C. M. Soukoulis, X. Jiang, J. Y. Xu, and H. Cao, "Dynamic response and relaxation oscillations in random lasers", *Physical Review B - Condensed Matter and Materials Physics*, vol. 71, no. 15, p. 041 103, 2005. DOI: 10.1103/PhysRevB.71.159902.

[92] I. Iparraguirre, J. Azkargorta, J. Fernández, R. Balda, S. García-Revilla, and N Hakmeh, "On the temporal behavior of $Nd^{3+}$ random lasers.", *Optics letters*, vol. 38, no. 18, pp. 3646–9, Sep. 2013.

[93] B. Redding, M. A. Choma, and H. Cao, "Speckle-free laser imaging using random laser illumination", *Nature Photonics*, vol. 6, no. 6, pp. 355–359, Apr. 2012. DOI: 10.1038/nphoton.2012.90.

[94] G. Zacharakis, N. A. Papadogiannis, G. Filippidis, and T. G. Papazoglou, "Photon statistics of laserlike emission from polymeric scattering gain media.", *Optics letters*, vol. 25, no. 12, pp. 923–5, Jun. 2000.

[95] M. Patra, "Theory for photon statistics of random lasers", *Physical Review A*, vol. 65, no. May 2001, p. 43 809, 2002. DOI: 10.1103/PhysRevA.65.043809. arXiv: 0105069 [quant-ph].

[96] B. Redding, M. A. Choma, and H. Cao, "Spatial coherence of random laser emission", *Optics Letters*, vol. 36, no. 17, pp. 3404–3406, 2011. DOI: 10.1364/OL.36.003404. arXiv: 1107.5586.

[97] L. Florescu and S. John, "Theory of photon statistics and optical coherence in a multiple-scattering random-laser medium", *Physical Review E*, vol. 69, no. 4, p. 046 603, Apr. 2004. DOI: 10.1103/PhysRevE.69.046603.

[98] ——, "Photon statistics and coherence in light emission from a random laser", *Physical Review Letters*, vol. 93, no. 1, pp. 13 602–13 604, Jul. 2004. DOI: 10.1103/PhysRevLett.93.013602.

[99] A. Mermillod-Blondin, H. Mentzel, and A. Rosenfeld, "Time-resolved microscopy with random lasers", *Optics letters*, vol. 38, no. 20, pp. 4112–5, Oct. 2013.

[100] J. D. Bhawalkar, G. S. He, and P. N. Prasad, "Nonlinear multiphoton processes in organic and polymeric materials", *Rep. Prog. Phys.*, vol. 59, pp. 1041–70, 1996.

[101] G. Zacharakis, N. A. Papadogiannis, and T. G. Papazoglou, "Random lasing following two-photon excitation of highly scattering gain media", *Applied Physics Letters*, vol. 81, no. 14, p. 2511, 2002. DOI: 10.1063/1.1511284.

[102] J. Chen, H. Mizuno, H. Kawano, A. Miyawaki, and K. Midorikawa, "Two-photon pumping of random lasers by picosecond and nanosecond lasers", *Applied Physics B: Lasers and Optics*, vol. 85, no. 1, pp. 45–48, 2006. DOI: 10.1007/s00340-006-2345-4.

[103] G Zhu, C. E. Small, and M. A. Noginov, "Single- and two-photon excitation of a GaAs random laser", *Optics letters*, vol. 33, no. 9, pp. 920–2, 2008. DOI: 10.1364/OL.33.000920.

[104] E. V. Chelnokov, N. Bityurin, I. Ozerov, and W. Marine, "Two-photon pumped random laser in nanocrystalline ZnO", *Applied Physics Letters*, vol. 89, no. 17, pp. 2006–2008, 2006. DOI: 10.1063/1.2370879.

[105] R. Bardoux, A. Kaneta, M. Funato, K. Okamoto, Y. Kawakami, A. Kikuchi, and K. Kishino, "Single mode emission and non-stochastic laser system based on disordered point-sized structures: toward a tuneable random laser.", *Optics express*, vol. 19, no. 10, pp. 9262–8, 2011. DOI: 10.1364/OE.19.009262.

[106] A. S. L. Gomes, M. T. Carvalho, C. T. Dominguez, C. B. De Araújo, P. N. Prasad, C. Zhang, F Zhang, T Xia, N Kumar, J. I. Hahm, J Liu, Z. L. Wang, and J Xu, "Direct three-photon excitation of upconversion random laser emission in a weakly scattering organic colloidal system", *Optics Express*, vol. 22, no. 12, pp. 14 305–14 310, 2014. DOI: 10.1364/OE.22.014305.

[107] C. Bouvy, E. Chelnokov, W. Marine, R. Sporken, and B. L. Su, "Quantum Size Effect and very localized random laser in ZnO@mesoporous silica nanocomposite following a two-photon absorption process", *Journal of Non-Crystalline Solids*, vol. 355, no. 18-21, pp. 1152–1156, 2009. DOI: 10.1016/j.jnoncrysol.2009.01.053.

[108] Z. C. Fu, J. Dai, T. Li, H. Y. Liu, Q. F. Dai, L. J. Wu, S. Lan, S. L. Tie, X. Wan, A. V. Gopal, V. A. Trofimov, and T. M. Lysak, "Femtosecond laser ablation of ZnO nanorods for two-photon-pumped random lasing and optical data storage", *Applied Physics B: Lasers and Optics*, vol. 108, no. 1, pp. 61–66, 2012. DOI: 10.1007/s00340-011-4833-4.

[109] D. J. Clark, L. Yuan, C. O. Otieno, G. Zhou, and J. I. Jang, "Impurity and morphological dependence on photoluminescence and enhanced impurity-induced two-photon absorption in ZnO", *Solid State Communications*, vol. 181, pp. 9–14, 2014. DOI: 10.1016/j.ssc.2013.11.020.

[110] A. L. Burin, H. Cao, and M. A. Ratner, "Two-photon pumping of a random laser", *IEEE Journal on Selected Topics in Quantum Electronics*, vol. 9, no. 1, pp. 124–127, 2003. DOI: 10.1109/JSTQE.2002.807965.

[111] K. Wang, J. Liu, J. Lu, and D. Xu, "Theoretical investigation on the saturation effects in two-photon pumping random lasers", *Optical and Quantum Electronics*, vol. 37, no. 11, pp. 1001–1009, 2005. DOI: 10.1007/s11082-005-8339-3.

[112] B. García-Ramiro, M. A. Illarramendi, S. García-Revilla, R. Balda, D. Levy, M. Zayat, and J. Fernández, "Lasing threshold of one-and two-photon-pumped dye-doped silica powder", *Applied Physics B*, pp. 11–14, 2014. DOI: 10.1007/s00340-014-5936-5.

[113] S. García-Revilla, E. Pecoraro, R. Balda, L. D. Carlos, and J. Fernández, "One- and two-photon pumped random laser action in Rhodamine B doped di-ureasil hybrids", *Proceedings of SPIE*, vol. 8257, pp. 825 708–825708–6, 2012. DOI: 10.1117/12.905372.

[114] E. Pecoraro, S. García-Revilla, R. A. S. Ferreira, R. Balda, L. D. Carlos, and J. Fernández, "Real time random laser properties of Rhodamine-doped di-ureasil hybrids.", *Optics express*, vol. 18, no. 7, pp. 7470–7478, 2010. DOI: 10.1364/OE.18.007470.

[115] I. A. Kenyon, *The light fantastic*. 2008.

[116] S. Venugopal Rao, N. K. M. Naga Srinivas, and D. Narayana Rao, "Nonlinear absorption and excited state dynamics in Rhodamine B studied using Z-scan and degenerate four wave mixing techniques", *Chemical Physics Letters*, vol. 361, no. August, pp. 439–445, 2002. DOI: 10.1016/S0009-2614(02)00928-4.

[117] L. D. Carlos, V. de Zea Bermudez, R. A. Sá Ferreira, L. Marques, and M. Assunção, "SolGel Derived Urea Cross-Linked Organically Modified Silicates. 2. Blue-Light Emission", *Chemistry of Materials*, vol. 11, p. 581, 1999. DOI: 10.1021/CM980373N.

[118] R. A. S. Ferreira, L. D. Carlos, and V. de Zea Bermudez, "Excitation energy dependence of luminescent sol-gel organically modified silicates", *Thin Solid Films*, vol. 343, p. 476, 1999.

[119] L. Fu, R. A. Sá Ferreira, N. J. Silva, L. D. Carlos, V. De Zea Bermudez, and J. Rocha, "Photoluminescence and Quantum Yields of Urea and Urethane Cross-Linked Nanohybrids Derived from Carboxylic Acid Solvolysis", *Chemistry of Materials*, vol. 16, no. 8, pp. 1507–1516, 2004. DOI: 10.1021/cm035028z.

[120] J. Fernández, S. García-Revilla, L. D. Carlos, E. Pecoraro, M. A. Arriandiaga, and R. Balda, "Time-resolved random laser spectroscopy of inhomogeneously broadened systems", *Laser & Photonics Reviews*, vol. 8, no. 3, pp. L32–L36, 2014. DOI: 10.1002/lpor.201300191.

[121] S. García-Revilla, J. Fernández, M. Barredo-Zuriarrain, L. D. Carlos, E. Pecoraro, I. Iparraguirre, J. Azkargorta, and R. Balda, "Diffusive random laser modes under a spatiotemporal scope", *Optics Express*, vol. 23, no. 2, p. 1456, 2015. DOI: 10.1364/OE.23.001456.

[122] M. Fox, *Quantum Optics*. Oxford University Press, 2006.

[123] D. F. Walls and G. J. Milburn, *Quantum Optics*. Springer-Verlag Berlin Heidelberg, 1994.

[124] S. García-Revilla, J. Fernández, M. Barredo-Zuriarrain, and E Pecoraro, "Coherence characteristics of random lasing in a dye doped hybrid powder", *Journal of Luminescence*, vol. 169, pp. 472–477, 2016. DOI: 10.1016/j.jlumin.2014.11.051.

[125] L. De Boni, P. L. Franzen, P. J. Gonçalves, I. E. Borissevitch, L. Misoguti, C. R. Mendonça, and S. C. Zilio, "Pulse train fluorescence technique for measuring triplet state dynamics", *Optics Express*, vol. 19, no. 11, pp. 10 813–10 823, 2011. DOI: 10.1016/j.saa.2011.05.012.1..

[126] N. S. Makarov, M. Drobizhev, and A. Rebane, "Two-photon absorption standards in the 550-1600 nm excitation wavelength range.", *Optics express*, vol. 16, no. 6, pp. 4029–4047, 2008. DOI: 10.1364/OE.16.004029.

[127] S. García-Revilla, J. Fernández, M. Barredo-Zuriarrain, L. D. Carlos, E. Pecoraro, I. Iparraguirre, J. Azkargorta, and R. Balda, "Spectral dynamics of a diffusive random laser under two photon pumping", *Advanced Device Materials*, vol. 1, no. October 2014, pp. 38–45, 2015. DOI: 10.1179/2055031614Y.0000000008.

[128] M. Bahoura, K. J. Morris, G. Zhu, and M. A. Noginov, "Dependence of the neodymium random laser threshold on the diameter of the pumped spot", *IEEE Journal of Quantum Electronics*, vol. 41, no. 5, pp. 677–685, 2005. DOI: 10.1109/JQE.2005.845027.

[129] M. Bahoura and M. A. Noginov, "Determination of the transport mean free path in a solid-state random laser", *Journal of the Optical Society of America B: Optical Physics*, vol. 20, no. 11, pp. 2389–2394, 2003. DOI: 10.1364/JOSAB.20.002389.

[130] S. García-Revilla, I. Iparraguirre, C. Cascales, J. Azkargorta, R. Balda, M. A. Illarramendi, M. Al-Saleh, and J. Fernández, "Random laser performance of $Nd_xY_{1-x}Al_3(BO_3)_4$ laser crystal powders", *Optical Materials*, vol. 34, pp. 461–464, 2011. DOI: 10.1016/j.optmat.2011.03.047.

[131] M. A. Noginov, N. E. Noginova, H. J. Caulfield, P. Venkateswarlu, T. Thompson, M. Mahdi, and V. Ostroumov, "Short pulsed stimulated emission in the powders of $NdAl_3(BO_3)_4$, $NdSc_3(BO_3)_4$, and Nd:$Sr_5(PO_4)_3F$ laser crystals", *Journal of the Optical Society of America B*, vol. 13, no. 9, p. 2024, 1996. DOI: 10.1364/JOSAB.13.002024.

[132] G. Kumar, J. Lu, A. Kaminskii, K.-I. Ueda, H. Yagi, and T. Yanagitani, "Spectroscopic and Stimulated Emission Characteristics of $Nd^{3+}$ in Transparent $Y_2O_3$ Ceramics", *IEEE Journal of Quantum Electronics*, vol. 42, no. 7, pp. 643–650, Jul. 2006. DOI: 10.1109/JQE.2006.875868.

[133] Y. V. Orlovskii, T. T. Basiev, K. K. Pukhov, M. V. Polyachenkova, P. P. Fedorov, O. K. Alimov, E. I. Gorokhova, V. A. Demidenko, O. A. Khristich, and R. M. Zakalyukin, "Oxysulfide optical ceramics doped by $Nd^{3+}$ for one micron lasing", *Journal of Luminescence*, vol. 125, no. 1-2, pp. 201–215, Jul. 2007. DOI: 10.1016/j.jlumin.2006.08.031.

[134] I. Iparraguirre, J. Azkargorta, O. Merdrignac-Conanec, M. Al-Saleh, C. Chlique, X. Zhang, R. Balda, and J. Fernández, "Laser action in $Nd^{3+}$-doped lanthanum oxysulfide powders", *Optics express*, vol. 20, no. 21, pp. 23 690–9, 2012. DOI: 10.1364/OE.20.023690.

[135] M. J. Weber, "Rare earth lasers", in *Handbook of the Physics and Chemistry of Rare Earths, 4*, K. A. Gschneidner Jr and L Eyring, Eds., North-Holland, 1979, ch. Rare earth, p. 275.

[136] J. Azkargorta, I. Iparraguirre, M. Bettinelli, E. Cavalli, M. Barredo-Zuriarrain, S. García-Revilla, R. Balda, and J. Fernández, "Effects of pumping wavelength and pump density on the random laser performance of stoichiometric Nd crystal powders", *Optics Express*, vol. 22, no. 22, p. 27 365, 2014. DOI: 10.1364/OE.22.027365.

[137] R. C. Powell, *Physics of Solid-State Laser Materials*. New York: Springer-Verlag New York, 1998.

[138] F. Luan, B. Gu, A. S. L. Gomes, K. T. Yong, S. Wen, and P. N. Prasad, "Lasing in nanocomposite random media", *Nano Today*, vol. 10, no. 2, pp. 168–192, 2015. DOI: 10.1016/j.nantod.2015.02.006.

[139] C. Maunier, J. L. Doualan, R. Moncorge, A. Speghini, M. Bettinelli, and E. Cavalli, "Growth , spectroscopic characterization , and laser performance of Nd:$LuVO_4$, a new infrared", *Journal of the Optical Society of America B*, vol. 19, no. 8, pp. 1794–1800, 2002.

[140] W. Strek, L Marciniak, A. Lukowiak, A. Bednarkiewicz, D. Hreniak, and R. Wiglusz, "Synthesis and luminescence properties of $LiLa_{1-x}Nd_xP_4O_{12}$ nanocrystals", *Optical Materials*, vol. 33, no. 2, pp. 131–135, 2010. DOI: 10.1016/j.optmat.2010.07.026.

[141] I. Iparraguirre, J. Azkargorta, K. Kamada, A. Yoshikawa, U. R. Rodríguez-Mendoza, V Lavín, M. Barredo-Zuriarrain, R. Balda, and J. Fernández, "Random laser action in stoichiometric $Nd_3Ga_5O_{12}$ garnet crystal powder", *Laser Physics Letters*, vol. 13, p. 035 402, 2016. DOI: 10.1088/1612-2011/13/3/035402.

[142] M. A. Noginov, N. E. Noginova, S. Egarievwe, H. J. Caulfield, P. Venkateswarlu, a. Williams, and S. Mirov, "Color-center powder laser: The effect of pulverization on color-center characteristics", *Journal of the Optical Society of America B: Optical Physics*, vol. 14, no. 8, pp. 2153–2160, 1997.

[143] W. M. Yen, S. Shionoya, and H. Yamamoto, *Phosphor Handbook*, 2nd ed. CRC Press, 2007.

[144] R. V. Alves, R. A. Buchanan, K. A. Wickersheim, and E. A. C. Yates, "Neodymium-activated lanthanum oxysulfide: A new high-gain laser material", *Journal of Applied Physics*, vol. 42, no. 8, pp. 3043–3048, Jul. 1971. DOI: 10.1063/1.1660681.

[145] G. I. Abutalibov, D. I. Guseynov, and A. A. Mamedov, "$Nd^{3+}$-ion luminescence in $La_2O_2S$ and $Y_2O_2S$ single crystals", *Physica Status Solidi (C)*, vol. 6, no. 5, pp. 1127–1129, 2009. DOI: 10.1002/pssc.200881132.

[146] V. M. Markushev, N. E. Ter-Gabriélyan, C. M. Briskina, V. R. Belan, and V. F. Zolin, "Stimulated emission kinetics of neodymium powder lasers", *Soviet Journal of Quantum Electronics*, vol. 20, no. 7, pp. 773–777, Jul. 1990. DOI: 10.1070/QE1990v020n07ABEH006817.

[147] T. Myers, C. Brauer, F.-Y. Su, T. Blake, R. Tonkyn, A. Ertel, T. Johnson, and R. Richardson, "Quantitative reflectance spectra of solid powders as a function of particle size", *Applied Optics*, vol. 54, no. 15, 2015. DOI: 10.1364/AO.54.004863.

[148] W Koechner, *Solid-State Laser Engineering*. Springer-Verlag New York, 2006.

[149] Y. Feng and K.-I. Ueda, "One-mirror random laser", *Physical Review A*, vol. 68, no. 2, p. 02 583, 2003. DOI: 10.1103/PhysRevA.68.025803.

[150] Y. Feng, J.-F. Bisson, J. Lu, S. Huang, K. Takaichi, A. Shirakawa, M. Musha, and K.-I. Ueda, "Thermal effects in quasi-continuous-wave $Nd^{3+}$:$Y_3Al_5O_{12}$ nanocrystalline-powder random laser", *Applied Physics Letters*, vol. 84, no. 7, p. 1040, 2004. DOI: 10.1063/1.1647285.

[151] Y. Feng, S. Huang, G. Qin, M. Musha, and K.-I. Ueda, "Random microchip laser.", *Optics express*, vol. 13, no. 1, pp. 121–6, 2005. DOI: 10.1364/OPEX.13.000121.

[152] J. Azkargorta, I. Iparraguirre, M. Barredo-Zuriarrain, S. García-Revilla, R. Balda, and J. Fernández, "Random Laser Action in Nd : YAG Crystal Powder", *materials*, vol. 9, no. 5, p. 369, 2016. DOI: 10.3390/ma9050369.

[153] B. Redding, M. A. Choma, and H. Cao, "Speckle Free Laser Imaging", *Conference on Lasers and Electro-Optics 2012*, vol. i, JTh2A.86, 2012. DOI: 10.1364/CLEO_AT.2012.JTh2A.86.

[154] B. H Hokr, M. S. Schmidt, B. J. N, P. N. Dyer, G. D. Noojin, B. Redding, R. J. Thomas, B. a. Rockwell, H. Cao, V. V. Yakovlev, and M. O. Scully, "A narrow-band speckle-free light source via random Raman lasing", *Journal of Modern Optics*, vol. 63, no. 1, pp. 46–49, 2015. DOI: 10.1080/09500340.2015.1078919. arXiv: arXiv:1505.07156v1.

[155] M. Barredo-Zuriarrain, I. Iparraguirre, J. Fernández, J. Azkargorta, and R. Balda, "Speckle-free near-infrared imaging using a $Nd^{3+}$ random laser source", *Laser Physics Letters*, vol. Accepted,

[156] P. Pringsheim, "Fluorescence and temperature radiation", *Zeitschrift für Physik*, vol. 57, pp. 739–46, 1929.

[157] A. Kastler, "Quelques suggestions concernant la production optique et la détection optique d'une inégalité de population des niveaux de quantifigation spatiale des atomes. Application à l'expérience de Stern et Gerlach et à la résonance magnétique", *Journal de Physique et le Radium*, vol. 11, no. 6, pp. 255–265, Jun. 1950. DOI: 10.1051/jphysrad:01950001106025500.

[158] R. Balda, N. Hakmeh, M. Barredo-Zuriarrain, O. Merdrignac-Conanec, S. García-Revilla, M. A. Arriandiaga, and J. Fernández, "Influence of Upconversion Processes in the Optically-Induced Inhomogeneous Thermal Behaviorof Erbium-Doped Lanthanum Oxysulfide Powders", *materials*, vol. 9, no. 353, p. 13, 2016. DOI: 10.3390/ma9050353.

[159] A. J. Garcia-Adeva, R. Balda, and J. Fernández, "Upconversion cooling of Er-doped low-phonon fluorescent solids", *Physical Review B - Condensed Matter and Materials Physics*, vol. 79, no. 3, pp. 5–8, 2009. DOI: 10.1103/PhysRevB.79.033110. arXiv: 0808.0569.

[160] A. J. Garcia-Adeva, R. Balda, M. Al Saleh, and J. Fernandez, "Local internal and bulk optical cooling in Nd-doped crystals and nanocrystalline powders", in *Proceedings of SPIE*, R. I. Epstein and M. Sheik-Bahae, Eds., International Society for Optics and Photonics, Feb. 2010, 76140A. DOI: 10.1117/12.842116.

[161] J. Fernández, R. Balda, M. Barredo-Zuriarrain, O. Merdrignac-Conanec, N. Hakmeh, and S. García-Revilla, "Progress in the spectroscopic and thermal studies of Er-doped oxysulfide crystal powders", in *Proceedings of SPIE*, vol. 9765, 2016, pp. 1–11. DOI: 10.1117/12.2208601.